Analysing the role of the anterior visceral endoderm in anterior-posterior axis establishment in the mouse embryo

Daniel William Stuckey

A thesis submitted for the degree of Doctor of Philosophy

2008

Imperial College

Dedicated to my family who have offered me endless love and support.

Thank you so much

Abstract

Anterior-posterior (A-P) axis specification requires signalling from a specialised extra-embryonic tissue called the anterior visceral endoderm (AVE). AVE precursors are induced at the distal tip of the pre-gastrulating mammalian embryo and move to the prospective anterior. This movement is essential in correctly positioning the A-P axis.

Firstly, the contribution of proliferation to AVE movements has been tested. Previous studies have suggested that differential proliferation within the visceral endoderm (VE) is required to determine its direction by passive displacement. High-resolution imaging and embryo culture experiments have been used to assess the distribution and requirements of proliferation during AVE movements. Differential proliferation was not observed along the A-P axis of the VE. However, proliferation within the epiblast was found to be required for correct AVE movements in a *Nodal*-dependant manner.

Secondly, to address the function of the AVE *in vivo*, this tissue was genetically ablated. Diphtheria toxin A was knocked-in to the *Hex* locus (an early AVE marker) by homologous recombination in embryonic stem cells. Depending on the time of ablation the AVE or its precursors could be ablated as demonstrated by AVE marker analysis. Ablation of the AVE precursors prior to 5.5 dpc resulted in embryos that displayed greatly disturbed patterning and were unable to gastrulate. AVE ablation between 5.5-6.5 dpc resulted in delayed formation of the primitive streak, epithelial to mesenchymal transition defects and a mispatterning of the anterior primitive streak. A decrease in

Nodal signalling was found to be a likely cause for the defects observed in these ablated embryos, indicating that AVE maintains Nodal signalling levels in the epiblast.

Together these experiments find a role for epiblast proliferation in AVE migration and identify a novel role for the AVE in patterning the primitive streak. Therefore this investigation provides a critical insight into how the A-P axis is established in mammals.

Acknowledgements

I would like to express special thanks to my supervisor Dr Tristan Rodriguez for all of his support, encouragement and interesting discussion throughout the course of this PhD. A big thanks also to the rest of the Molecular Embryology Group, past and present for their help, humour and scientific advice. Last-but-not-least the MRC Clinical Sciences Centre Transgenic facility, especially Zoe Webster and Jonathan Godwin for help with ES cell targeting and general mouse advice. This work was funded by the Medical Research Council.

List of contents

Chapter 1 – Introduction

1.1. Aim of the study…… 10
1.2. Embryogenesis in the mouse…… 12
1.2.1. Preimplantation development……... 12
1.2.2. Peri-implantation development…… 16
1.2.2.1. How early is the A-P axis established?.....
1.2.2.2. Morphological asymmetries in the peri-implantation embryo…….. 17
1.2.2.3. Evidence of molecular asymmetries in the implanting blastocyst…….. 18
1.2.2.4. Evidence of molecular asymmetries in the peri-implantation embryo…… 20
1.2.2.5. Induction of the DVE…… 22
1.2.2.6. Movements of the AVE……... 26
1.2.2.7. Roles of the AVE……. 34
1.2.2.8. The AVE determines the site of primitive streak formation……. 35
1.2.2.9. Role of AVE in forebrain development……. 37
1.2.3. Gastrulation……. 41
1.2.3.1. Formation of the primitive streak……. 41
1.2.3.2. Cell movement through the primitive streak…… 43
1.2.3.3. Signals regulating lineage choice during gastrulation……. 47
1.3. This investigation…… 48

Chapter 2 – Materials and methods

2.1. Mice and procedures…….. 50
2.1.1. Mouse strains……... 50
2.1.2. Transgenic lines……... 50
2.2. Embryology methods……. 53
2.2.1. Embryo recovery……. 53
2.2.2. Wholemount RNA *in situ* hybridisation……... 53
2.2.2.1. Fixation…….. 53
2.2.2.2. Embryo processing…… 53
2.2.2.3. Hybridisation of riboprobe…… 54
2.2.2.4. Incubation with anti-DIG antibody…….. 54
2.2.2.5. Signal detection…….. 55
2.2.3. Wholemount β-galactosidase staining…….. 55
2.2.3.1. Fixation…….. 55
2.2.3.2. Staining…….. 56
2.2.4. TUNEL staining…….. 56
2.2.5. Antibody staining…… 57
2.2.5.1. Wholemount anti-phospho-Histone H3 staining……. 57
2.2.5.2. Wholemount GFP and BrdU staining – Embryo culture protocol I…… 57

2.2.5.3. Wholemount GFP and BrdU staining – Injection of BrdU……... 59
2.2.5.4. Wholemount GFP and BrdU staining – Embryo culture protocol II……. 59
2.2.6. Embryo culture…….. 61
2.2.6.1. Nocodazole, Genistein and Okadaic acid…… 61
2.2.6.2. SB-431542…… 62
2.2.7. Confocal acquisition…….. 62
2.3. Molecular biology……. 64
2.3.1. Transcription of riboprobes for wholemount RNA *in situ* hybridisation…… 64
2.3.2. Generation of targeting vector Hex-XneoSTOP^{R}X-DTA…. 65
2.3.3. Isolation and restriction digestion of genomic DNA from ES cells for Southern blot…….. 66
2.3.4. Synthesis and purification of DNA probes for Southern blot 66
2.3.5. Southern blot analysis of Hexd targeted ES cell clones…… 67
2.3.6. Extraction of genomic DNA from murine tail biopsies for Southern blot analysis…… 68
2.3.7. Extraction of genomic DNA from murine tail biopsies for PCR genotyping…….. 69
2.3.8. Digestion of transgenic embryos for genotyping…… 69
2.3.9. Genotyping of transgenic mouse lines by PCR…….. 69
2.3.9.1. The standard PCR reaction…… 71
2.3.9.2. Exon 1 PCR reaction…….. 71
2.4. Tissue culture……... 72
2.4.1. General passaging techniques……. 72
2.4.2. Generation of targeted clones……. 72
2.4.2.1. Preparation of DNA……... 72
2.4.2.2. Electroporation and processing of targeted clones... 72
2.4.2.3. Karyotyping ES cells…….. 74
2.4.2.4. Transient transfections of targeted ES cells with pTurboCre…….. 75

Chapter 3 – Proliferation at the time of DVE movements

3.1. Introduction…… 76
3.1.1. Proliferation and DVE movement……. 77
3.2. Results……. 80
3.2.1. BrdU incorporation shows no regional bias in the VE at the onset of DVE movements……. 80
3.2.2. Low levels of mitosis in the VE at the onset of DVE movements 84
3.2.3. Distribution of mitotic nuclei within the VE during DVE movements……. 88
3.2.4. No evidence of a proliferative burst during DVE movement 91
3.3. Discussion……... 95

Chapter 4 – The role of proliferation at 6.25 dpc

4.1. Introduction…… 99
4.2. Results……. 103

4.2.1. The AVE shows a similar incorporation index to the rest of the VE, but the success of BrdU incorporation is sensitive to the Protocol used……. 103
4.2.2. At 6.25 dpc the VE displays low levels of randomly distributed mitotic nuclei…….. 106
4.2.3. At 6.25 dpc the AVE and VE cycle at a similar rate…… 110
4.2.4. *Nodal* is not required for proliferation in the VE, but is required for AVE movement…… 113
4.2.5. Disrupting cell division throughout the embryo perturbs AVE movement…… 117
4.3. Discussion…… 121

Chapter 5 – Creating the Hexd mouse line

5.1. Introduction…… 126
5.2. Results……. 128
5.2.1. A genetic strategy for AVE/DVE ablation…… 128
5.2.2. Characterisation of positively targeted clones…….. 128
5.2.3. The ablation system is functional *in vivo*……... 133
5.2.4. The decrease in *Hex*-expressing cells is accompanied by a reduction in other AVE markers……. 139
5.2.5. The ability to correctly position the primitive streak is impaired in a proportion of mutants…… 142
5.3. Discussion…… 146

Chapter 6 – Characterisation of Hexd^{act} embryos

6.1. Introduction…… 150
6.2. Results……. 151
6.2.1. Hexd^{act} embryos display two Classes of phenotype depending on the time of ablation…….. 151
6.2.2. Class I mutants display severe patterning defects of the AVE 151
6.2.3. Class I mutants show a failure to specify the anterior primitive streak and exhibit EMT defects…….. 157
6.2.4. There are no apparent defects in the anterior definitive endoderm of Class I mutants……. 161
6.2.5. There are no apparent defects in the anterior neurectoderm of Class I mutants……. 164
6.2.6. Class II mutants are unable to gastrulate……. 164
6.2.7. Nodal signalling is aberrant in both Classes of mutant…... 168
6.3. Discussion…… 172

Chapter 7 – General discussion

7.1. Proliferation during AVE movements…… .. 178
7.2. Genetic ablation in Hexd embryos……. 182
Bibliography…… 188
Appendix ……..……...……... 217

Abbreviations

Abbreviation	Full Term
A-P	**Anterior-Posterior**
AVE	**Anterior Visceral Endoderm**
BMP	**Bone Morphogenetic Protein**
BSA	**Bovine Serum Albumin**
BrdU	**5-bromo-2-deoxyuridine**
dpc	**Days Post Coitum**
D-V	**Dorso-Ventral**
DVE	**Distal Visceral Endoderm**
ECM	**Extracellular Matrix**
EGO	**Early gastrula organiser**
Em-Ab	**Embryonic-Abembryonic**
EMT	**Epithelial to Mesenchymal Transition**
EpC	**Ectoplacental Cone**
ExE	**Extraembryonic Ectoderm**
FCS	**Fetal Calf Serum**
FGF	**Fibroblast Growth Factor**
GFP	**Green Fluorescent Protein**
GMEM	**Glasgow Minimum Essential Media**
hrs	**Hours**
ICM	**Inner Cell Mass**
LIF	**Leukocyte Inhibitory Factor**
mAb	**Monoclonal Antibody**
MI	**Mitotic Index**
NGS	**Normal Goat Serum**
P-D	**Proximal-Distal**
PE	**Primitive Endoderm**
PH3	**Phospho-Histone-H3**
PS	**Primitive Streak**
RNA	**Ribonucleic acid**
SEM	**Standard Error of Mean**
TGF-β	**Transforming Growth Factor-β**
TE	**Trophectoderm**
TUNEL	**Terminal deoxynucleotidyl transferase dUTP nick end labelling**
VE	**Visceral Endoderm**
WISH	**Wholemount *in situ* hybridisation**
ZP	**Zona pellucida**

Chapter 1

1.1. Aim of the study

How the embryo is patterned remains a fascinating biological conundrum. Conversion of a single celled egg into a multi-cellular, multilayered foetus relies upon exquisite genetic and cellular coordination. Underpinning these events is the acquisition of successive asymmetries that culminate in the establishment of three embryonic axes: anterior-posterior (A-P), dorso-ventral (D-V) and left-right. These axes are initiated from appropriately positioned signalling centres and form the blueprint for the mature body plan.

Fertilization of the egg by the sperm marks the first embryonic asymmetry. However, whether this event causally relates to later patterning events is controversial. In mouse, formation of the A-P axis is the first definitive embryonic axis to be associated with a manifest asymmetry. A complex network of signalling molecules and cell movements have been identified that are important in establishing the A-P axis; eventually defining the head at the anterior side from trunk and associated structures at the posterior.

The anterior visceral endoderm (AVE) is a specialised extra-embryonic signalling centre that is essential for A-P patterning. The AVE is characterised by the expression of a unique set of molecular markers that are restricted to the distal tip of the visceral endoderm at 5.5 dpc. By 5.75-6.0 dpc, the AVE has traversed unilaterally along the prospective anterior of the epiblast. The endpoint of this movement will

define the anterior of the embryo. The posterior of the embryo, opposite the AVE, is where the primitive streak (PS) will form.

Despite the significant role of the AVE in anterior patterning, many questions remain unanswered: The mechanisms involved in its movement and appropriate positioning is a contentious issue, as is its exact contribution to A-P patterning events. This thesis aims to tackle these two fundamental aspects of AVE function.

1.2. Embryogenesis in the mouse

1.2.1. Preimplantation development

Mammalian preimplantation spans the period from fertilisation to implantation and is defined by dynamic genetic programming (reviewed in Wang and Dey, 2006). Fertilization occurs when the sperm penetrates the oocyte resulting in a 1-cell embryo containing haploid maternal and paternal pronuclei. Both pronuclei undergo DNA replication before entering into mitosis and forming a 2-cell zygote. At this point, 90% of the maternal RNA transcripts have been degraded and activation of the zygotic genome commences to enable further development (Nothias *et al*., 1995). The zygote undergoes two additional cleavages, and the 8-cell embryos undergo a process of compaction to form the morula. This is followed by differentiation of the morula into the blastocyst at 3.5 days post coitum (dpc) (Fig. 1A).

At this stage the blastocyst is composed of two cell types: the outer epithelial trophectoderm (TE) and the inner cell mass (ICM) positioned to one side of the TE. The TE in contact with the ICM is the polar TE, whilst the TE surrounding the blastocoel is the mural TE (Fig. 1A). The TE will make the first contact with the luminal epithelium of the uterus during implantation. In addition, its lineages will give rise to extraembryonic tissues such as the placenta. The pluripotent ICM will generate all the future cell lineages of the embryo proper.

At 3.5 dpc, the blastocyst has an embryonic-abembryonic (Em-Ab) axis, defined by the position of the ICM. However this axis is topological rather than relating to a definitive body axis.

Figure 1 – Preimplantation development

A. *Diagrammatic representation of events from fertilisation to implantation*. At fertilisation the sperm penetrates the female oocyte and the two pro-nuclei fuse to form the diploid nucleus. Fertilisation results in completion of the second meiotic division, producing the second polar body (2PB) (yellow). In the next 3.5 days the conceptus becomes a multilayered blastocyst. The outermost layer is the trophectoderm (TE; shown in light blue), which is classified into two hemispheres, the mural and polar TE, relating to the position of the inner cell mass (ICM; shown in pink). The TE forms extraembryonic tissues such as the ectoplacental cone and eventually forms the placenta. The ICM is a mass of pluripotent cells, which go on to form every tissue of the animal itself. The asymmetric location of the ICM defines the Embryonic-Abembryonic (Em-Ab) axis, which later becomes the post-implantation proximal-distal (PD) axis. By 4.0 dpc a subpopulation of cells within the ICM move to the inner surface and form the primitive endoderm (PE; shown in green). At 4.5 dpc the blastocyst hatches from the protective outer zona pellucida (ZP) and implants into the uterine wall. The conceptus is now referred to as the egg cylinder. The ICM has become the embryonic ectoderm, which is referred to as the epiblast (also shown in pink).

B. *Genes responsible for lineage segregation*. A flow diagram showing the genes responsible for converting a totipotent precursor cell into the three lineages of the hatched blastocyst. Note the reciprocal inhibitory interactions which stabilize and reinforce lineage commitment.

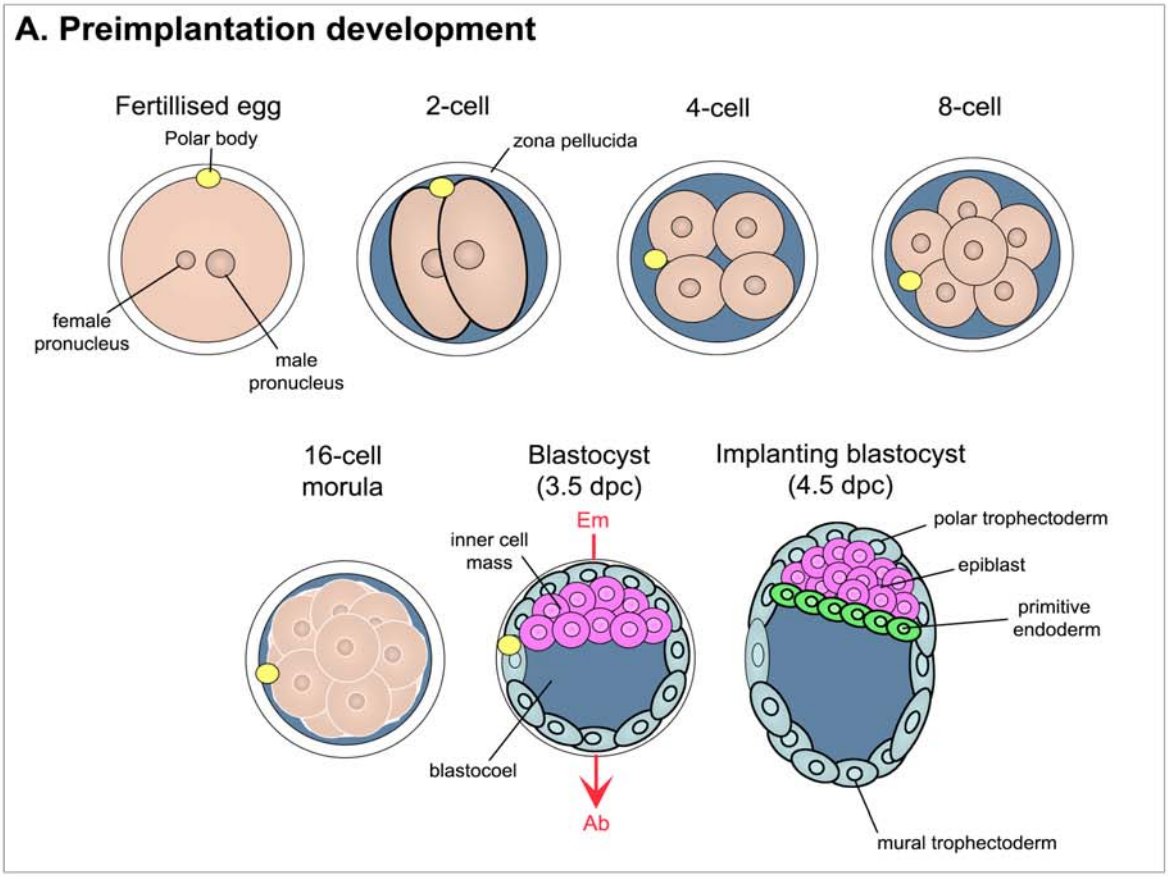
A. Preimplantation development
Fertillised egg
Polar body
female pronucleus
male pronucleus
2-cell
zona pellucida
4-cell
8-cell
16-cell morula
Blastocyst (3.5 dpc)
Em
inner cell mass
blastocoel
Ab
Implanting blastocyst (4.5 dpc)
polar trophectoderm
epiblast
primitive endoderm
mural trophectoderm

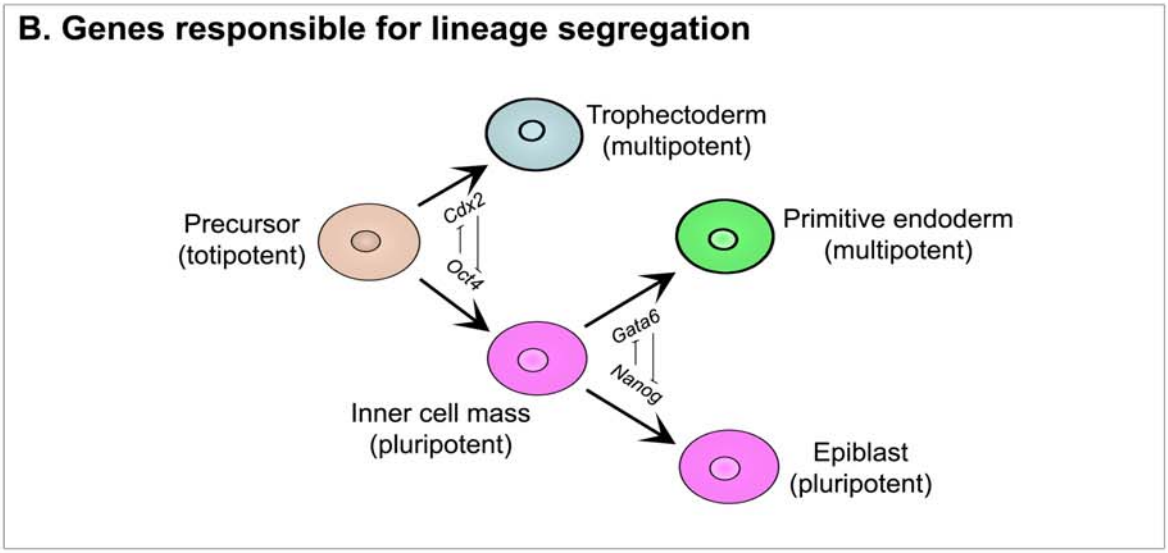
B. Genes responsible for lineage segregation
Trophectoderm (multipotent)
Precursor (totipotent)
Cdx2
Oct4
Primitive endoderm (multipotent)
Gata6
Nanog
Inner cell mass (pluripotent)
Epiblast (pluripotent)

The existence of prepatterning in the embryo before implantation is controversial but to date no irrefutable evidence has proven that asymmetries within the zygote are related to establishment of the definitive embryonic axes (reviewed in Rossant and Tam, 2004).

Important molecular pathways that segregate and differentiate the two cell types of the blastocyst at this stage have been identified by genetic analysis. ICM formation depends on OCT4, which is encoded by *Pou5f1* (Nichols *et al.*, 1998). Additionally, the ICM comprises a mixture of *Gata6* expressing Primitive Endoderm (PE) precursors and *Nanog* expressing epiblast precursors expressed in a mutually exclusive manner (reviewed in Rossant, and Tam 2004; Brewer *et al.*, 2002; Chazaud *et al.*, 2006a). Eventually PE cells move to the surface of the ICM to form the distinct PE layer, whilst *Nanog* expressing cells give rise to the epiblast (Chazaud *et al.*, 2006a). Maintaining pluripotency of the epiblast also requires the TGFβ-related molecules Nodal and Bone morphogenetic proteins (BMPs), and in their absence the epiblast prematurely differentiates into neurectoderm (Camus *et al.*, 2006; Mesnard *et al.*, 2006; Di-Gregorio *et al.*, 2007). The TE lineage not only requires an absence of OCT4, but the presence of the caudal-type homeodomain protein, CDX2, to repress OCT4 and NANOG in the TE (Strumpf *et al.*, 2005). Together this signalling network is responsible for forming the mature blastocyst at 4.5 dpc (Fig. 1B).

Implantation into the uterine wall occurs between 4.5 and 5.0 dpc. The blastocyst hatches from the surrounding zona pellucida and attaches to the uterine wall. TE cells invade the uterine wall and eventually form the placenta. It is at this peri-implantation stage the embryo begins to form the egg cylinder. The ICM has now become the embryonic ectoderm, which is referred to as the epiblast. Polar TE rapidly

proliferates in response to FGF-4, and pushes down the epiblast into the blastocoel cavity, forming the extraembryonic ectoderm (ExE) and ectoplacental cone (Tanaka *et al*., 1998). Also around the time of implantation the epiblast is transformed into a columnar epithelium around a central cavity, the proamniotic cavity (Coucouvanis and Martin, 1995). This is achieved via a process of programmed cell death and modulation of cell adhesion. (Coucouvanis and Martin, 1995) and (Murray and Edgar, 2000) demonstrated that the surrounding visceral endoderm (VE) induces cell death in the epiblast and cells are rescued from this fate only if they are in contact with the extracellular basement membrane, between the VE and epiblast. Surviving cells are now polarised as they have an apical and basal surface, defined by their contact with the basement membrane. The epiblast goes on to form the germ layers and thus all the precursors of the embryo proper. Between 4.5 and 5.0 dpc the primitive endoderm differentiates to become the VE and the parietal endoderm. The VE covers the ExE and epiblast and will eventually form part of the yolk sac at later stages. The parietal endoderm forms the Reichert's membrane, a protective membrane that envelops the entire egg cylinder; this too will later contribute to the yolk sac.

1.2.2. Peri-implantation development

1.2.2.1. How early is the A-P axis established?

In many organisms polarity is established in the oocyte, or shortly after fertilisation by the reorganisation of positional determinants. Therefore perturbation of the early conceptus, such as deletion of a blastomere, results in abnormal development. The mouse embryo however, is remarkably tolerant to such manipulations (reviewed in Beddington and Robertson, 1999 and Rossant and Tam, 2004). For example, the

removal of a substantial volume from either the animal or vegetal pole of the egg still results in viable offspring (Zernicka-Goetz, 1998). This led to the tentative conclusion that mouse development was not determinative, but regulative.

This assertion continues to be contentious; although the embryo can seemingly bypass major disruptions of the egg, this does not mean that positional events in an undisturbed embryo are not important. In light of this, the quest for finding asymmetries in the embryo and relating them to definitive embryonic axes remains voracious.

1.2.2.2. Morphological asymmetries in the peri-implantation embryo

A correlation between asymmetries in the attached blastocyst relating to embryonic axis orientation was first documented by Smith (Smith, 1980, 1985). Serial histological sections of embryos between implantation to 9.5 dpc were examined and an axis fate map was constructed. Smith proposed that the ICM/PE tilt observed in the implanted blastocyst related to the later bending of the ectoplacental cone, and that this bend predicted the future A-P axis (Smith, 1985). This hypothesis was tested by marking the VE on the tilted side with horseradish peroxidase, and culturing embryos until gastrulation (Gardner *et al*., 1992). Although the ectoplacental cone tilt did generally correspond to the A-P axis, labelled cells were equally likely to reside by or opposite the primitive streak; suggesting that the orientation but not polarity of the embryo was specified at the blastocyst stage.

Weber and colleagues proposed that polarity of the mouse embryo was anticipated before implantation (Weber *et al*., 1999). By injecting single ICM cells of a 3.5 dpc blastocyst with mRNA encoding a robust marker, it was possible to lineage trace descendants. ICM-derived VE cells originating from near the polar body tended

to localise distally in the egg cylinder, whilst VE cells derived from ICM cells situated away from the polar body tended to colonise more proximal regions (Weber *et al*., 1999). This suggested that the bilateral asymmetry of the blastocyst did indeed anticipate the polarity of the later conceptus, with asymmetric VE movements forming along the proximal-distal (P-D) axis of the post-implantation egg cylinder. Although this finding was the first of its type, it has yet to be independently replicated.

The first unequivocal morphological asymmetry relating to definitive axis establishment in the embryo is that of the distal visceral endoderm (DVE). At approximately 5.5 dpc, a collection of visceral endoderm (VE) cells at the distal tip of the egg cylinder differentiate into a morphologically distinct tissue, known as the DVE. Cells of the DVE are a columnar epithelium compared to the squamous epithelium of the surrounding VE (Rivera-Perez *et al*., 2003; Srinivas *et al*., 2004). The distal DVE begins to tilt and then move unilaterally to the future anterior of the embryo (Srinivas *et al*., 2004). The direction of this tilt always predicts the prospective anterior of the embryo and is regarded as the first symmetry-breaking step; responsible for converting the transient P-D axis into the definitive A-P axis.

1.2.2.3. Evidence of molecular asymmetries in the implanting blastocyst

Numerous molecular asymmetries have been reported before DVE movements, although their exact roles in establishing the future A-P axis are largely speculative (reviewed in Pfister *et al*., 2007). What is apparent is the importance of reciprocal interactions between extra-embryonic tissues and the epiblast in refining expression domains essential for correct patterning.

Molecular asymmetries implicated in A-P patterning have been reported in the implanting blastocyst (Takaoka *et al*., 2006; Chazaud and Rossant, 2006b). In the first instance, the Nodal antagonist *Lefty1* was found to be expressed in primitive endoderm cells located towards the top of the tilted ICM (Takaoka *et al*., 2006). The asymmetric localisation of endogenous *Lefty1* transcript was corroborated by *Lefty1*-LacZ expression. Furthermore, asymmetric expression was shown not to require interaction with the uterus and was induced by Nodal signalling (Takaoka *et al*., 2006).

However, the presence of *Lefty1* asymmetry and its functional significance in polarity formation should be taken with caution. Firstly, other groups were unable to detect the asymmetric localisation of endogenous *Lefty1* transcript in the implanting blastocyst (Chazaud and Rossant, 2006b; Mesnard *et al*., 2006). Secondly *Lefty1* expression has not been detected between 4.75-5.0 dpc, before being detected again in the DVE at 5.5 dpc (Chazaud and Rossant, 2006b; Mesnard *et al*., 2006). As *Lefty1* is not continually expressed between implantation to DVE induction, whether its later expression corresponds to the same cell lineage as its early expression is unknown. Finally no asymmetry in the expression of *Nodal* or its effectors have been reported in the ICM throughout implantation (Takaoka *et al*., 2006; Mesnard *et al*., 2006). This leaves the mechanism of asymmetric restriction of *Lefty1*, and indeed its functional significance unknown.

Chazaud and Rossant used fluorescent *in situ* hybridisation analysis to look for molecular asymmetries in the implanting blastocyst (Chazaud and Rossant, 2006b). The authors reported non-uniform, transient expression of the homeobox genes *Pem* and *Hex* (*haematopoietically expressed homeobox*) in the primitive endoderm, with

greater expression in cells next to the trophectoderm (Chazaud and Rossant, 2006b). Additionally, in about 15% of the 4.5 dpc blastocysts analysed, β-catenin nuclear localisation was detected in a single trophectoderm cell situated near the primitive endoderm. β-catenin expression was situated opposite the *Hex* expression domain in a non-overlapping manner (Chazaud and Rossant, 2006b). The expression of β-catenin might signify sites of active Wnt signalling although other effector molecules that would presumably be asymmetrically localised have not been identified.

Although interesting observations, as with *Lefty1*, the expression of *Hex* is switched off by 5.0 dpc (Mesnard *et al*., 2006). This hinders the inference that *Hex*-expressing primitive endoderm cells correspond to later *Hex*-expressing cells of the DVE. Furthermore, a recent study looking at *Cerl* expression claim that the AVE is established from both preimplantation precursor cells and *de novo* gene expression after implantation (Torres-Padilla *et al*., 2007). This finding implies that the ontogeny of the AVE comprise multiple cell populations in which AVE commitment occurs at different developmental stages.

1.2.2.4. Evidence of molecular asymmetries in the peri-implantation embryo

It is apparent that in the implanting blastocyst, the detection of molecular asymmetries and their biological significance in polarity establishment remains an ongoing topic of research and intense debate. However the molecular asymmetries associated with the conversion of the P-D axis of the implanted embryo into the A-P axis is equally as contentious.

Soon after implantation molecular heterogeneities within the VE can be detected. The VE overlying the ExE starts to express a different set of genes compared to the VE

overlying the epiblast (EmVE) (reviewed in Pfister *et al*., 2007). At 5.5 dpc the distal EmVE forms a thickening which defines the distal VE (DVE). The DVE expresses a unique set of genes including *Hex*, *Lefty1* and *Cerl*, which set them apart from the surrounding EmVE (reviewed in Pfister *et al*., 2007). Careful examination has revealed that these domains of expression do not completely overlap; *Hex* is distally restricted in a symmetrical domain, while *Cerl* and *Lefty1* both extend asymmetrically to one side (Takaoka *et al*., 2006; Yamamoto *et al*., 2004). This tilt is presumed to be towards the prospective anterior of the embryo as both genes are expressed in the AVE, although this has not been formally proven.

Another asymmetry has been observed before DVE movements. On one side of the VE overlying the proximal epiblast, *Wnt3* transcript is evident (Rivera-Perez and Magnuson, 2005). Again this tilt is regarded to mark the prospective posterior of the embryo, as *Wnt3* is expressed in the primitive streak, although this too has yet to be proven.

As well as asymmetries existing within the VE prior to DVE movements, there also appears to be regionalised signalling within the ExE. Rodriguez *et al*. (2005) demonstrated that signalling within this tissue represses the expression of DVE-specific genes such as *Hex*. Moreover, the source of signalling activity was proposed to emanate from the posterior portion, but not the anterior portion of the ExE (Richardson *et al*., 2006). However this study relied on the tilt of the DVE to demarcate the A-P axis, suggesting that the observed signalling asymmetry might follow those initially required to tilt the DVE.

Nevertheless a growing body of evidence indicates that A-P axis establishment may be initiated prior to DVE movements. Whilst the patterns of gene expression remain radially symmetrical and widespread within the epiblast in the

DVE stage embryo, it is asymmetries within extra-embryonic tissues that initiate subsequent patterning events. This will be discussed in the next section.

1.2.2.5. Induction of the DVE

Recently much progress has been made in understanding how the DVE is induced (reviewed in Takaoka, *et al*., 2007; Srinivas, 2006). Analysis of mouse mutants and embryological manipulation has enabled the identification of signalling pathways and tissue interactions required. The TGFβ-related family member Nodal has a central role in this process, although is not the sole contributor. This section will first focus on Nodal's involvement in these events, then describe recent evidence implicating the Wnt pathway.

Nodal is a secreted TGFβ-related protein that is crucial in establishing polarity in the early mouse embryo (reviewed in Ang and Constam, 2004). Nodal signals via the Alk4 or Alk7 type I receptor in association with either the ActRIIA or ActRIIB type II receptor (reviewed in Whitman, 2001). This activated receptor complex phosphorylates the intracellular molecules Smad2 and Smad3, which associate with Smad4 and translocate to the nucleus (Massague *et al*., 2000). Smad proteins interact with DNA-binding proteins to regulate the transcription of target genes (reviewed in Wotton and Massague, 2001).

Embryos null for *Nodal* display an absence of DVE markers including *Hex, Lefty1* and *Lim1* at 5.5 dpc, indicating its fundamental requirement in the induction of this tissue (Brennan, *et al*., 2001). Careful analysis of embryos at peri-implantation stages have shown *Nodal* and its effector genes including the proprotein convertases *Furin* and *Pace4*, are expressed in the hatched blastocyst (Mesnard *et al*., 2006). At

5.5 dpc these two serine proteases are expressed in the ExE and are required for the proteolytic maturation of Nodal; converting an inactive proprotein into one that is cleaved and active (Beck *et al*., 2002). Interestingly, compound mutants lacking both convertases phenocopy *Nodal* null mutants by failing to induce a DVE (Beck *et al*., 2002), indicating that active Nodal is required to induce this tissue.

Whilst Nodal is essential in specifying the DVE, how its widespread expression is able to induce the DVE towards the distal portion of the egg cylinder remains unclear. Rodriguez *et al.,* (2005) demonstrated that the ExE was responsible for restricting the DVE to the distal tip of the 5.5 dpc embryo. Firstly, microsurgical removal of the entire extra-embryonic region lead to ectopic, *de novo* expression of *Hex*GFP, *Lim1* and *Cerl* throughout the VE (Rodriguez *et al*., 2005). Furthermore injection of dissociated ExE cells into the distal tips of 5.5 dpc embryos resulted in the inhibition of AVE markers (Rodriguez *et al*., 2005). The precise mechanism of how the ExE inhibits AVE formation is unclear.

One possibility is that the ExE could secrete an inhibitor that actively represses the expansion of the DVE. In support of this hypothesis is the fact that upregulation of AVE genes is observed one hour after ExE ablation, with no apparent change in *Nodal* transcript levels as AVE expression is expanding (Rodriguez *et al*., 2005), making an indirect effect temporally unlikely. Alternatively the removal of the ExE could expose the proximal visceral endoderm to low levels of Nodal compatible with AVE induction. Indeed, removal of the ExE will effectively remove *Furin* and *Pace4*, resulting in a block in Nodal activation. As lowest levels of Nodal signalling are required to specify the AVE (Robertson *et al*., 2003; Norris *et al*., 2002), this might explain the ectopic expansion of AVE observed.

Interestingly *Elf5* null mutants lack an ExE, yet still induce and correctly position the AVE (Donnison *et al*., 2005). These mutants do possess an ectoplacental cone which expresse *Furin* and *Pace4* (Donnison *et al.*, 2005). Thus the ectoplacental cone could take over the signalling role from the absent ExE. However, this does not preclude the possibility that the ectoplacental cone also expresses an unknown inhibitor expressed in the ExE, responsible for directly repressing DVE expansion.

Although the repressive effects of the ExE on DVE induction have been demonstrated (Rodriguez *et al.*, 2005; Richardson *et al*., 2006), they are not sufficient in this process. As previously reported, culturing embryo explants in which the extraembryonic portion had been removed resulted in ectopic DVE formation (Rodriguez *et al*., 2005). However, culturing these explants in the Nodal inhibitor SB-431542 abolished DVE expansion as shown by a loss of Hex-GFP and *Lim1* mRNA (Mesnard *et al*., 2006). This suggests that Nodal signalling is required even in the absence of the negative influence of the ExE.

Additional roles for Nodal in DVE specification arose from careful *in situ* hybridisation analysis of *Nodal* and its effector genes in embryos during implantation. An early role was inferred by the observation that Nodal mutants at 5.0 dpc also exhibit a failure to specify EmVE markers (including *Lim1*, *Bmp2* and *Otx2*), and instead express ectopic ExE VE markers such as *Gata4*, *Hnf4* and *Ttr* (Mesnard *et al*., 2006). This suggested that even before DVE induction, Nodal is required to define an EmVE compartment, which is then competent to give rise to a DVE lineage depending upon subsequent signalling events (Mesnard *et al*., 2006).

Mesnard and colleagues then noted that DVE was induced only when the distance between the ExE and distal tip of the egg cylinder exceeded 70 μm, and when the conceptus reached a minimum length of 180 μm (Mesnard *et al*., 2006). Furthermore, in Nodal mutants lacking a DVE, the average length of the egg cylinder at 5.5 dpc was reduced by 24%, suggesting Nodal had an indirect role by promoting proliferation and thereby increasing the egg cylinder to a permissive length (Mesnard *et al*., 2006).

This lead to proposal of a dual role for Nodal during the process of DVE induction (Mesnard *et al*., 2006). Firstly Nodal is required to define the EmVE compartment. At a later stage Nodal is required to promote proliferation in the egg cylinder allowing the distal EmVE to escape the negative influence of the ExE (Rodriguez *et al.*, 2005; Richardson *et al*., 2006).

Nodal signalling is clearly important for the induction of the DVE, though evidence suggests that the canonical Wnt pathway is also required. Wnt/β-catenin signalling is involved in many developmental events, and the formation of the A-P axis is no exception (reviewed in Logan and Nusse, 2004). Briefly, Wnt proteins bind to the Frizzled (Fz)/low density lipoprotein (LDL) receptor-related protein (LRP) complex at the cell surface. Successful binding results in signal transduction to several intracellular proteins including Dishevelled (Dsh), glycogen synthase kinase-3β (GSK-3), Axin, Adenomatous Polyposis Coli (APC) and the transcriptional regulator, β-catenin. In the absence of Wnt signalling, cytosolic β-catenin levels are kept low by continual proteosome-mediated degradation, via the GSK-3/APC/Axin complex. When Wnt binds, the degradation pathway is inhibited resulting in an increase in free β-catenin, which translocates into the nucleus and interacts with members of the

Lef/Tcf transcription factor family to affect transcription (Logan and Nusse, 2004, and references within).

Loss of function in the *Apc* gene leads to constitutive β-catenin activity, as the degradation pathway is unable to function properly. The embryological consequences of having high levels of widespread nuclear β-catenin is the proximalisation of the epiblast and inability to pattern the overlying VE and induce a DVE, as shown by an absence of *Hex*, *Cerl* and *Gsc* expression (Chazaud and Rossant, 2006b). This defect in DVE induction and/or embryonic VE formation appears to be independent from Nodal signalling defects, as its expression and that of its co-receptor Cripto were unaffected (Chazaud and Rossant, 2006b).

Taken together, it is evident that DVE induction requires reciprocal interactions between extra-embryonic tissues and the epiblast to regulate Nodal and Wnt signalling. Perturbation in the spatial or molecular regulation of these events can profoundly affect this process. It remains to be seen whether additional signalling pathways participate in these events.

1.2.2.6. Movements of the AVE

The first morphological evidence of asymmetry relating to the future A-P axis is the tilt of the DVE at 5.5 dpc (reviewed in Srinivas, 2006). VE cells at the distal tip of the egg cylinder adopt a tall, columnar epithelial morphology, distinguishing them from the surrounding squamous VE (Kimura *et al*., 2000; Rivera-Perez *et al*., 2003; Srinivas *et al*., 2004). The columnar nature of the DVE might be modulated by the extracellular matrix (ECM), as when embryonic stem (ES) cells were seeded on the ECM protein hensin, a terminally differentiated epithelium formed that resembled the columnar epithelia of the DVE (Takito and Al-Awqati, 2004). Furthermore, *in vivo*

hensin expression coincides with the formation of columnar cells, and is lost as the cells moved to the prospective anterior of the egg cylinder (Takito and Al-Awqati, 2004).

DVE movements were first described in 1998 by Thomas *et al.,* who labelled VE cells at the distal tip of a 5.5 dpc conceptus with DiI (Thomas *et al*., 1998). Surprisingly, labelled VE cells were shown to move unilaterally, and always towards the prospective anterior of the embryo where they are referred to as the anterior VE (AVE) (Thomas *et al.*, 1998). This finding has since been supported by iontophoretic lineage tracing (Rivera-Perez *et al*., 2003) and directly observing DVE movements using transgenic lines that express GFP in a DVE-specific manner (Srinivas, *et al*., 2004; Mesnard *et al*., 2004) (Fig. 2).

This latter technology combined with high resolution imaging has allowed the direct observation of DVE movements, enabling a more thorough understanding of this process. Time-lapse imaging of transgenic embryos that drive GFP using *Hex* regulatory elements (Rodriguez *et al*., 2001) has afforded the greatest cellular insight into DVE movements (Srinivas *et al*., 2004, and movie links within). This paper describes the dynamic morphological events during this anteriorwards movement with cells becoming flatter and starting to project filopodial processes in the direction of their movement-indicative of active cell migration (Srinivas *et al*., 2004). AVE cells migrated as a single layer in direct contact with the epiblast.

Figure 2 – Conversion of the proximal-distal axis into the anterior posterior axis in the post-implantation embryo

At about 5.5 dpc the first definitive embryonic axis, the anterior-posterior (A-P) axis begins to form. A group of VE cells at the distal tip become morphologically different from their neighbours and begin to express a distinct of set markers. These cells are referred to as the distal VE (DVE; shown in green). They actively migrate towards the prospective anterior of the egg cylinder (red arrows). It remains unclear how early the first asymmetries are present in the DVE. Once at the anterior, these cells are referred to as the anterior VE (AVE) and they signal to the underlying epiblast to form anterior structures such as forebrain (shown in light blue). The AVE restricts posteriorising signals such as *Nodal* (purple dots and white inhibitory arrows), to the opposite side of the epiblast (black arrow), therefore defining a clear A-P axis. At 6.5 dpc this results in formation of the primitive streak at the posterior of the epiblast (also purple). (Adapted from Beddington and Robertson, 1999).

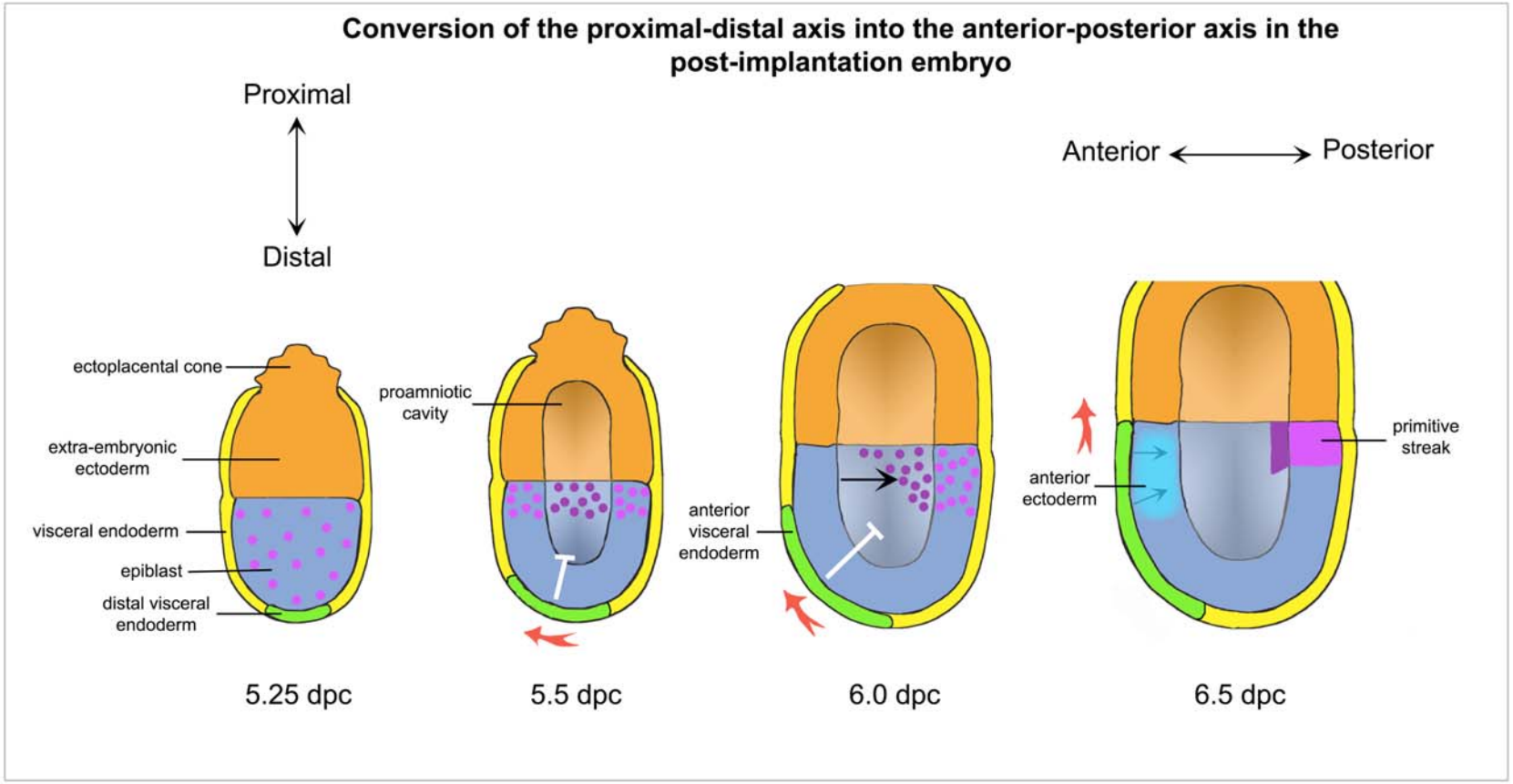
Conversion of the proximal-distal axis into the anterior-posterior axis in the post-implantation embryo
Proximal
Distal
Anterior
Posterior
ectoplacental cone
extra-embryonic ectoderm
visceral endoderm
epiblast
distal visceral endoderm
proamniotic cavity
anterior visceral endoderm
anterior ectoderm
primitive streak
5.25 dpc
5.5 dpc
6.0 dpc
6.5 dpc

When the leading cells reached the junction between the epiblast and the ExE, migration halted, and cells began spreading laterally (Srinivas *et al*., 2004). The inability of AVE cells to pass beyond this juncture is corroborated in other studies looking at cell movements within the VE (Lawson and Pederson, 1987; Thomas *et al*., 1998; Rivera-Perez *et al*., 2003), although the mechanism for migratory arrest is currently unknown.

Nevertheless, the migratory behaviour of the DVE was supported by the analysis of *Nap1* mutants (Rakeman and Anderson, 2006). *Nap1* is a regulator of WAVE-mediated actin branching, and therefore important in the process of polarised cell movements. In *Nap1* null embryos the DVE fails to migrate away from the distal tip and show a rounded, non-polarised morphology, highlighting the importance of dynamic intracellular rearrangements during migration (Rakeman and Anderson, 2006).

Interestingly, between 5.5-6.0 dpc the embryo is transformed from a radially symmetrical egg cylinder, to one that is bilaterally symmetrical (possessing a long and short axis in the transverse plane). The A-P axis is first aligned with the short axis as the DVE begins to migrate (Mesnard *et al*., 2004; Perea-Gomez *et al*., 2004). However, at the onset of gastrulation the A-P axis has shifted to the long axis (Mesnard *et al*., 2004; Perea-Gomez *et al*., 2004). Both groups agree that this apparent shift in A-P axis orientation is associated with tissue remodelling of the epiblast, rather than altering gene expression patterns or cell migration, such that the initial transverse ellipse forms a circle, then reforms another ellipse perpendicular to

the first (Mesnard *et al.*, 2004; Perea-Gomez *et al.*, 2004). Following this logic, the DVE migrates initially from the distal tip along the short axis of the embryo.

The process of DVE cells located at the distal tip reaching the epiblast-ExE boundary takes between 4-5 hours, as determined by time-lapse analysis (Srinivas *et al.*, 2004). This anteriorwards movement of *Hex*GFP-expressing cells is reflected in the expression of other AVE markers such as *Cerberus-like* (*Cerl*) (and *Cerl*GFP), *Lim1* (Belo *et al.*, 1997; Mesnard *et al.*, 2004), *Frizzled-8* (*Fz8*) (Lu *et al.*, 2004a) and *left-right determination factor 1* (*Lefty1*) (and *Lefty-LacZ*) (Meno *et al.*, 1999; Perea-Gomez *et al.*, 1999; Takaoka *et al.*, 2006). However, it should be noted that the AVE and its precursors are heterogeneous tissues comprising multiple subpopulations of cells (Srinivas *et al.*, 2004; Yamamoto *et al.*, 2004; Takaoka *et al.*, 2006). The significance of variegated gene expression within the AVE on its function is only beginning to be understood. Two examples will be discussed below; both relating to the fundamental question of what determines the direction of the DVE.

The migration of the DVE defines the orientation of the A-P axis, but the mechanism(s) responsible for this movement are currently a source of active investigation. Two possibilities exist: either DVE movements are stochastic, with the DVE traversing randomly up one side of the egg cylinder, or the direction of DVE movements are molecularly pre-determined. A growing body of evidence suggests the latter scenario is likely. Molecular asymmetries prior to DVE movements have been discussed in an earlier section, but two examples are particularly pertinent to DVE directional determination.

Kimura-Yoshida and colleagues proposed that Wnt/β-catenin signalling mediates DVE movements by guiding cell migration towards the prospective anterior of the embryo (Kimura-Yoshida *et al*., 2005). Specifically, the Wnt antagonist Dkk1 can act as a guidance cue, whilst canonical Wnt can act as a repulsive cue to DVE migration (Kimura-Yoshida *et al*., 2005). *In vivo,* prior to migration, *Dkk1* is initially detected in the proximal portion of the VE. As the DVE tilts, *Dkk1* expression is shifted to the future anterior side and is absent from the posterior side, forming a crescent over the leading front of *Cerl*-positive migratory cells (Kimura-Yoshida *et al*., 2005). Moreover, *Otx2* null embryos form a functional DVE that is unable to move (Kimura *et al*., 2000). Notably *Dkk1* expression is absent from all mutant embryos, suggesting that *Otx2* is essential for *Dkk1* induction, and its induction might play an important role in affecting DVE movement (Kimura-Yoshida *et al*., 2005).

Indeed, the migration defects caused by *Otx2* deficiency could be rescued by knocking-in *Dkk1* into the *Otx2* locus, strongly suggesting that *Dkk1* was necessary in this process (Kimura-Yoshida *et al*., 2005). Furthermore, partial rescue of migratory behaviour in *Otx2* mutants could be elicited by reducing the level of β-catenin in the embryo, implicating the Wnt/β-catenin pathway in establishing A-P polarity (Kimura-Yoshida *et al*., 2005). In support of this possibility Kimura-Yoshida and colleagues demonstrated that misexpression of the canonical Wnt ligand, *Wnt8,* perturbed cell movement; whilst in an *in vitro* situation, beads soaked in Dkk1 or Wnt3a could act as attractive and repulsive guidance cues respectively, controlling directional migration of VE cells (Kimura-Yoshida *et al*., 2005). Taken together this paper provides compelling evidence that DVE movements are directed along a Wnt/β-catenin signalling gradient, towards a region where Wnt is antagonised and levels of activated β-catenin are low. This movement is reinforced by the repulsive effect of Wnt ligands

expressed in the prospective posterior of the VE (Kimura-Yoshida *et al*., 2005; Rivera-Perez and Magnuson, 2005). It should be noted that *Dkk1* null embryos are able to undergo normal A-P axis formation at an early stage (Mukhopadhyay *et al*., 2001). Although other Wnt antagonists and negative regulators of the Wnt/β-catenin signalling pathway are expressed in the anterior VE at the right time including *Cerl*, *Sfrp5* and *Axin*, all of which might functionally compensate for the absence of *Dkk1* in correctly forming the A-P axis (Logan and Nusse, 2004; reviewed in Pfister *et al*., 2007).

Another putative mechanism for directing DVE migration was put forward by Yamamoto and colleagues who proposed that differential proliferation within the VE was responsible for directing DVE movements (Yamamoto *et al*., 2004). This group observed that the Nodal antagonists *Cerl* and *Lefty1* were shifted to one side of the embryo before the onset of DVE migration (Yamamoto *et al*., 2004); a finding that they later corroborated (Takaoka *et al*., 2006). It was presumed that the shift corresponded to the prospective anterior of the embryo, resulting in localised antagonism of Nodal along the A-P axis of the VE, with lower levels on the anterior.

To test if Nodal antagonism could direct DVE movements, *Nodal* and *Cerl* and/or *Lefty1* were ectopically expressed in the embryo just prior to the DVE tilt (Yamamoto *et al*., 2004). The DVE tended to migrate away from the side with higher Nodal activity, and towards the region of low Nodal activity elicited by the co-injection of *Cerl* and *Lefty1*, indicating that the level of Nodal did influence DVE directionality (Yamamoto *et al*., 2004). This was consistent with previous findings that Nodal activity has a crucial role in promoting cell movements that position the A-P axis (Norris *et* al., 2002; Ding *et al*., 1998). Additionally, an absence of cell

proliferation in the VE was shown to correspond to the region of VE co-expressing *Cerl* and *Lefty1*, as demonstrated by a failure to incorporate Bromodeoxyuridine (BrdU) (Yamamoto *et al.*, 2004). The implication that Nodal itself was responsible for promoting cell division was demonstrated by injecting VE cells with a *Nodal* vector and showing that the replicative capacity of these VE cells was increased compared to non-treated control embryos. Conversely, a decrease in the replicative capacity of VE cells was observed when embryos were co-injected with *Cerl* and *Lefty1* effector genes (Yamamoto *et al*., 2004). Furthermore, DVE cells tended to move away from areas of high proliferation, as induced by *Cdk2*, whilst dominant negative *Cdk2* was unable to affect DVE directionality (Yamamoto *et al*., 2004).

In summary, Yamamoto *et al*., (2004) proposed that the driving force of DVE movement was due to Nodal stimulating the proliferation of VE cells, whilst directionality was determined by the asymmetric antagonism of Nodal by Cerl and Lefty1 on the future anterior side. How this passive model mechanism incorporates the migratory cell movements of the DVE is not clear, and has formed the basis of one of my PhD projects. It is possible that both active and passive movements of the DVE both contribute, thus enabling a reconciliatory model to be constructed (Srinivas, 2006). Alternatively, other mechanisms might be involved that are yet to be described. Only careful analysis of cell movements and gene expression patterns will resolve this fascinating and essential biological phenomenon.

1.2.2.7. Roles of the AVE

The function of the AVE has been inferred by using a combination of microsurgical ablation experiments, explant experiments and by analysing the phenotype of embryos carrying mutations in genes expressed in the AVE. These approaches have

given invaluable insights into the role of the AVE, yet assigning exact function(s) remains controversial. The following section will summarise what is currently known about AVE function and how this fits with the contemporary model of A-P axis establishment.

1.2.2.8. The AVE determines the site of primitive streak formation

The unilateral movement of AVE cells is mirrored by a shift in the expression of genes from the embryonic-extraembryonic boundary towards the prospective posterior of the epiblast. These events effectively convert the proximal-distal (P-D) axis of the pregastrula embryo into that of the A-P axis (reviewed in Beddington and Robertson, 1999; Rossant and Tam, 2004) (Fig. 2). The DVE (AVE precursors) expresses a number of secreted antagonists that can act upon the underlying epiblast, prior to their movement. *Cerl* and *Lefty1* both inhibit Nodal signalling, and are responsible for restricting its expression firstly to the proximal epiblast, then as the AVE moves anteriorly, to the posterior side (Norris and Robertson, 1999; Perea-Gomez *et al*., 2001a; Perea-Gomez *et al.*, 2002). Likewise, the WNT antagonists *Dkk1*, *Sfrp1* (Kemp *et al.*, 2005) and *Sfrp5* (Finley *et al*., 2003) are expressed in the AVE and might act to suppress WNT signalling in the anterior epiblast (reviewed in Tam and Loebel, 2007). The pattern of Nodal mRNA restriction to the proximal then posterior epiblast is replicated by the expression of its co-receptor *Cripto* (Ding *et al*., 1998) and *Wnt3* (Liu *et al*., 1999), whilst *Brachyury,* which is initially expressed throughout the distal ExE becomes posteriorly restricted during AVE movements (Perea-Gomez *et al.*, 2004; Rivera-Perez and Magnuson, 2005). Thus a radially symmetrical pattern of gene expression in a P-D orientation is rotated into an A-P axis, perpendicular to that of the original P-D axis (Thomas *et al.,* 1998). The anterior

side of the epiblast cup will give rise to anterior structures, whilst the posterior side will form the primitive streak in which epiblast cells undergo an epithelial to mesenchymal transition (EMT) before delaminating and migrating through the primitive streak (Fig. 2). The process of gastrulation will be discussed in more detail later.

A role for the AVE can be inferred by analysing mouse mutants that form a functional AVE, but which fail to move anteriorwards. Two such examples are *Cripto* (Ding *et al*., 1998) and *Otx2* (Acampora *et al*., 1998; Rhinn *et al*., 1998; Kimura *et al*., 2000) mutants in which the primitive streak is ectopically formed in the proximal epiblast. These observations led to the logical conclusion that the AVE was responsible for positioning the site of primitive streak formation (Kimura *et al*., 2000; Perea-Gomez *et al*., 2001a; reviewed in Perea-Gomez *et al*., 2001b).

It is not clear exactly how the primitive streak is initiated, although genetic analysis in mouse has indicated the essential requirements of Wnt, Nodal and BMP signalling pathways. Embryos lacking *Wnt3* (Liu *et al*., 1999) or its co-receptor proteins Lrp5 and Lrp6 (Kelly *et al*., 2004) fail to initiate *Brachyury* (and *Nodal* in the case of Wnt3 mutants) or form a primitive streak. Furthermore, *Brachyury* is a direct transcriptional target gene of the Wnt signalling pathway (Arnold *et al*., 2000; Yamaguchi *et al*., 1999). Mutant embryos lacking *Nodal* also fail to correctly form a primitive streak and fail to express *Wnt3* (Conlon *et al*., 1994; Brennan *et al*., 2001). BMP4 is required for the formation of the node and primitive streak morphogenesis (Fujiwara *et al*., 2002; Winnier *et al*., 1995). In sum a complex interplay between these signalling pathways is required to initiate the primitive streak and restrict its formation to the posterior (Constam and Robertson, 2000; reviewed in Perea-Gomez

et al., 2001b). Failure of the AVE to move results in ectopic initiation of primitive streak gene expression in the proximal epiblast, as the secreted antagonists within the AVE fail to act in an A-P orientation. This is best exemplified in *Cerl*$^{-/-}$*;Lefty1*$^{-/-}$ compound mutants in which inappropriate posterior restriction of *Nodal* results in ectopic primitive streak formation (Perea-Gomez *et al*., 2002).

The widely accepted idea that the P-D axis is converted into the A-P axis has recently been challenged in light of evidence suggesting that molecular asymmetries relating to the A-P axis are already present before AVE movements. Specifically, Rivera-Perez and Magnuson (2005) reported that *Wnt3* is expressed in the prospective posterior VE at 5.5 dpc before the DVE has moved (Rivera-Perez and Magnuson, 2005). The implication is that formation of the primitive streak does not depend on the regionalisation of gene expression from proximal epiblast cells, but that the epiblast has already pre-determined the site of the primitive streak. However, studies thus far have failed to corroborate or repudiate such a notion.

1.2.2.9. Role of AVE in forebrain development

Heterotopic transplantation of the mouse node from gastrulating embryos was shown to induce a secondary neural axis in the host, although midbrain and forebrain regions failed to develop (Beddington, 1994; Tam and Steiner, 1999). This suggested that unlike amphibians and chick, the node alone was not the sole organiser but required an additional signalling contribution to form a complete A-P axis. Embryological and genetic analysis has since revealed the AVE to be required for anterior patterning (reviewed in Beddington and Robertson, 1998 and 1999; Martinez-Barbera and Beddington, 2001). Microsurgical ablation of the AVE at the onset of gastrulation

reduces or abolishes the forebrain marker *Hesx1* in the underlying anterior neural ectoderm (Thomas and Beddington, 1996). The role for the AVE in anterior patterning was strengthened by the fact that many of the genes expressed in the node and its derivatives were also expressed in the AVE; these include *Hex* (Thomas *et al*., 1998), *HNF3β* (Ang and Rossant, 1994), *Lim1* (Shawlot and Behringer, 1995), *Cerl* (Belo *et al*., 1997) and *Otx2* (Ang and Rossant, 1994; Acampora *et al*., 1995).

Not surprisingly in light of the AVE ablation experiment, mutants homozygous for many of these genes result in severe forebrain defects. Loss of *Lim1* (Shawlot and Behringer, 1995), *HNF3β* (Ang and Rossant, 1994) and *Otx2* (Ang and Rossant, 1994; Acampora *et al*., 1995) causes anterior truncations. Chimeric embryos possessing different embryonic and extraembryonic genotypes were used to show a requirement for these genes in the AVE (Beddington and Robertson, 1989; reviewed in Martinez-Barbera and Beddington, 2001).

Using *Lim1* as an example, when wildtype ES cells were injected into $Lim1^{-/-}$ blastocysts, the extraembryonic tissues of the resulting chimeras were almost exclusively of the genotype $Lim1^{-/-}$. These embryos were phenotypically indistinguishable from $Lim1^{-/-}$ embryos which lack rostral brain structures, suggesting that *Lim1* was required in extraembryonic tissues for normal forebrain formation (Shawlot *et al*., 1999). When the converse experiment was performed and $Lim1^{-/-}$ ES cells were injected into wildtype blastocysts, mutant cells contributed to the entire embryo proper, and constrictions observed between the embryonic and extraembryonic regions in $Lim1^{-/-}$ mutants at 7.5 dpc were rescued (Shawlot *et al*., 1999). This rescue was presumably a consequence of the chimera possessing largely wildtype extraembryonic tissues, thus strengthening the requirements of *Lim1* in the VE for correct head formation.

The sufficiency of wildtype extraembryonic tissue rescuing chimeras in which the embryo proper is predominantly mutant was phenocopied in *nodal*, *Otx2*, and *HNF3β* chimeras (Varlet *et al*., 1997; Rhinn *et al*., 1998; Acampora *et al*., 1998; Dufort *et al*., 1998). Therefore in combination with the AVE ablation experiment and this genetic evidence, the general consensus is that visceral endoderm is required in normal forebrain and midbrain development.

This is only part of the story; whilst it is true that AVE is required to establish anterior character in the underlying ectoderm, this signalling centre alone is insufficient to initiate rostral patterning. Firstly, grafts of mouse AVE fail to induce neural character in non-neural ectoderm (Tam and Steiner, 1999), but do suppress posterior markers (Kimura *et al*., 2000). A complete ectopic axis requires a combination of a posterior epiblast fragment (or early gastrula organiser (EGO)), AVE and anterior epiblast, suggesting that a combinatorial mode of action between these germ layers is necessary (Tam and Steiner, 1999), in addition to preventing posteriorising signals (Kimura *et al*., 2000). Furthermore, as previously discussed, chimeras with a mutant embryonic but wildtype extraembryonic tissues are able to induce normal anterior development (reviewed in Beddington and Robertson, 1999). However, anterior neural structures degenerate at later stages suggesting that after induction additional signals are required to maintain and/or embellish neural development.

Are the roles of the AVE and node and its derivatives interdependent or functionally separable? It is true that both structures co-express a number of the same genes, and that axial mesendoderm (comprising the anterior definitive endoderm (ADE), prechordal and notochordal plates) displaces the AVE at 7.0 dpc, and so is apposed to

the same portion of anterior epiblast previously subjected to the AVE (Thomas and Beddington, 1996) (Fig. 3A). There are examples of genes that are expendable in the AVE, but are absolutely required in the derivatives of the node. Both *Hex* and *Hesx1* are expressed in the AVE, and then later in the ADE and AME respectively (Thomas *et al*., 1998; Hermesz *et al*., 1996; Thomas and Beddington, 1996). When either gene is knocked out, patterning of the AVE is normal as assessed by marker analysis, although at later stages embryos develop variable forebrain truncations (Martinez-Barbera *et al*., 2000a; Martinez-Barbera *et al*., 2000b; Dattani *et al*., 1998). Chimeric analysis has indicated that both genes are required in epiblast-derived tissues for normal forebrain development; ADE in the case of *Hex*, and anterior neurectoderm (ANE) in the case of *Hesx1* (Martinez-Barbera *et al*., 2000a; Martinez-Barbera *et al*., 2000b). This provides solid evidence that it is tissues derived from the epiblast that are important in the maintenance of anterior neural character. The fact that these genes are not required in the AVE might reflect redundancy within this tissue.

To summarise, this wealth of embryological and genetic data has led to the construction of a model for forebrain development. The model comprises a sequence of inductive steps starting with the initiation of neural patterning from the AVE and EGO on the underlying ectoderm. This is shortly followed by signalling from the AME which passes through the node and displaces the AVE, resulting in maintenance and embellishment of neural patterning (reviewed in Beddington and Robertson, 1998 and 1999; Martinez-Barbera and Beddington, 2001).

1.2.3. Gastrulation

Gastrulation is a defining point in the post-implantation embryo in which the three definitive germ layers are established. At about 6.5 dpc the primitive streak forms at the posterior of the epiblast. The primitive streak is the morphological landmark of the site of gastrulation. It is here that cells of the epiblast delaminate from their epithelial sheet and move towards the posterior, through the streak, and emerge having taken on either an endodermal or mesodermal fate. Those cells that do not ingress through the streak are fated to become the ectoderm (reviewed in Tam and Behringer, 1997; Tam and Loebel, 2007) (Fig. 3A). The proceeding sections will outline the signalling pathways involved in the formation of the primitive streak, and also how these signals are integrated to produce the necessary tissue movements and lineage choices that encompass gastrulation.

1.2.3.1. Formation of the Primitive Streak

The onset of gastrulation is marked by the formation of the primitive streak. As previously discussed, the correct site of primitive streak formation depends on the correct establishment of the A-P axis, where the AVE has an integral role by antagonising the activity of Nodal. Nodal has multiple roles in primitive streak formation, both directly and more indirectly in feedback loops (reviewed in Tam and Loebel, 1997). For example, Nodal precursor protein in the proximal epiblast is required to maintain *Bmp4* expression in the ExE, which in turn is necessary to induce expression of primitive streak markers and activate the transcription of Nodal convertases, which perpetuate its activity (Winnier *et al.*, 1995; Mishina *et al.*, 1995; Beppu *et al.*, 2000; Ben-Haim *et al.*, 2006). Uncleaved Nodal also activates *Fgf8* and

Wnt3, which indirectly maintains Nodal expression in the epiblast (Brennan *et al*., 2001; Ben-Haim *et al*., 2006) and positions the site of primitive streak formation via β-catenin and the Wnt co-receptors Lrp5/6 (Liu *et al*., 1999; Huelsken *et al*., 2000; Kelly *et al*., 2004; Mohamed *et al*., 2004).

However, the epiblast must also reach a certain number of cells for gastrulation to take place, confirmed by ultrastructural analysis and the study of proliferation rates and its perturbation in pregastrulae embryos (reviewed in Tam *et al*., 1993; Tam and Behringer, 1997). Snow calculated a 4.5- to 5-fold increase in epiblast population between 5.5 and 6.5 dpc, which increased by 12-fold between 6.5 and 7.5 dpc (Snow, 1977). This dramatic growth in epiblast number is required to sustain the recruitment of ectoderm cells through the primitive streak. Mouse embryos can compensate for an earlier loss of cells, showing the highly regulative nature of the embryo. This was demonstrated by removing 1 cell from a 4-cell embryo and showing that a complete restoration of body size was possible by compensatory growth at gastrulation (Power and Tam, 1993; reviewed in Tam and Behringer, 1997). What factors are responsible for eliciting proliferation of the epiblast? Nodal is a growth factor that can promote cell proliferation (Yamamoto *et al*., 2004; Mesnard *et al*., 2006), so presumably another role for this important molecule is to enable the epiblast to reach a critical threshold of cells prior to gastrulation. Whether other growth factors that are present contribute to proliferation in the epiblast is not clear; nevertheless the epiblast requires approximately 660 cells for gastrulation to commence (Snow, 1977).

1.2.3.2. Cell movement through the primitive streak

The primitive streak marks the site where epithelial cells of the epiblast delaminate from their epithelium, undergo an epithelial to mesenchymal transition (EMT) and emerge as mesoderm or endoderm. EMT describes the process by which an epithelial layer, such as the epiblast, loses integrity via changes in cell shape and adhesion (reviewed in Shook and Keller, 2003). As cells move through the primitive streak they must disassemble their basement membrane and change shape, thus facilitating morphogenesis of the tissue and ultimately ingression through the streak (Tam *et al*., 1993).

As gastrulation progresses, the primitive streak lengthens and eventually reaches the distal tip of the egg cylinder. Epiblast cells ingress through the primitive streak when it has extended into their vicinity, establishing a sequential recruitment of epiblast cells dependent upon their distance from the primitive streak. Accordingly, epiblast cell fates have been mapped onto the pre-gastrula stage egg cylinder by lineage tracing studies, thereby determining the temporal and morphological sequence of gastrulation (Lawson *et al*., 1991; Tam and Behringer, 1997).

It appears that clonal descendants of single cells passing through the streak often intermingle, suggesting that mesodermal and endodermal derivatives do not comprise distinct epiblast cell clones (Lawson *et al*., 1991; Tam and Behringer, 1997). The mesoderm emerges as a new layer between the epiblast and the overlying VE, which moves around the egg cylinder as lateral 'wings' (Tam *et al*., 1993). Gastrulating cells that emerge from the node intercalate into the surrounding VE and form the definitive endoderm, displacing the AVE and ultimately giving rise to the gut, and organs including the liver and pancreas (Tam *et al*., 2007) (Fig. 3A). The

ectoderm forms from those anterior and distal epiblast cells that do not ingress through the streak (Lawson *et al*., 1991).

The migration of mesodermal cells is dependent on FGF signalling, and the absence of either *Fgf8* or its receptor *Fgfr1* (fibroblast growth factor receptor 1) result in problems in cell movement through the primitive streak (Sun *et al*., 1999; Ciruna and Rossant, 2001). In embryos lacking FGF-8, epiblast cells undergo an EMT and move to the streak, but are then retained, resulting in the absence of any mesoderm- or endoderm-derived tissues (Sun *et al*., 1999). When the *Fgfr1* receptor is knocked-out, epiblast cells are unable to undergo EMT, most likely a result of the inability to upregulate *Snail1* (Snail homologue 1) and therefore downregulate E-cadherin (Ciruna and Rossant, 2001). Furthermore, mesoderm cell fate specification is hindered, as shown by the downregulation of *Brachyury* and *Tbx6* (Ciruna and Rossant, 2001). *Brachyury* is necessary for correct mesoderm migration (Wilson *et al*., 1995) and is also a direct target of *Wnt3a* (Yamaguchi *et al*., 1999). Therefore FGF and Wnt signalling are intimately linked at the primitive streak, involved in both morphogenetic cell movement and cell fate specification.

Figure 3 – Formation of the primitive streak and gastrulation

A. *Primitive streak formation.* By 7.0 dpc, extraembryonic mesoderm (red) emanates from the posterior portion of the primitive streak. Cells from the embryonic ectoderm ingress through the anterior primitive streak and form the organiser (node, purple). These cells give rise to axial mesendoderm (brown) which move anteriorly (red arrow) and displace the AVE (green). Axial mesendoderm and its derivatives will give rise to dorsal mesoderm and gut endoderm.

B. *Lineage allocation during gastrulation. Brachyury* transcript (dark blue) marks the entire primitive streak in a 7.5 dpc embryo. Epiblast cells delaminate from the epithelium and ingress through the primitive streak. This process results in the formation of the embryonic germ layers. Cells that move through the streak emerge as either definitive endoderm or various mesodermal derivatives depending upon their location within the primitive streak (red, node/some axial mesendoderm; orange, paraxial mesoderm; green, lateral plate mesoderm; yellow, extraembryonic mesoderm). Cells that do not ingress through the streak will become embryonic ectoderm (blue) (adapted from Tam and Loebel, 2007).

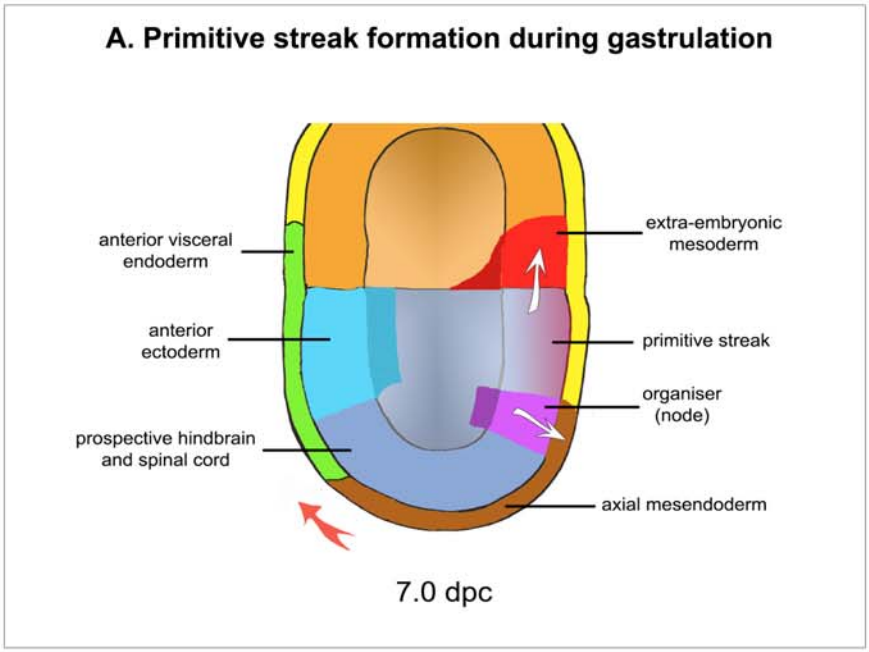
A. Primitive streak formation during gastrulation
anterior visceral endoderm
anterior ectoderm
prospective hindbrain and spinal cord
extra-embryonic mesoderm
primitive streak
organiser (node)
axial mesendoderm
7.0 dpc

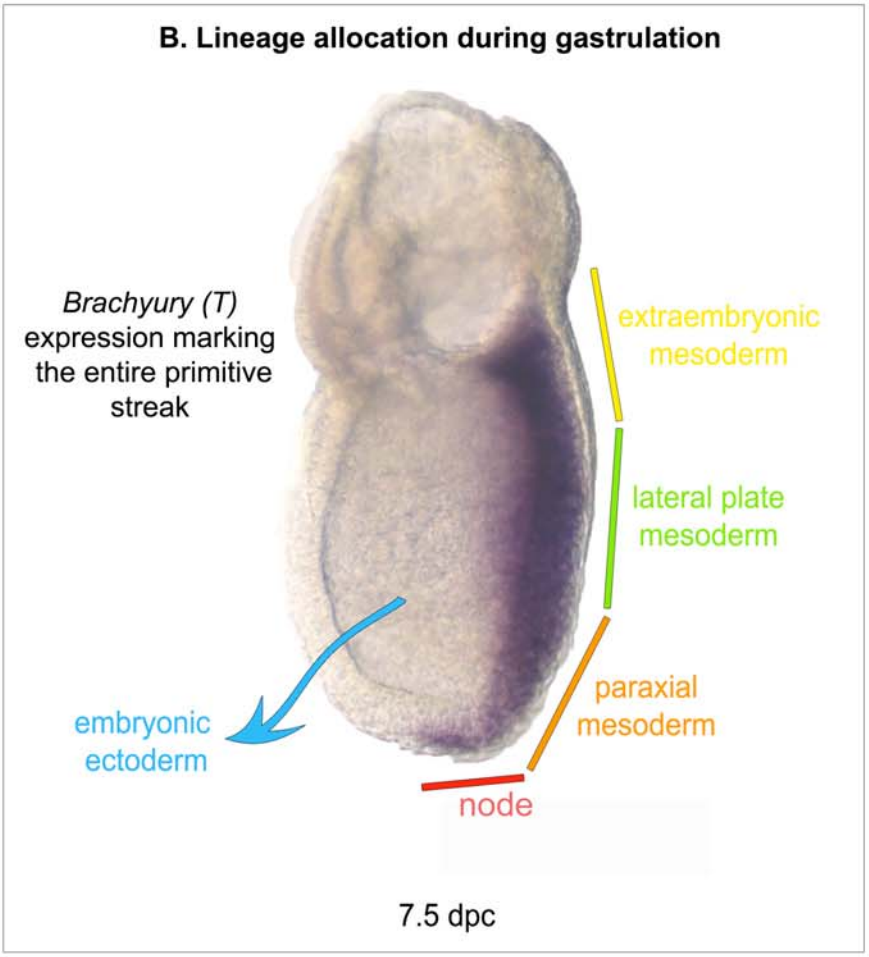
B. Lineage allocation during gastrulation
Brachyury (T) expression marking the entire primitive streak
extraembryonic mesoderm
lateral plate mesoderm
paraxial mesoderm
node
embryonic ectoderm
7.5 dpc

1.2.3.3. Signals regulating lineage choice during gastrulation

Fate map studies of the primitive streak have revealed that different regions of the streak display different mesodermal and endodermal fates (Tam and Beddington, 1987; Lawson *et al.*, 1991). The primitive streak can be divided into individual but overlapping regions depending on the contribution of labelled cells to a particular tissue-type (Fig. 3B). For example, the node region of the late gastrula will give rise to axial mesoderm and definitive endoderm, the anterior-third of the primitive streak will give rise to the paraxial mesoderm, the middle-third lateral plate mesoderm and the posterior-third will form extraembryonic mesoderm. Cells that remain in the epiblast are allocated to the ectoderm (reviewed in Tam and Behringer, 1997; Tam and Loebel, 2007). It is becoming increasingly clear that the allocation of these different lineages depend upon varying combinations of TGFβ signalling molecules Nodal and BMP, as well as FGF and Wnt signalling (Tam and Loebel, 2007).

Genetic studies have shown a loss of Nodal signalling results in the abolition of anterior primitive streak-derived tissue including axial and paraxial mesoderm and definitive endoderm (Beck *et al.*, 2002; Hoodless *et al.*, 2001; Episkopou *et al.*, 2001). Conversely, loss of *Bmp4* results in the loss of posterior primitive streak derivatives such as extraembryonic mesoderm (Winnier *et al.*, 1995). Paraxial mesoderm, derived from anterior and middle primitive streak, is not formed when *Fgfr1* is absent (Deng *et al.*, 1994; Yamaguchi *et al.*, 1994) or when *Wnt3a* is deleted (Yoshikawa *et al.*, 1997) implicating both FGF and Wnt signalling in the formation of the paraxial mesoderm lineage. Therefore, a model can be proposed whereby BMP and Nodal signalling are required in the posterior and anterior primitive streak respectively, with middle-streak derivatives requiring a combination of FGF and Wnt signalling (reviewed in Tam and Behringer, 1997; Tam and Loebel, 2007).

To conclude, gastrulation is a complex process involving the integration of signalling pathways and morphogenetic movements. Many aspects remain elusive. A recent paper proposed that the *Argonaute2* protein was essential for proper mesoderm formation in mouse by modulating FGF signalling (Alisch *et al.*, 2007). Argonaute2 is involved in the process of RNA interference (RNAi), opening up the possibility that this method of post-transcriptional gene regulation is implicit during gastrulation. What we know is continually being built upon; the process becoming both better understood and evermore intriguing. It is this resolution of this dichotomy that continues to drive research forward.

1.3. This investigation

It is clear that the AVE is inexorably linked to A-P axis establishment, although its exact functions are poorly defined. This PhD has focused on two aspects of AVE function; firstly, what role does cell proliferation have in defining its movements, and secondly, is this signalling centre responsible for other undefined events in the embryo?

The movement of the AVE not only defines the anterior side of the embryo, but is also essential in positioning the site of primitive streak formation. What is not well understood are the mechanisms responsible for its appropriate localisation. As discussed, hypotheses have been proposed tending towards active or passive cell movements. Evidence of differential proliferation and its involvement in AVE movements was published in 2004 (Yamamoto *et al*, 2004). This project has investigated this possibility by analysing patterns of cell proliferation during AVE

movements in detail using a combination of high resolution imaging and culturing techniques.

Functions of the AVE have been ascribed using embryological micromanipulation and genetic mutation techniques. To address the function of the AVE as a whole and *in vivo*, the AVE has been genetically ablated. This was achieved by targeting Diphtheria toxin A (DTA) into the *Hex* locus by homologous recombination. DTA is placed under the control of the endogenous *Hex* regulatory sequence and is inducible using the Cre-*loxP* recombinase system. This project describes the making of this mouse line and the subsequent characterisation of embryos in which, depending on the timing of genetic ablation, have provided further insights into the function of the DVE and AVE.

Chapter 2 - Materials and Methods

Note all chemicals were obtained from Sigma-Aldrich UK unless otherwise stated.

2.1. Mice and procedures

2.1.1. Mouse strains

All mice used in this investigation were maintained in the Biological Services Unit, Clinical Sciences Centre, Imperial College, UK. All transgenic strains were purchased from Harlan Olac, UK. All transgenic strains were produced by the Transgenic Facility, Clinical Sciences Centre, Imperial College, UK. Hexd32 mice were derived by ES cell injection into C57BL/6 blastocysts. This was carried out in house by the CSC Transgenic facility. These mice were studied on either a mixed 129sv, C57BL/6 or CD1, C57BL/6 background. All mice were maintained and treated under the Home Office's animals (scientific procedures) Act 1986.

2.1.2. Transgenic lines

In total six transgenic mouse lines were used during this investigation. The Hexd32 line was generated by homologous recombination of a *DTA* cassette into the endogenous *Hex* locus. The ATG start codon of *DTA* was separated from its open reading frame (ORF) by an intervening *Neomycin*-resistant cassette flanked by *Lox*P sites (Neo^R-STOP). Cre recombination excised Neo^R-STOP and resulted in the DTA's ORF uniting inframe to its start codon. This event placed *DTA* under the control of the *Hex* regulatory sequences allowing activation of *DTA* in *Hex*-expressing cells.

Two Cre-expressing lines were crossed to the Hexd32 line. The first was β-actin-*Cre* that expresses *Cre* recombinase ubiquitously under the control of the β-actin promoter/CMV enhancer (Lewandoski *et al*., 1997). The second Cre-expressing mouse line was *Sox2Cre* that expresses *Cre* under the upstream regulatory sequence of the *Sox2* gene (Hayashi *et al*., 2002). If the *Sox2Cre* transgene is inherited maternally all of the offspring will carry *Cre* ubiquitously (Hayashi *et al*., 2003, Vincent *et al*., 2003), whilst paternal transmission is restricted to epiblast-derived tissues in progeny possessing the *Cre* transgene (Hayashi *et al*., 2002). Both *Cre* mouse lines were crossed to Hexd32 mice and embryos were characterised throughout development. A small number of embryos resulting from the β-actin-*Cre*;Hexd32 cross escaped genetic ablation, were born and were fertile. These mice carried one activated DTA allele, negating the need for further *Cre* mediated recombination. These mice were named Hexd^{act} and the nature of the genetic ablation in mice harbouring the activated DTA allele was characterised by crossing to either 129sv or CD1 wildtypes, or other Hexd^{act} mice to double the level of activated DTA to test if the efficiency of the ablation system was enhanced. Hexd^{act} mice were also crossed to *Nodal.LacZ* mice in which the endogenous *nodal* minimal promoter drives β-galactosidase expression (Norris and Robertson, 1999).

Throughout the investigation *Hex*GFP mice were used as a way of visualising *Hex*-expressing cells (Rodriguez *et al*., 2001). GFP expression in these mice is driven by *Hex* regulatory elements and embryos carrying the *Hex*GFP transgene were generated by crossing homozygous/heterozygous *Hex*GFP males to CD1 females. Additionally Hexd32:*Hex*GFP studs were generated to give another means to characterise the genetic ablation.

The final transgenic line used to study the efficiency of β-actin-*Cre* recombination was the ROSA26 *Cre* (*R26R*) reporter strain (Soriano, 1999). This line possesses an interrupted *LacZ* cassette in the constitutively expressed *Rosa26* locus. *Cre*-mediated recombination is required for reporter activity, and once expressed all descendents will express *LacZ.*

2.2. Embryology methods

2.2.1. Embryo recovery

Mice were maintained on a 12 hour light, 12 hour dark cycle. Mice were mated and noon of finding a vaginal plug was designated 0.5 days *post coitum* (dpc). Pregnant females were sacrificed at the dpc required for the procedure and the uterus was removed. Embryos were dissected from the uterus in M2 media (see Appendix I). Embryos were then processed according to the appropriate protocol.

2.2.2. Wholemount RNA *in situ* hybridization

2.2.2.1. Fixation

Harvested embryos were immediately fixed in 4% Paraformaldehyde in PBS at 4 °C overnight. The following day they were dehydrated through a Methanol series (25%, 50%, 75% in PBS and 100%) at room temperature (RT), 5 mins for each condition. Embryos were stored at -20 °C until use.

2.2.2.2. Embryo processing

Embryos were rehydrated through a Methanol series (75%, 50%, 25% in PBS) at RT then washed twice in PBT (0.1% Tween-20 in PBS), 5 mins for each condition. Embryos were sorted and placed in 15 mm Netwells with either a 500 μm or 74 μm mesh depending on embryo size. The Netwells were positioned into 12-well plates (VWR, UK). All steps were carried out in this format. Embryos were bleached in 6% Hydrogen peroxide in PBT for 1 hr at RT and washed in PBT three times, 5 mins each. They were placed in 10 μg/ml Proteinase K in PBT and incubated at room temperature for the following times: 5.5 dpc for 1 min, 6.5 dpc for 2.5 mins, 7.5-8.5

dpc for 4 mins and 9.5 dpc 6 mins. Embryos were immediately placed in 2 mg/ml Glycine in PBT for 5 mins followed by two, 5 min washes in PBT. Embryos were then re-fixed in a solution of 4% Paraformaldehyde, 0.2% Gluteraldehyde in PBT at RT for 20 mins. This was followed by two, 5 min washes in PBT.

2.2.2.3. Hybridisation of riboprobe

Embryos were placed in Pre-hyb buffer (50% Formamide, 5x SSC, 50 μg/ml Heparin sulphate and 0.1% Tween-20 in dH_2O) and incubated at 70 °C for 1-2 hrs. Embryos were then placed in pre-warmed hybridisation buffer (1 mg/ml torula RNA and 1 mg/ml Herring sperm DNA in Pre-hyb buffer) containing the denatured riboprobe. Probes were used at a dilution between 1:100 or 1:200 depending on their quality and approximate concentration. Hybridisation was carried out at 70 °C overnight.

2.2.2.4. Incubation with anti-DIG antibody

Next day embryos were placed in Solution I (50% Formamide, 4x SSC pH 4.5, 10% SDS in dH_2O) two times for 30 mins at 70 °C. Following this was a 10 min incubation at 70 °C in 1:1 Solution I: Solution II (500 mM NaCl, 10mM Tris-HCl pH 7.5 and 0.1% Tween-20 in dH_2O). Embryos were then washed twice at RT in Solution II for 5 mins each. Unbound riboprobe was removed by two incubations in 100 μg/ml RNAse A (Roche Diagnostics, Germany) in Solution II for 30 mins each at 37 °C. Embryos were washed once more in Solution II and once in pre-warmed Solution III (50% Formamide, 2x SSC pH 4.5 in dH_2O) for 5 mins at RT. They were then incubated at 65 °C in pre-warmed Solution III twice for 30 mins each. Embryos were washed three times at RT in TBST (137 mM NaCl, 1.34 mM Potassium chloride, 12.5 mM Tris-HCl pH 7.5 and 0.1% Tween-20 in dH_2O). Embryos were blocked at RT in

10% sheep serum in TBST for 1-2.5 hrs. After blocking embryos were incubated with 1:2000 anti-Digioxin FAB antibody (Roche Diagnostics, Germany) in 1% Sheep serum in TBST at 4 °C overnight while rocking. Next day embryos underwent six 1 hr washes at RT in TBST to remove unbound antibody and thus reduce unspecific signal. Embryos were left rocking overnight in TBST at 4 °C.

2.2.2.5. Signal detection

Next day embryos were carefully removed from the Netwells and placed into glass embryo dishes (RA Lamb, UK) containing NTMT (100 Mm NaCl, 100 mM Tris-HCl pH 9.5, 50 mM $MgCl_2$ and 0.1% Tween-20 made up in dH_2O). The embryo dishes had been previously treated with Repelcote (BDH, UK). Embryos were washed three times in NTMT, for 10 mins each at RT. The staining reaction was carried out with 20 μl NBT/BCIP solution (Roche Diagnostics, Germany) in 1 ml NTMT at room temperature in the dark. The reaction was left to proceed until a clean specific staining was achieved. In cases where staining took a long time to appear embryos were washed and left in fresh NTMT, overnight at 4 °C and the NBT/BCIP stain replaced the following day to continue the reaction. This allowed the reaction to proceed more slowly overnight therefore preventing the appearance of background staining.

2.2.3. Wholemount β-galactosidase staining

2.2.3.1. Fixation

After harvesting, embryos were immediately fixed at 4 °C as follows: preimplantation stages were fixed in 0.2% Gluteraldehyde in PBT for 10 mins. Postimplantation stage 6.5 dpc were fixed in 0.2% Gluteraldehyde, 2% Formaldehyde in PBT for 7 mins.

2.2.3.2. Staining

Embryos were then washed three times, 5 mins each at RT in rinse solution, pH 7.3 (21 parts 0.1 M $NaHPO_4$ to 4 parts 0.1 M NaH_2PO_4, 0.1% Sodium deoxycholate, 0.2% Igepal, 5 mM EGTA, 2 mM $MgCl_2$). Embryos were then placed in Stain (5 mM Potassium ferrocyanide, 5 mM Potassium ferricyanide and 1 mg/ml X-gal in the rinse solution). Embryos were incubated in stain at 37 °C in a humid chamber overnight or until an adequate level of staining was achieved.

2.2.4. TUNEL staining

Embryos were fixed, dehydrated, rehydrated and PK-treated using exactly the same procedure as the wholemount *in situ* hybridisation protocol as described previously. Embryos were re-fixed in fresh 4% PFA/0.1% Tween-20 for 20 mins and washed 5 times with PBT (0.1% Tween-20 in PBS), 5 mins. Embryos were plunged into ice-cold Ethanol:Acetic acid (2:1), and incubated at -20°C for 20 mins. Embryos were then washed 5 times in PBT (0.1% Tween-20 in PBS), 5 mins, and transferred in the smallest possible volume into a 1.5 ml Eppendorf tube. Embryos were treated as described in the TUNEL Staining kit (Upstate Cat. No: S7101). Briefly, 100 µl equilibration buffer was added to the embryos for 4 mins, removed and repeated, this time for 1 hr at RT. Equilibration buffer was removed and 100 µl Reaction buffer and TdT enzyme (1:2) added. The embryos were incubated at 37°C overnight. The following day the Reaction mix was aspirated and 100 µl Stop buffer/dH_2O (34:1) was added and incubated for 1 hr. This was repeated 4 times, before washing in PBT (0.1% Tween-20 in PBS), 3 times, 20 mins each. Embryos were then blocked in 10% Sheep serum and signal was detected using NBT/BCIP in exactly the same way as described in the wholemount *in situ* hybridisation protocol. It should be noted that

unlike the majority of the *in situ* cases, signal develops quickly using the TUNEL kit, and often needed stopping before 5 mins.

2.2.5. Antibody staining

2.2.5.1. Wholemount anti-phospho-Histone H3 staining

Freshly dissected 5.5-7.5 dpc *Hex*GFP embryos were fixed in 4% Paraformaldehyde overnight at 4 °C. After fixation they were washed three times for 5 mins each in PBS at RT. Embryos were then incubated in blocking solution (5% Goat serum, 1% Fish skin gelatin, 0.5% Triton X-100 in PBS) for 1 hr, then transferred to primary antibody solution [rabbit anti-phospho-Histone H3 (Ser28) (Upstate Cat No. 07-145) diluted 1:500 in blocking solution] and incubated at 4 °C overnight. The following morning embryos were washed three times in blocking solution and incubated in secondary antibody solution [Alexa Fluor 568 goat anti-rabbit IgG (Molecular Probes Cat No. A-11036) diluted 1:250 in secondary block (1% Fish skin gelatin, 0.5% Triton X-100 in PBS)] for 4 hrs at RT. Embryos were rinsed three times in PBT and once in PBS for 5 mins and counterstained with DAPI-Vectashield mounting medium (4', 6-diamidino-2-phenylindole dihydrochloride) for 20 mins.

2.2.5.2. Wholemount GFP and BrdU staining – Embryo culture protocol I

This protocol has been modified from the Whole mount BrdU staining protocol as found on the Rossant web page (www.sickkids.ca/rossant/protocols). BrdU was prepared as a stock concentration of 10 mg/ml in PBS. Aliquots were kept at -20 °C and diluted to a final concentration of 20 μM in 1:1 DMEM: rat serum. Culture medium containing BrdU was pipetted into 80 μl drops in 10 cm culture dishes (VWR, UK). Drops were covered in mineral oil and equilibrated at 37 °C, 5% CO_2

for 2-3 hrs. Freshly dissected 5.5-6.25 dpc *Hex*GFP embryos were placed into the drops and cultured for 1 hr. Control embryos underwent culture in medium in which BrdU had been omitted. Following culture embryos were transferred to a 4-well dish and washed three times in PBS for 5 mins and fixed in 4% Paraformaldehyde overnight at 4 °C. Typically embryos in a 4-well dish were placed in a volume of 400 μl solution. This format was maintained throughout all culture protocols.

After fixation embryos were washed three times, 5 mins each with 0.1% PBS Triton X-100 at RT. Embryos were blocked in 10% heat-inactivated Sheep serum (inactivated at 56 °C for 20 mins then aliquoted and stored at -20 °C) in 0.1% PBS Triton X-100 for 20 mins at RT with constant rocking. Blocking solution was removed and replaced with the first primary antibody solution [Rabbit anti-GFP (Molecular Probes, Cat No.A11122) diluted 1:1000 in blocking solution] thus amplifying the GFP signal which would otherwise be abolished in the harsh conditions later in the protcol. The embryos were incubated for 5 hrs at RT with constant rocking. The primary antibody solution was then removed and embryos were washed three times for 5 mins in 0.1% Triton X-100, followed by one more wash for 1 hr at RT. Embryos were incubated in secondary antibody [Alexa Fluor 488 goat anti-rabbit IgG (Molecular Probes, Cat No.A11008) diluted 1:500 in blocking solution] for 2 hrs at RT with rocking. Embryos were washed three times for 5 mins in 0.1% Triton X-100, followed by one more wash for 1 hr at RT.

After removing non-bound secondary antibody embryos were post-fixed in 4% Paraformaldehyde for 10 mins at RT, then washed three times in 0.1% Triton X-100, 5 mins each. For the BrdU to be detected its antigenic sites must be accessible to the antibody. To achieve this DNA must be denatured. Embryos were placed in 2M HCl for 30 mins at 37 °C. Following DNA denaturation the HCl was neutralized by

washing the embryos three times, 5 mins each at RT in Borate buffer (6.18 g Boric acid in 1 L dH_2O, pH 8.5) with constant rocking. Embryos were then incubated with the second primary antibody solution [rat anti-BrdU (Oxford Biotech, Cat No. OBT0030S) diluted 1:100 in blocking solution] overnight at RT with constant rocking. The following day embryos were washed three times for 5 mins in 0.1% Triton X-100, followed by one more wash for 1 hr at RT. Incubation with the second secondary solution followed [Alexa Fluor Cy3 Goat anti-rat IgG (Abcam, Cat No.ab6953) diluted 1:500 with blocking solution] for 2 hrs at RT with rocking. Embryos were washed three times, 5 min at RT to remove any non-bound secondary antibody, followed by one more wash for 1 hr. Embryos were counterstained with To-pro-3 iodide (Molecular Probes, Cat No. T3605) to visualise DNA, mounted and acquired using confocal microscopy.

2.2.5.3. Wholemount GFP and BrdU staining – Injection of BrdU

Matings between *Hex*GFP homozygous stud males and CD1 female mice were set up. At 6.5 dpc, pregnant mice were administered 50 mg/kg BrdU by intraperitoneal (IP) injection and sacrificed 1 or 3 hrs later. Control mice were injected with PBS alone. Embryos were recovered from the uterus, washed three times, 5 mins each with PBS at RT and fixed overnight in 4% Paraformaldehyde. The immunofluorescent detection of GFP and BrdU was conducted identically to the relevant part of the protocol as previously described.

2.2.5.4. Wholemount GFP and BrdU staining – Embryo culture protocol II

This protocol has been modified from the Wholemount BrdU staining protocol as found on the Rossant web page (www.sickkids.ca/rossant/protocols). BrdU (32.56

mM) was diluted to a final concentration of 20 μM in 1:1 DMEM: rat serum and pipetted into 80 μl drops in 10 cm culture dishes (VWR, UK). Drops were covered in mineral oil and equilibrated at 37 °C, 5% CO_2 for 2-3 hrs. Freshly dissected 5.5-6.25 dpc *Hex*GFP embryos were placed into the drops and cultured for 30 mins. Control embryos underwent culture in medium in which BrdU had been omitted. Following culture embryos were transferred to a 4-well dish, washed three times in PBS for 5 mins and fixed in 4% Paraformaldehyde containing 2 mM EGTA for 1.5 hrs at 4 °C. Embryos were washed in PBT (PBS containing 0.1% Tween-20) for 1 hr at 4 °C then blocked in 10% Normal goat serum (NGS) in 0.1% PBS Triton X-100 at RT for 1.5 hrs. Embryos were transferred to the first primary antibody solution [Rabbit anti-GFP (Molecular Probes, Cat No.A11122) diluted 1:1000 in blocking solution] and incubated at 4 °C for a minimum of 2 days.

Non-bound primary antibody was removed during three 5 min rinses in 0.1% Triton X-100, and followed by one more wash for 1 hr at RT. Incubation with the second secondary solution followed [Alexa Fluor 488 Goat anti-rabbit IgG (Molecular Probes, Cat No.A11008) diluted to 1:500 with blocking solution] for 2 hrs at RT with rocking. Embryos were washed three times, 5 min at RT to remove any non-bound secondary antibody, followed by one more wash for 1 hr. Embryos were then post-fixed in 4% Paraformaldehyde for 10 mins and transferred to 2M HCl in PBS 0.1% Tween-20 for 30 mins at 37 °C to denature the DNA. The HCl was quenched by washing three times for 5 mins in borate buffer at RT. Quenching was followed by blocking in MABT (100 mM Maleic acid, pH 7.5, 150 mM NaCl in 0.1% Tween-20) containing 10% Sheep serum for a minimum of 1.5 hrs at RT. The embryos were then incubated overnight in the second primary antibody solution [Rat

anti-BrdU (Abcam, Cat no. ab6326) diluted 1:100 in MABT, 1% Sheep serum] at RT with constant rocking.

The following day embryos were washed three times, 5 mins each in MABT containing 10% Sheep serum, then an additional five times, 1 hr each in MABT. Embryos were blocked in MABT containing 10% sheep serum for 1.5 hrs at RT. Secondary antibody was then added [polyclonal Cy3 Goat anti-rat IgG (Abcam, Cat No.ab6953) diluted to 1:500 with the same blocking solution and To-pro-3 iodide (Molecular Probes, Cat No. T3605) diluted 1:500] and embryos were incubated at 4 °C overnight. Finally embryos were washed five times, 1 hr each in MABT to removed non-bound secondary antibody, mounted and acquired using confocal microscopy.

2.2.6. Embryo culture

2.2.6.1. Nocodazole, Genistein and Okadaic acid

The basic protocol for embryo culture is as described when embryos were cultured with BrdU. The basic format is stock solutions are made, aliquoted and stored at -20 °C. The mitotic inhibitors used in this investigation were all diluted in Dimethylsulfoxide (DMSO) to a stock concentration as follows: Nocodazole (5 mM), Genistein (5 mM) and Okadaic acid (1 μM). Stock solutions were thawed when required and diluted to the appropriate concentration in 1:1 DMEM: rat serum. The culture medium containing mitotic inhibitor was pipetted into 10 cm culture dishes as 80 μl drops. Drops were covered in mineral oil and equilibrated at 37 °C, 5% CO_2 for 2-3 hrs. Non-treated controls contained an equivalent volume of DMSO in the embryo culture medium.

During equilibration of the culture medium, embryos were dissected from the uterus and if necessary screened for the *Hex*GFP transgene under a fluorescent lamp with a GFP filter. GFP positive embryos were placed in the drop and pictures were taken before and after culture (usually 16 hrs, but in the case of nocodazole at multiple time points) using a Leica MZ FLIII dissection microscope with a Leica Image Manager 50 software package. These images were processed in Adobe Photoshop CS2. Post-culture embryos were washed three times in PBS for 5 mins and fixed in 4% Paraformaldehyde overnight at 4 °C. They then underwent antibody staining as described.

2.2.6.2. SB-431542

Freshly dissected 5.5 dpc embryos were cultured for 16 hrs in the chemical inhibitor of activin/nodal, SB-431542 at a concentration of 10 μM. 30 mins before completion the embryos were transferred to another drop containing both SB-431542 and 20 μM BrdU. These embryos were cultured for a further 30 mins at which point they were washed three times, 5 mins in PBS and fixed in 4% PFA containing 2 mM EGTA for 1.5 hrs at 4 °C. These embryos then underwent GFP and BrdU staining as previously described.

2.2.7. Confocal acquisition

Stained embryos were mounted on either a Glass Bottom Microwell dish (MatTek Corp, USA, Cat No. P35G-1.5-14-C) or a μ-Slide (Ibidi, Germany, Cat No. 81821) in a drop of 1:1 Glycerol:PBS. Confocal images of each embryo were captured on a Leica DM IRB upright confocal microscope through either a 10x/0.30 PH1 air objective or 40x/1.00 PH3 oil immersion objective. The microscope was equipped

with an argon, helium-neon and UV laser. Stacks were generally taken at 4 μm intervals through the embryo, with each channel being acquired sequentially. Stacks were reconstructed using the downloadable package, ImageJ 1.33u.

2.3. Molecular biology

2.3.1. Transcription of riboprobes for wholemount RNA *in situ* hybridisation

Table 1

Gene	Enzyme for antisense linearisation	RNA polymerase (Roche, Germany)	Source of probe
Brachyury	*BamH*I	T7	Wilkinson *et al.*, 1990
Cerberus	*Sal*I	SP6	Shawlot *et al.*, 1998
Cripto	*BamH*I	T7	Ding *et al.*, 1998
Dkk1	*Sal*I	T7	Glinka *et al.*, 1998
Eomesodermin	*Sal*I	T7	Ciruna and Rossant, 1999
FGF 8	*Eco*RI	T3	Mahmood *et al.*, 1995
Frizzled 8	*Eco*RI	T3	Lu *et al.*, 2004
Hesx1	*BamH*I	T3	Thomas *et al.*, 1995
Hex	*Eco*RI	T3	Bedford *et al.*, 1993
HNF3β	*Hind*III	T7	Ang *et al.*, 1993
Lefty1/2	*Xho*I	T7	Meno *et al.*, 1997
Lim1	*Hind*III	T7	Shawlot and Behringer, 1995
Nodal	*Eco*RI	T3	Varlet *et al.*, 1997
Oct4	*Hind*III	T7	Rosner *et al.*, 1990
Otx2	*Eco*RI	SP6	Ang *et al.*, 1996
Sfrp5	*Eco*RI	T3	Leaf *et al.*, 2006
Six3	*Xba*I		Oliver *et al.*, 1995
Snail	*BamH*I	SP6	Nieto *et al.*, 1992
Sox17	*Eco*RI	T3	Kanai *et al.*, 1996
Tbx6	*Not*I		Chapman *et al.*, 1996
TTR	*Xba*I	T3	Makover *et al.*, 1998
Wnt3	*Xba*I	T3	Roelink *et al.*, 1990

Plasmids containing the appropriate cDNAs were first linearised using restriction enzymes as listed in Table 1. All enzymes were obtained from New England Biolabs. Digests were set up in a 50 μl volume according to their specifications and 1.5 mg total plasmid was digested. Complete linearisation was confirmed by agarose gel separation after which the DNA was purified by phenol/chloroform/isoamyl alcohol (25:24:1) extraction. DNA was precipitated using 1/10 volume of 3 M Sodium acetate pH 5.2 and 2 volumes of 100% Ethanol (Fisher Scientific, UK) at -20 °C. Samples

were then centrifuged at 16, 000 x g, 4 °C for 15 mins. Precipitated DNA was washed in 70% Ethanol, re-suspended in 10 ml dH_2O, and if necessary stored at -20 °C until transcription of the riboprobe.

In vitro transcription of riboprobes was carried out using the appropriate RNA polymerase, shown in Table 1. Reactions were as follows: 50 μl total volume containing 1 mg plasmid DNA, 100 units of T3, T7 or SP6 polymerase, 1x transcription buffer, 25 units RNAse Inhibitor and 5 μl DIG-labelled nucleotide mix (all Roche Diagnostics, Germany). Transcription was carried out at 37 °C for 2 hrs after which 30 units of RNAse-free DNAse I (Roche, Germany) was added to the reaction and incubated at 37 °C for 15 mins to destroy the plasmid template. 3 μl of the reaction was fractionated by electrophoresis in a 1% agarose gel containing Ethidium bromide and visualised under UV light to assess the yield of the transcription reaction. Riboprobes were purified using ChromoSpin columns (BD Biosciences, UK) and 3 μl was again fractionated on a 1% agarose gel to assess the quality and approximate concentration of the probe to determine its working dilution.

2.3.2. Generation of targeting vector Hex-XneoSTOP^{R}X-DTA

The *Hex-XneoSTOP^{R}X-DTA* targeting construct was generated by inserting a 3 kb cassette consisting of an internal ribosome entry site (IRES), followed by a reverse PGK-*Neomycin* gene flanked by *loxP* sites, and the DTA coding sequence (a gift from T. Jessell) into a *Hex* genomic clone at an *ApaI* site immediately 3' to the *Hex* start ATG.

2.3.3. Isolation and restriction digestion of genomic DNA from ES cells for Southern blot

DNA was isolated from ES cells and expanded in 96 well format. Cells were grown until confluent and growth media turned yellow daily. Growth medium was aspirated from the plate and cells were washed twice with PBS. 50 μl lysis buffer (10 mM Tris-HCl, pH 7.5, 10 mM EDTA, 10 mM NaCl, 0.5% Sarcosyl) containing 1 mg/ml Proteinase K (Roche, Germany) was added to each well and the plate incubated overnight at 55 °C in a humidified chamber.

Next day 100 μl of -20 °C Ethanol/salt solution (75 mM NaCl in 100% Ethanol) was added to each well. The plate was incubated at RT for 30 mins and subsequently inverted onto paper towels so the liquid drained away. Genomic DNA was left attached to the base of each well. DNA was washed three times with 70% Ethanol, 150 μl per well. After the final wash the plate was left inverted on paper towels for 5 mins to dry the DNA. During this time the restriction digest mix was prepared (1x NEB buffer, 1 mM Spermidine, 100 μg/ml BSA, 100 μg/ml RNAse A, 20 units of enzyme made up to a total of 30 μl with dH_2O per well). After loading the digest mix the plate was incubated overnight at 37 °C in a humidified chamber. *EcoRV* was used to digest the targeted clones.

2.3.4. Synthesis and purification of DNA probes for Southern blot

Two DNA probes were used to screen for homologous recombinant clones. The first sequence hybridised 5' external to the site of recombination. This was created by cutting the targeting vector with *KpnI* which liberated a 400 bp fragment. In wildtype clones this probe bound to an *EcoRV*-cut fragment 11.8 kb in length. This could be differentiated from the targeted allele by the additional binding of the 5' probe to a 7

kb fragment, brought about by the addition of another *EcoRV* site situated within the *Neomycin* gene. To confirm single insertion of the targeting vector blots were also hybridised with a DTA probe that recognised a single 5 kb *EcoRV*-cut fragment. The probes were labelled with ^{32}P-dCTP using the Megaprime® Random labelling kit according to the manufacturer's instructions, and purified using Sephadex G50 columns (all Amersham Biosciences, UK). Radiolabelling was measured using a scintillation counter. 15 million counts per minute (cpm) total activity was used for hybridisation to each membrane.

2.3.5. Southern blot analysis of Hexd targeted ES cell clones

Southern blot analysis was used to identify successfully targeted ES cell clones with a single copy of the targeted vector in the *Hex* locus. Southern blots were conducted according to the Amersham Biosciences Hybond membrane product protocol.

Digested genomic DNA was separated alongside a 1 kb ladder (Invitrogen, UK) on a 0.75% agarose gel run at 50 V for 8-10 hrs. DNA samples were visualised under UV against a ruler to allow accurate sizing of bands on the eventual Phosphor-imager scan. The agarose gel was placed in 0.125 M HCl to depurinate the DNA. The gel was gently rocked for 10 mins, after which it was rinsed twice in dH_2O. DNA was placed in denaturing buffer (0.5 M NaOH, 1.5 M NaCl) for 30 mins, and again gently rocked. This was followed by two rinses in dH_2O. Finally the gel was placed in neutralising buffer (0.5 M Tris, 1.5 M NaCl, pH 7.5) for 30 mins with gentle rocking and washed in dH_2O.

DNA was transferred by capillary blot from the gel to a PVDF membrane (Polyscreen, Perkin Elmer) using Transfer buffer (20x SSC containing 3 M NaCl, 0.3

M Sodium citrate) to promote binding of DNA to the membrane. DNA was then covalently bound to the membrane via UV crosslinking.

The membrane was placed in a hybridisation bottle to allow rolling incubation in the hybridisation oven. The membrane was incubated in RapidHyb buffer (Amersham Biosciences, UK) at 65 °C for a minimum of 1 hr to block non-specific binding. The membrane was incubated with ^{32}P-dCTP-labelled probe in RapidHyb buffer overnight at 65 °C allowing the probe to bind to the membrane-bound DNA. After hybridisation, the membrane was washed twice at high stringency (2x SSC/0.1% SDS) at 65 °C for 10 mins each, and twice at low stringency (0.2x SSC/0.1% SDS) at 65 °C for 10 mins each. Between washes the radioactive signal on the membrane was monitored using a Geiger counter. Washing in low stringency continued until the average signal over the membrane was less than 10 cpm.

The membrane was then wrapped in Saran Wrap and placed in a Phosphor-imager detection cassette (Amersham Biosciences, UK) and exposed overnight. Cassettes were analysed on a Storm Phosphor-imager (Amersham Biosciences, UK).

2.3.6. Extraction of genomic DNA from murine tail biopsies for Southern blot analysis

Tail biopsies obtained from transgenic mice were digested in tail buffer (50 mM Tris, pH 7.6, 100 mM EDTA, 0.5 % SDS, 100 mM NaCl) overnight at 55 °C in the presence of 400 μg/ml Proteinase K. DNA was purified by two phenol/chloroform/isoamyl alcohol (25:24:1) extractions, followed by a chloroform extraction. Genomic DNA was then precipitated by adding 1/10 volume of Sodium acetate (3 M, pH 5.2) and 1 volume of 100% Isopropanol (Fisher Scientific, UK). Precipitated DNA was washed in 70% Ethanol and resuspended in dH_2O. DNA

concentration was determined spectrophotometrically (Nanodrop®, ND1000), and 10 μg were digested with *EcoRV* overnight at 37 °C. These samples were then run on a 0.75% agarose gel and probed as previously described.

2.3.7. Extraction of genomic DNA from murine tail biopsies for PCR genotyping

Tail biopsies obtained from transgenic mice were digested in Rossant buffer (50 mM KCl, 10 mM Tris-HCl, pH 8.3, 2 mM $MgCl_2$, 0.1 mg/ml gelatin, 0.45% IGEPAL and 0.45% Tween-20) overnight at 55 °C in the presence of 500 μg/ml Proteinase K. The following morning, Proteinase K was inactivated at 95 °C for 10 mins. Samples were vortexed, spun down and stored at 4 °C. Typically 3 μl lysate was used for PCR genotyping.

2.3.8. Digestion of transgenic embryos for genotyping

Embryos obtained from transgenic mice were digested in embryo lysis buffer (50 mM Tris-HCl, pH 8.5, 1 mM EDTA, 0.5% Tween-20) overnight at 55 °C in the presence of 6 μg/ml Proteinase K. Proteinase K was inactivated by incubation of lysates at 95 °C for 10 mins. Samples were vortexed, spun down and stored at 4 °C. Depending on the size of the embryo different volumes of embryo buffer were used. Typically 5.5 dpc embryos were digested in 20 μl, 6.5 dpc embryos 30 μl, 7.5 dpc embryos 50 μl, 8.5 dpc embryos 70 μl and tail tips of 9.5 dpc embryos were digested in 90 μl. Depending on the specific PCR or embryo stage, between 3 and 7 μl of lysate were used per 50 μl PCR reaction.

2.3.9. Genotyping of transgenic mouse lines by PCR

Hexd32 transgenic mice were crossed to β-actin *Cre* mice to produce offspring of which one quarter harboured both transgenes. To identify Hexd^{act} mice three sets of primers were used. A single 5' and 3' oligo were used to amplify part of the *DTA* coding region and are thus referred to as 5' DTA and 3' DTA. Presence of β-actin *Cre* was confirmed by using a single 5' and 3' oligo that amplified a portion of the *Cre* recombinase coding region. To verify that the *Neomycin* cassette had been excised in embryos harbouring DTA and *Cre* recombinase a third pair of 5' and 3' oligos were used to amplify part of the *Neomycin* coding region (Table 2).

In subsequent crosses, surviving Hexd^{act} mice were intercrossed to produce offspring of which one quarter harboured two copies of the activated DTA allele. To distinguish the heterozygous (Hexd^{act}/+) from homozygous (Hexd^{act}/Hexd^{act}) allele an additional PCR strategy was designed which amplified a portion of Exon 1 of the endogenous Hex locus. Exon 1 is the site of targeting and is therefore disrupted by the exogenous targeting vector sequence. 5' and 3' oligos were designed to amplify up a portion of Exon 1, referred to as 5' Exon 1 and 3' Exon 1. The homozygous allele would fail to amplify this sequence whilst the heterozygous allele would produce a product.

*Hex*GFP mice were genotyped using 5'/3' GFP oligos, and nodal.*LacZ* and R26R were genotyped using 5'/3' *LacZ* oligos as summerised in Table 2

Name	5' Primer	3' Primer
DTA	CGACAATAAATACGACGCTGCGGG	CATCGCATCTTGGCCACGTTTTCC
Cre	CCAGCTAAACATGCTTCATC	CGCTCGACCAGTTTAGTTAC
Neo	CAAGATGGATTGCACGCAGG	CGGCAGGAGCAAGGTGAGAT
Exon 1	CGGAGGCGAATCTGAAGCCAG	GCATACAGCGGGACTCCCACG
GFP	TGCAGTGCTTCAGCCGCTAC	CCAGCAGGACCATGTGATCG
LacZ	CGCCAGCTGGCGTAATAGCGAAG	GATGGGCGCATCGTAACCGTGCA

2.3.9.1. The standard PCR reaction

Each PCR reaction was made up in 50 μl total volume containing 3-7 μl DNA lysate, 1 unit of Amplitaq, 125 ng of each primer (Sigma, UK), 5 μl 10x buffer and 0.2 mM of each dNTP (All Roche Diagnostics, Germany) made up in dH_2O. PCR was performed on a Peltier thermal cycler (PTC-100™) using the following program: Initial denaturation step at 95°C for 5 mins, then 39 amplification cycles of 30 secs at 94 °C, 30 secs annealing (60 °C for Cre and GFP, 59 °C for Neo, 56 °C DTA and 58 °C for LacZ), 45 secs at 72 °C, followed by a final elongation step of 7 mins at 72 °C. The resulting PCR products were size-fractionated by electrophoresis in 1% agarose gels containing Ethidium bromide and visualised under UV light.

2.3.9.2. Exon 1 PCR reaction

The Exon 1 PCR was made up in 50 μl total volume containing 3 μl DNA lysate, 0.625 μl of Taq DNA polymerase, 5 μl 10x buffer and 10 μl Q solution (Qiagen, UK), 125 ng of each primer (Sigma, UK), and 0.2 mM of each dNTP (Roche Diagnostics, Germany) made up in dH_2O. The following PCR program was used: Initial denaturation step at 94 °C for 2 mins, then 30 amplification cycles of 20 secs at 94 °C, 20 secs annealing at 58 °C, 20 secs at 72 °C followed by a final elongation step of 7 mins at 72 °C. The resulting PCR products were size-fractionated by electrophoresis in 1% agarose gels containing Ethidium bromide and visualised under UV light.

2.4. Tissue Culture

2.4.1. General passaging techniques

All ES cells used in this investigation were cultured in feeder-free conditions on gelatinised plasticware. Growth media was Glasgow Minimum Essential Medium (GMEM) supplemented with 80 nM β-mercaptoethanol, 100 nM non-essential amino acids, 2 mM L-glutamine, 1 mM Sodium pyruvate (all Gibco), plus 10% characterised fetal calf serum (FCS; Chemicon-Millipore, UK) and 9 x 10^5 units of ESGRO® Leukocyte Inhibitory Factor (LIF; Chemicon-Millipore, UK). ES cells were frozen in media containing 90% FCS, 10% tissue culture grade DMSO.

2.4.2. Generation of targeted clones

2.4.2.1. Preparation of DNA

50 μg of Hexd targeting vector was linearised by *NotI* restriction digest in a 50 μl volume. Complete linearization was assessed by visualisation of DNA in a 1% agarose gel containing Ethidium bromide under UV light. The Linearised vector was purified by phenol/chloroform/isoamyl alcohol (25:24:1) extraction. DNA was precipitated using 1/10 volume of 3 M Sodium acetate, pH 5.2 and 2 volumes of 100% Ethanol at -20 °C. DNA was centrifuged at 16,000 x g, 4 °C for 15 mins. Precipitated DNA was washed in 70% Ethanol, resuspended in dH_2O to a final concentration of 2 μg/μl.

2.4.2.2. Electroporation and processing of targeted clones

Low passage number (<10 times) ES cells were plated into a 75 cm^2 tissue culture flask (VWR, UK) and grown until confluent. Cells were trypsinised, collected,

resuspended in PBS and counted using a haemocytometer. Approximately 3 x 10^7 cells were used for electroporation in 1 ml PBS.

30 μg of linearised DNA was added to the 1 ml cells and transferred to a 0.4 cm electroporation cuvette (BioRad). Cells were electroporated using a BioRad Genepulser electroporation unit. Cells were exposed to two pulses: the first was at 0.23 Kv, and the second at 0.24 Kv with resistance set to 960 μF. Following the second pulse the cuvette was tapped on the bench and placed on ice for 10 mins. After this cells were plated on gelatinised 10 cm culture plates (VWR, UK) in their normal growth medium, GMEM.

After 24 hrs, selection media was added to the plates. For selection of positive clones cells were cultured in G418 (Sigma, UK) at a final concentration of 2 μg/ml. After 10 days selection colonies were well established on the plates. 96 colonies were picked into gelatinised, flat bottom 96 well plates and cultured. Once confluent, the clones were split into two duplicate 48 well plates. Approximately one fifth of cells were left in the 96 well plate and cultured until confluent to be used for DNA extraction and Southern blot analysis. The 48 well plates were also grown to confluency and then frozen down and stored at -80 °C for up to one month. A number of clones were indicated as containing correct *Hex* insertions in the initial Southern blot analysis. These were thawed and expanded and underwent further analysis by Southern blot to confirm the position of the insertion site and the presence of a single targeting event. Two correctly targeted clones were determined. These were thawed, expanded and used for injection into blastocysts to derive the Hexd mouse line.

2.4.2.3. Karyotyping ES cells

ES cells were plated into a 25 cm^2 tissue culture flask (VWR, UK) and grown until 50-75% confluent on the day of karyotyping. Medium was changed first thing in the morning and 2 hrs later Demecoline (Sigma, D6279) was added directly to the medium to a final concentration of 20 ng/ml. After 1 hr, cells were gently washed with PBS then thoroughly trypsinized and spun down (750 rpm, 5 mins). The pellet was washed once in PBS and respun. The pellet was resuspended in 5 ml hypotonic solution (0.56% w/v KCl) until a single cell suspension was obtained. Cells were kept in hypotonic solution at RT for exactly 6 mins, then spun at 750 rpm for 5 mins. The supernatent was removed, leaving a drop to resuspend the pellet in. Flicking the tube, 5 ml of ice-cold fixative (Methanol: Acetic acid, 3:1 made up fresh) was added dropwise. After 5 mins at RT, cells were spun down, and the fixing procedure was repeated a further 3 times. Each time the cells were spun down, a loose and flocculent pellet formed. To avoid losing the pellet 0.5-1.0 ml fixative was always left behind. After the last fixation step, cells were resuspended in a final volume of 1 ml fixative.

To observe mitotic spreads, cells were dropped using a Pasteur pipette from a height of around 40 cm onto acid-washed slides (slides were placed overnight into 5% acetic acid in ethanol). When slides have dryed thoroughly, they were stained in 10% Giemsa's (BDH Lab Supplies, Cat No. 35086 4X) in PBS for 20 mins. Slides were then washed gently in tap water twice, with a final wash in dH_2O. Slides were left to dry overnight and coverslips were mounted using DPX medium (BDH Lab Supplies, Cat No. 36029 4H). Slides were observed on a normal dissection microscope. Murine nuclei possess a full complement of 40 chromosomes. A 10% tolerance was allowable if ES cells were to be blastocyst injected.

2.4.2.4. Transient transfection of targeted ES cells with pTurboCre

To test the efficiency of DTA ablation *in vitro*, one of the targeted cell lines was transiently transfected with the Cre expression plasmid pTurboCre (Gibco). Cells were split onto a gelatinised 6 well plate (Nunc™) the day before transfection so they would be approximately 90% confluent on the day of transfection. Cells were grown overnight in GMEM (as previously described). Prior to transfection cells were washed with PBS and transfected according to the Lipofectamine 2000 reagent protocol (Invitrogen, UK). For each well 4.0 μg of pTurboCre or the positive control plasmid pTriExGFP was mixed with 250 μl OptiMEM. At the same time 10 μl Lipofectamine 2000 was mixed with 250 μl OptiMEM per well. These two mixes were combined and left at RT for 30 mins. Cells were washed once in OptiMEM, aspirated and 500 μl of the incubated mix was added to each well and incubated at 37 °C, 5% CO_2 for 5 hrs. All conditions were carried out in duplicate wells.

After incubation the transfection mix was aspirated and replaced with GMEM ES cell media. Given that *Hex* is only expressed in differentiating ES cells (T. Rodriguez, personal communication) media was changed daily using complete GMEM without LIF to allow differentiation of the ES cells. Pictures were taken daily for the duration of the three day experiment.

Chapter 3 – Proliferation at the time of DVE movements

3.1. Introduction

Cell proliferation has been shown to have multiple functions in developmental processes. Examples are diverse and include refining tissue shape during organogenesis, cell fate determination and regulating pattern formation (Schmahl and Capel., 2003; Baena-Lopez *et al.,* 2005). In rodents, proliferation in the post-implantation embryo has been investigated. Many of the early studies calculated cell cycle length in tissues of the pre-gastrulae embryo providing a descriptive map of proliferation (Snow, 1977; Poelmann, 1980; Lawson *et al.*, 1991). For example, Snow estimated the mean cell cycle length in the pregastrulating endoderm to be approximately 17 hrs, whilst cells of the epiblast could range from 9.5 hrs to as little as 3 hrs in a region termed the proliferative zone (Snow, 1977). Lawson's study calculated the cell cycle length of the endoderm to be 10.5 hrs, and the epiblast a mean length of 7.5 hrs, whilst evidence for a proliferative zone was not found (Lawson *et al.*, 1991). There appears to be an apparent degree of discordance when comparing studies, although there is agreement that tremendous variation in proliferative rates between and within tissues exists.

A more recent study used a stathmokinetic approach in rat embryos to calculate the cell cycle structure of epiblast cell populations (Mac Auley *et al.*, 1993). They found, like Snow did, that epiblast cells of the primitive streak (PS) divided unusually rapidly compared to surrounding epiblast cells (Snow, 1977; Snow and Bennett, 1978). Furthermore this increase in growth rate during gastrulation was shown to be associated with extensive modification of the cell cycle.

Lewis and Rossant investigated size regulation in normal and double-sized pre-gastrulae mouse embryos and demonstrated that normal embryos were able to

alter their size by shortening cell cycle length such that gastrulation commenced at the same time, despite the initial discrepancy in total cell number (Lewis and Rossant, 1982). Taken together it is apparent that the post-implantation embryo possesses a tremendous capacity to regulate cell cycle composition in certain tissues. However to what extent this occurs, the mechanisms involved in achieving this regulation and the processes that are affected are poorly understood.

3.1.1. Proliferation and DVE movement

The unilateral movement of the DVE from the distal tip of the embryo to the future anterior side is essential in correctly establishing the A-P axis. However, the mechanisms involved in initiating, driving and halting this process are not well understood. In 2004, Yamamoto and colleagues proposed that differential proliferation in the VE along the future A-P axis regulated DVE direction and constituted the engine for its movement (Yamamoto *et al*., 2004). They demonstrated that around the time of DVE movements, anterior VE cells were unable to incorporate BrdU, whilst the rest of the VE did.

Nodal signalling was proposed to drive distal DVE movement by stimulating the proliferation of VE cells, whilst the Nodal antagonists *Lefty1* and *Cerl* determined the direction of migration by asymmetrically inhibiting Nodal activity on the future anterior side of the epiblast and thus creating differential proliferation between the anterior and posterior of the embryo (Yamamoto *et al*., 2004). This was demonstrated by injecting embryos with a *Nodal* expression vector and observing an increase in cell proliferation. Conversely co-injection of the Nodal antagonists *Lefty1* and *Cerl* resulted in the inhibition of proliferation. Moreover the DVE tended to move away

from the side where proliferation was stimulated and towards the side where proliferation had been inhibited (Yamamoto *et al.,* 2004).

In the same year, another study indicated that an active cell migration process drove DVE cells towards the prospective anterior of the embryo (Srinivas *et al.,* 2004). In this study, embryos at the time of DVE movement were imaged in real time at single cell resolution. DVE cells were shown to migrate as a single layer in direct contact with the epiblast, projecting filopodial processes in the direction of motion. These migrating cells took 4-5 hours to reach the boundary between the epiblast and the extra-embryonic ectoderm, whereupon they halted. This paper provided good evidence for active migration driving AVE movement.

Shortly after, a report implicated canonical Wnt signalling in controlling directional movement of VE cells (Kimura-Yoshida *et al.,* 2005). *In vivo* and *in vitro* experiments demonstrated that the Wnt antagonist *dickkopf1 (Dkk1)* could act as an attractive guidance cue for DVE cells. Furthermore, *Dkk1*-positive cells are located at the forefront of migrating VE cells and were shown to attract *Cerl*-positive DVE cells; providing a possible cue that could guide migrating AVE cells.

Therefore despite the differential proliferation mechanism being an attractive model, how it accounts for the following findings has remained unresolved: (a) DVE cells move in as little as 4-5 hours in a proposed active migration process, possibly in response to a molecular cue (Srinivas *et al.,* 2004; Kimura-Yoshida *et al.,* 2005); (b) the average cell cycle length in the VE at the time of DVE movement is estimated to be 17 hours (Snow, 1977); (c) detailed analysis of clonal populations in the VE at this stage failed to outline major differences in proliferation rates between the 4 sub-

regions of the distal VE (Perea-Gomez, 2001a); (d) the patch of BrdU-negative cells on the anterior side expands considerably despite being non-proliferating.

Is it possible to reconcile these points in the context of a differential proliferation model?

This Chapter aims to resolve these contradictions by providing a detailed characterisation of proliferation levels and distribution within the embryo at the time DVE movements are initiated. Proliferation will be assessed by BrdU incorporation (S phase) and by anti-phospho-Histone-H3 staining (M phase) in combination with high resolution imaging and culturing techniques. *Hex*GFP transgenic mice will be used which express GFP in the *Hex*-expressing cells of the DVE (Rodriguez *et al.*, 2001). Thus proliferation within the VE can be mapped with respect to the exact position of the DVE. Using this approach it will be possible to confirm the presence of differential proliferation within the VE, and if so, accurately relate these patterns of proliferation to DVE movements.

3.2. Results

3.2.1. BrdU incorporation shows no regional bias in the VE at the onset of DVE movements

BrdU incorporation was the first method used to measure proliferation in the VE during DVE movements. *Hex*GFP embryos that express GFP in the DVE, were cultured in 20 μM BrdU for 15 mins, and analysed by confocal microscopy allowing cellular resolution and accurate visualisation of DVE position in relation to proliferating cells of the VE.

A total of 16 *Hex*GFP embryos were acquired and divided into three groups depending upon the position of the DVE. The first was named the pre-distal group and displayed low level GFP expression throughout the VE (Fig. 1A+A'). Group two constituted those embryos in which the DVE had resolved to the distal tip, referred to as the distal group (Fig. 1D+D'). The final group showed a definite tilt of the DVE and was therefore referred to as the tilted group (Fig. 1H+H').

Several longitudinal sections were acquired at different levels for each embryo. The number of BrdU-positive nuclei were counted and expressed as a percentage of the total cell number, referred to as the incorporation index. In the pre-distal group, due to the diffuse expression of GFP throughout the VE this tissue was not regionally sub-divided (Fig. 1B). The mean incorporation index of the VE in this group was 76% (n=5, SEM ± 2.66%)(Fig. 1C), with non-incorporated nuclei not appearing to cluster in any particular region of the VE.

Although an A-P axis could not be assigned to the distal group, embryos were divided into DVE and VE domains (Fig. 1E).

Figure 1 - BrdU incorporation at the onset of the DVE movement

Freshly dissected *Hex*GFP embryos were cultured in 20 μM BrdU for 15 mins and immunofluorescently stained for BrdU and GFP. Longitudinal sections were acquired on the confocal microscope at multiple levels. Embryos were divided into three groups depending on their developmental stage. (A+A') The pre-distal group exhibited GFP (green) at low levels throughout the entire VE. Nuclei (blue) and BrdU-positive nuclei (red) are easily distinguishable. (B) The number of BrdU-positive nuclei in the embryonic VE was counted and expressed as a percentage of the total cell number, referred to as the incorporation index. (C) Mean incorporation index in pre-distal embryonic VE (n=5). (D+D') The distal group exhibits strong GFP staining at the distal tip. (E) Embryonic VE was divided into two portions: DVE and flanking VE. The incorporation index for both regions were calculated. (F) Mean incorporation index in the distal group (n=6). (G) Relative fold difference of BrdU incorporation between the flanking VE regions. The red line indicates no relative difference between the two areas. Any deviation from the red line indicates a relative difference in proliferation. (H+H') The tilted group exhibits strong GFP staining in a tilted DVE. (I) Embryonic VE was divided into three portions: Anterior VE, DVE and posterior VE. (J) Mean incorporation index in tilted embryonic VE group (n=5). Error bar = ± SEM. (K) Relative fold difference of BrdU incorporation between anterior VE and posterior VE were calculated for each embryo (anterior VE /posterior VE). The red line indicates no relative difference between the two areas. A positive deviation from the red line indicates relatively more proliferation in the anterior VE compared to the posterior VE. A negative deviation would imply the converse was true. Scale bar 40 μm.

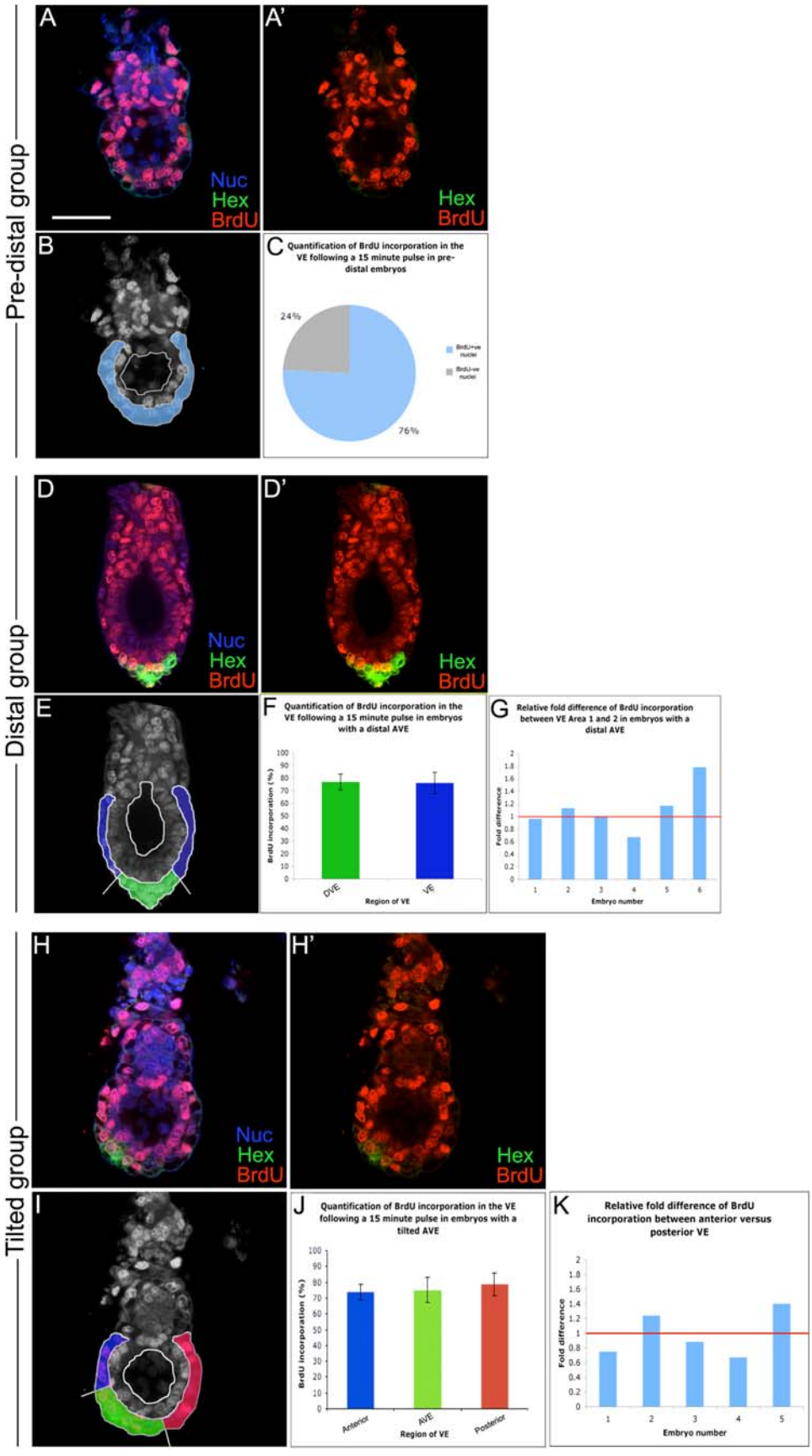
Pre-distal group
A
Nuc
Hex
BrdU
A'
Hex
BrdU
B
C
Quantification of BrdU incorporation in the VE following a 15 minute pulse in pre-distal embryos
24%
76%
BrdU+ve nuclei
BrdU-ve nuclei
Distal group
D
Nuc
Hex
BrdU
D'
Hex
BrdU
E
F
Quantification of BrdU incorporation in the VE following a 15 minute pulse in embryos with a distal AVE
BrdU incorporation (%)
DVE
VE
Region of VE
G
Relative fold difference of BrdU incorporation between VE Area 1 and 2 in embryos with a distal AVE
Fold difference
Embryo number
Tilted group
H
Nuc
Hex
BrdU
H'
Hex
BrdU
I
J
Quantification of BrdU incorporation in the VE following a 15 minute pulse in embryos with a tilted AVE
BrdU incorporation (%)
Anterior
AVE
Posterior
Region of VE
K
Relative fold difference of BrdU incorporation between anterior versus posterior VE
Fold difference
Embryo number

The mean incorporation index of these areas was quantified: DVE, 76.85% (n=6, SEM ± 6.33%) and VE, 76.07% (n=6, SEM ± 8.45%)(Fig. 1F). The two VE areas flanking the DVE for each embryo were then plotted as a ratio of each other to give an indication of differential proliferation within individual embryos. If each side divided at an equal rate then a value of 1 would be obtained. Any relative difference in proliferation would result in a deviation from this number, proportional to the degree of difference.

4/6 embryos showed a relative fold difference of no greater than 1.17 indicating the two regions of VE possessed similar levels of proliferating cells (Fig. 1G). Two embryos did exhibit more pronounced differential proliferation with values of 1.78 and 0.66 (Fig. 1G). However whether differential proliferation was greatest in the prospective anterior or posterior VE could not be determined in this experiment.

The tilted group could be assigned an A-P axis and the VE was divided up according to the position relative to the DVE (Fig. 1I). The mean incorporation index of these areas was quantified: VE anterior to the DVE, 73.83% (n=5, SEM ± 4.84%), DVE, 75.05% (n=5, SEM ± 7.93%) and posterior VE, 78.74% (n=5, SEM ±7.18%) (Fig. 1J). There was a slight increase in proliferation from anterior to posterior VE with DVE having an incorporation index intermediate of the two, though this difference was not statistically significant (χ^2 P=0.587). As in the distal group, each embryo had the ratio of its anterior versus posterior VE proliferation index plotted (Fig. 1K). This time a value exceeding 1 would indicate more proliferation in the anterior compared to the posterior VE, whilst a value less than 1 would indicate the converse was true. Of the five embryos in the group, two displayed values exceeding 1 (1.24 and 1.40).

The remaining embryos had values of 0.75, 0.88 and 0.67 indicating a marginal increase in posterior VE proliferation compared to anterior VE.

This BrdU-incorporation experiment showed firstly that following a 15 min pulse, between 70-80% of VE cells were in S phase at the time DVE movements are being initiated. Furthermore unlike the Yamamoto *et al* (2004) study, at no point during this process was there evidence of any consistent or marked differential proliferation between the anterior and posterior VE.

3.2.2. Low levels of mitosis in the VE at the onset of DVE movements

In order to confirm the BrdU findings it was necessary to assess levels and distribution of proliferation using a different cell cycle marker. For this purpose an antibody raised against phospho-Histone-H3 (PH3) was used. This antibody specifically binds to nuclei in M phase of the cell cycle, providing another means to investigate the proliferative capacity of the embryo at the time of DVE movement. Again *Hex*GFP embryos were used to allow visualisation of the DVE.

Embryos were harvested at 5.5 dpc and stained with anti-PH3 antibody. Confocal stacks were taken through the whole embryo, allowing the entire embryo to be reconstructed and complete quantification to be performed. Initially, 53 embryos were acquired and numbers of mitotic nuclei were pooled irrespective of their exact stage. This provided a general indicator of the proliferative capacity of each tissue compartment during DVE movement (Fig. 2A). The ectoplacental cone was excluded from the study as different amounts of tissue were lost during dissection. It is clear, at least when comparing absolute numbers of mitotic nuclei within each tissue, that there were large variations in the numbers of dividing cells in each tissue compartment (Fig. 2B).

Figure 2 – Embryonic distribution of mitotic nuclei at the onset of the DVE movement

Freshly dissected *Hex*GFP embryos were immunofluorescently stained with the M phase marker anti-phospho-Histone-H3. Complete stacks of 53 embryos were taken at 4 μm intervals by confocal microscopy. The number of mitotic nuclei were counted allowing the mean number of divisions in each tissue per embryo to be calculated. (A) Confocal section of a stained embryo divided into its tissue compartments: visceral endoderm (VE), epiblast, extra-embryonic ectoderm (ExE) and ectoplacental cone (EPC). Mitotic nuclei (red), all nuclei (blue), DVE domain expressing GFP (green). (B) A mitotic map of the embryo at the time of DVE movement. Colour key represents mean number of divisions found in tissue compartment per embryo. EPC was excluded as tissue was lost during dissection. (C) Embryos were divided into three groups by virtue of GFP expression. The pre-distal group displayed weak GFP expression throughout the VE. Strong GFP expression at the distal tip defined the distal group whilst embryos with a tilt in the GFP domain defined the tilted group. It was possible to assign an A-P axis to embryos in the tilted group. (D) Mean number of mitotic nuclei in the VE, epiblast and ExE per embryo, plotted for the three groups. Embryos in each group: pre-distal (n=11), distal (n=22), tilted (n=20). (E) Five embryos from each group were randomly picked and the mitotic index was calculated in the epiblast and VE. The mitotic index (MI) was defined as the percentage of mitotic nuclei. 4-6 confocal sections were quantified per embryo and mean values have been presented. Error bar = ± SEM.

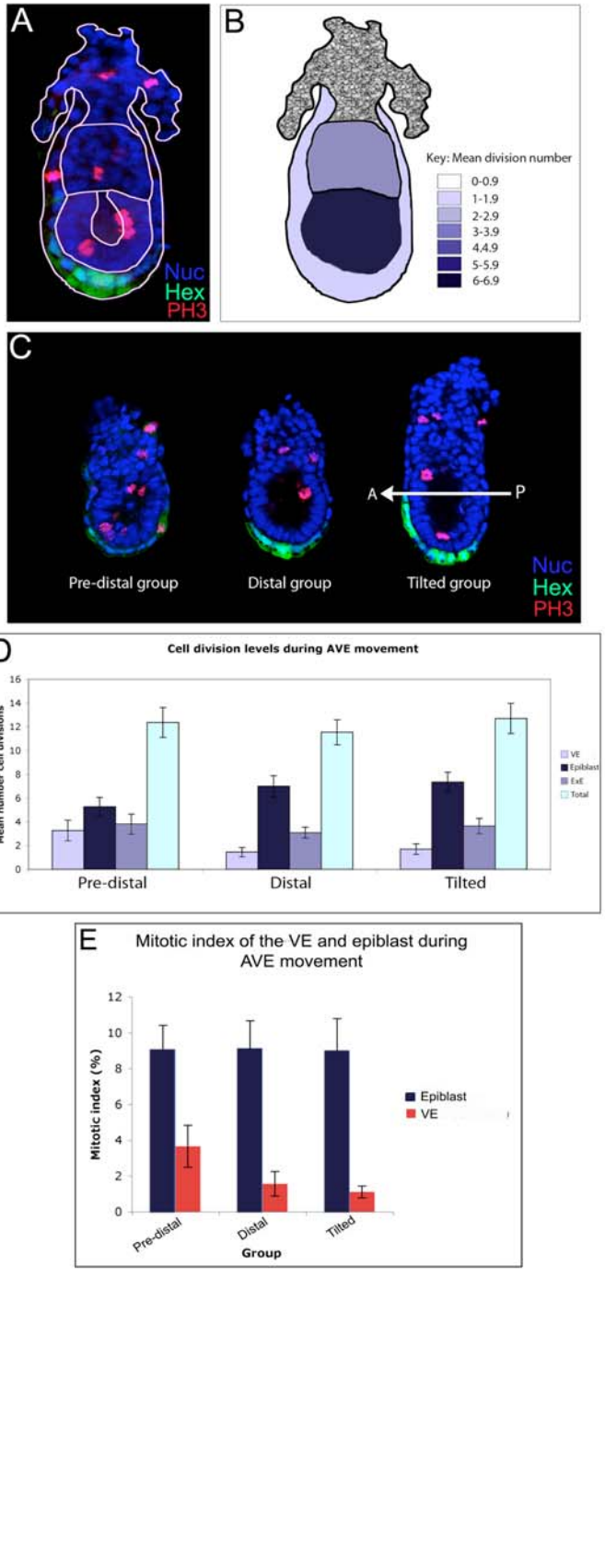
A
Nuc
Hex
PH3
B
Key: Mean division number
0-0.9
1-1.9
2-2.9
3-3.9
4-4.9
5-5.9
6-6.9
C
A
P
Pre-distal group
Distal group
Tilted group
Nuc
Hex
PH3
D
Cell division levels during AVE movement
Mean number cell divisions
16
14
12
10
8
6
4
2
0
Pre-distal
Distal
Tilted
VE
Epiblast
ExE
Total
E
Mitotic index of the VE and epiblast during AVE movement
Mitotic index (%)
12
10
8
6
4
2
0
Pre-distal
Distal
Tilted
Group
Epiblast
VE

The epiblast displayed the greatest number of mitotic nuclei, with a mean of 6.77 per embryo (n=53, SEM ± 0.51). Next was the extra-embryonic ectoderm (ExE) with a mean value of 3.45 divisions per embryo (n=53, SEM ±0.35), followed by the VE with a mean value of 1.92 divisions per embryo (n=53, SEM ± 0.19) (Fig. 2B).

To address whether this relatively low level of division was maintained in the VE throughout DVE movement, pooled embryos were divided into three groups by virtue of their morphology and location of GFP-expression (Fig. 2C). The total number of divisions between the three groups remained remarkably similar (Fig. 2D), as observed in the previous BrdU-labelling experiment. The mean number of divisions in the VE of the pre-distal group was 3.27 (n=11, SEM ± 0.86), slightly greater than levels found in the distal group, 1.45 (n=22, SEM ± 0.39) or tilted group, 1.7 (n=20, SEM ± 0.45). Levels of mitosis were slightly lower in the epiblast of the pre-distal group (5.27 divisions per epiblast, SEM ± 2.61), compared to the distal group (7.0 divisions per epiblast, SEM ± 4.14) or tilted group (7.35 divisions per epiblast, SEM ± 3.67) (Fig. 2D).

Instead of comparing absolute numbers of dividing cells, a more accurate way was to calculate the mitotic index (MI). The MI was calculated as the percentage of dividing nuclei and provided an estimate of the proportion of cells in M phase of the cell cycle at a given time. Five embryos from each stage of DVE movement were selected and the MI was calculated in the epiblast and VE (Fig. 2E). The epiblast displayed little variation in its MI between stages with almost identical mean values (pre-distal group, 9.07%; distal group, 9.14%; tilted group, 9.0%). As seen when looking at absolute numbers, the VE in the pre-distal group displayed a greater MI compared to either the distal or tilted groups (3.65% versus 1.56% and 1.11%

respectively) indicating a decrease in proliferation within the VE just prior to the initiation of the DVE movements. Furthermore the VE irrespective of stage clearly proliferates relatively slowly compared to the underlying epiblast.

3.2.3. Distribution of mitotic nuclei within the VE during DVE movement

Despite the low proportion of mitotic cells in the VE at the time when DVE movements are initiated, it was important to assess their regional distribution within the tissue in relation to DVE position. It was possible that, although the proliferative capacity of the VE was low, mitotic nuclei were regionalised such that differential accretion could produce mechanical forces within the plane of the VE.

The VE of six distal embryos were divided into three regions; DVE, Embryonic VE (Emb VE) and Extra-embryonic VE (ExE VE) (Fig. 3A). Dividing nuclei were then counted with respect to which region they resided, and the mitotic index was calculated. The mean mitotic index of the DVE was 2.34% (SEM ± 1.71%), which represented a significantly greater value than that of the Emb VE at 1.33% (SEM ± 0.99%) and ExE VE at 1.63% (SEM ± 0.89%) (χ^2 P=0.039). This indicates that just prior to the DVE movements, greater levels of cell division occur in the DVE compared to the rest of the VE, although effectively this equates to a relative increase in levels of mitosis of approximately 1% (Fig. 3A).

In the tilted group it was possible to assign an A-P axis, allowing us to readily test the presence of differential division. Five embryos from the tilted group were randomly chosen and the mitotic index for each quadrant was calculated. The anterior quadrant possessed a mean MI of 1.44% (SEM ± 0.62%), similar to the 1.43% (SEM ± 0.66%) calculated in the posterior quadrant (Fig. 3B).

Figure 3 – Distribution of mitotic nuclei within the VE at the onset of DVE movement

(A) The VE of six distal embryos were divided into three regions; DVE, Embryonic VE (Emb VE) and extra-embryonic VE (ExE VE). The mitotic index of each region was counted and represented as a percentage of the total number. Values equal actual mean mitotic index. (B) Five embryos from the tilted group were randomly selected. This time the VE was divided into anterior, posterior, lateral left and lateral right quadrants. The mitotic index of each quadrant was counted and represented as a percentage of the total number. Values equal actual mean mitotic index. (C+C') A 3D reconstruction of one of the two embryos that displayed a proliferative burst, defined as a region of the VE with 4 or more mitotic nuclei relative to the other VE quadrants. Mitotic nuclei (red), all nuclei (blue), DVE expressing GFP (green).

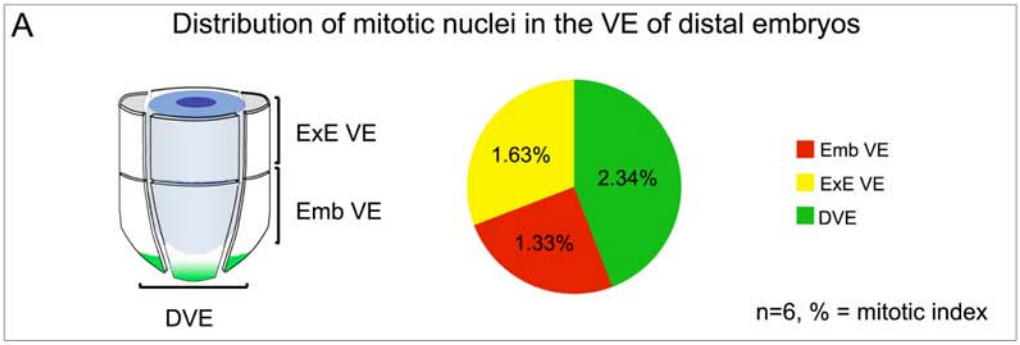
A
Distribution of mitotic nuclei in the VE of distal embryos
ExE VE
Emb VE
DVE
1.63%
2.34%
1.33%
Emb VE
ExE VE
DVE
n=6, % = mitotic index

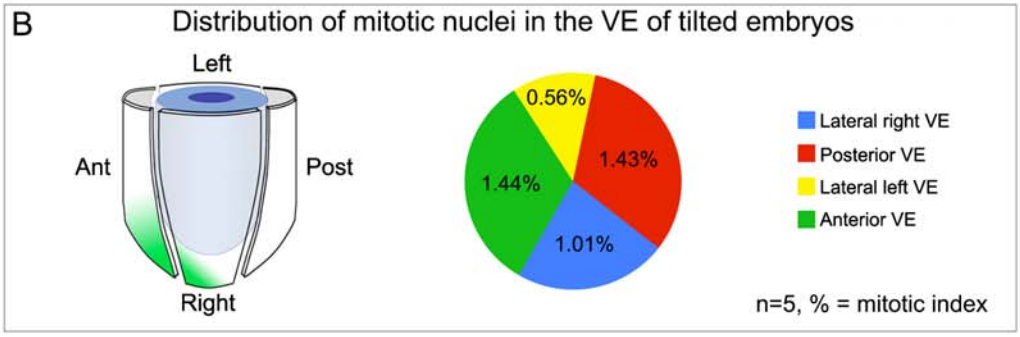
B
Distribution of mitotic nuclei in the VE of tilted embryos
Left
Ant
Post
Right
0.56%
1.43%
1.44%
1.01%
Lateral right VE
Posterior VE
Lateral left VE
Anterior VE
n=5, % = mitotic index

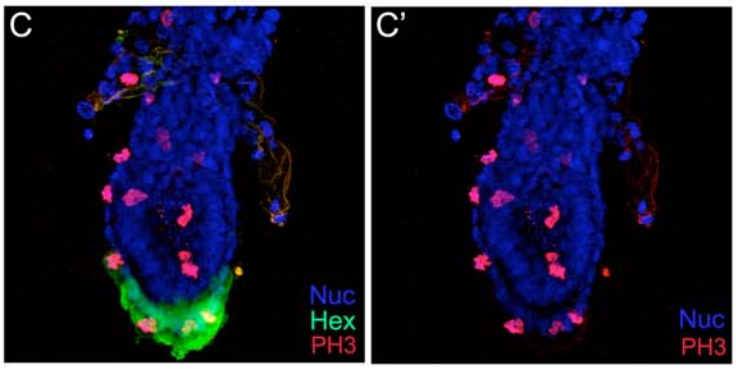
C
Nuc
Hex
PH3
C'
Nuc
PH3

The lateral left quadrant possessed an MI of 0.56% (SEM ± 0.55%), whilst the lateral right quadrant possessed an MI of 1.01% (SEM ± 0.65%). The distribution of cell division within the VE did deviate from the expected 25% in each quadrant assuming a random distribution (χ^2 P=0.02). This experiment indicates that although the greatest proportion of dividing cells fall along the anterior-posterior axis, there is no difference in the relative MI between the anterior and posterior regions of the VE. This supports the previous BrdU experiment.

3.2.4. No evidence of a proliferative burst during DVE movement

A proliferative burst, defined here as a region of VE with more than 4 mitotic nuclei relative to the other quadrants, was observed in 2/53 of the embryos in this study (Fig. 3B+B'). It was important to test if these embryos represented a random distribution of mitotic nuclei or were examples of synchronisation within the VE that were being missed in the majority of the embryos. To differentiate these two possibilities embryos were cultured in the mitotic inhibitor nocodazole at the time of DVE movements. Nocodazole disrupts microtubule formation, preventing sister chromatids from separating during mitosis. It was therefore possible to culture embryos in nocodazole to allow mitotic nuclei to accumulate. Any patterns of division such as a proliferative burst would be readily observable (Fig. 4A).

*Hex*GFP embryos were cultured for 4 hrs in 200 nM nocodazole (Fig. 4B) and stained with an antibody against phospho-Histone-H3 (Fig. 4C). Treated embryos showed a mean number of total dividing cells of 69.29 ± 18.48 compared to 22.44 ± 7.98 divisions in control embryos-in excess of a 3-fold difference (Fig. 4D).

Figure 4 – Testing for the presence of a proliferative burst in the VE at the onset of DVE movement

(A) Schematic representation of the approach taken (B) A freshly dissected *Hex*GFP embryo used for culture. (C) Cultured embryos were immunofluorescently stained with anti-PH3 and stacks taken at 5 μm intervals were acquired on the confocal microscope. Mitotic nuclei (red), all nuclei (blue), DVE expressing GFP (green). (D) Accumulated mitotic nuclei in the total embryo and VE were quantified in control (n=16) and treated (n=14) groups. Values indicate mean cell division ± SD. (E) Distribution of mitotic nuclei within the VE was determined. The VE was divided into anterior, posterior, lateral left and lateral right quadrants and the mitotic index of each quadrant was calculated. This has been represented diagrammatically showing the relative mitotic index values as a percentage. Actual mitotic index values can be found in the Results section.

A

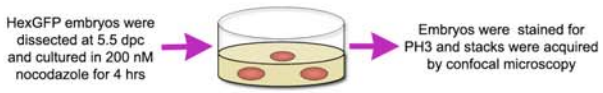

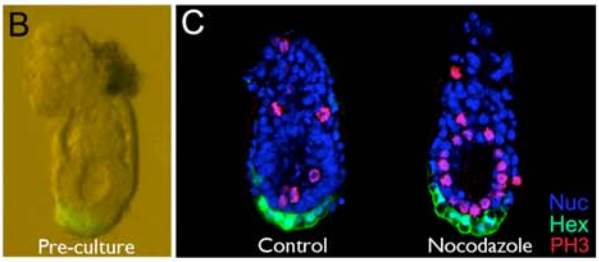

D

Group	Number	Total mean cell division +/- sd	VE mean cell division +/- sd
Control	16	22.44 +/- 7.98	3.13 +/- 2.70
200nM Nocodazole	14	69.29 +/- 18.48	10.79 +/- 3.29

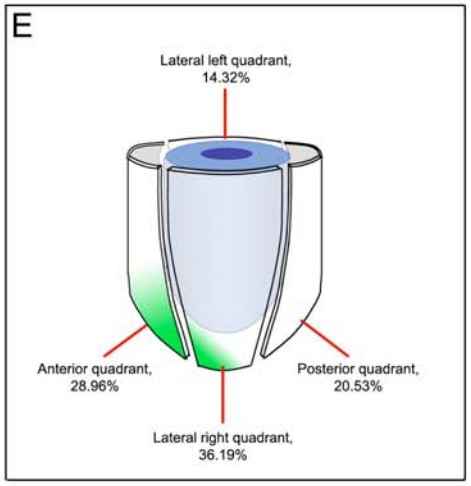

Within the VE, treated embryos showed a mean number of dividing cells of 10.79 ± 3.29 compared to 3.13 ± 2.70 divisions in control embryos, again displaying a similar fold increase in dividing cells (Fig. 4D).

Dividing nuclei were positioned in relation to the quadrant with which they resided and a mitotic index was calculated. The anterior quadrant in the treated group possessed an MI of 9.89% (SEM ± 3.08%) whilst the posterior quadrant had an MI of 7.01% (SEM ± 2.86%). The lateral right quadrant had an MI of 12.36% (SEM ± 1.54%) and the lateral left quadrant had an MI of 4.89% (SEM ± 2.16%) (Fig. 4E). These values represented a statistically significant deviation from the expected 25% per quadrant assuming a random distribution (χ^2 P=0.0119), although not in the A-P orientation (χ^2 P=0.2579). This indicates that reduced proliferation in the anterior VE relative to the posterior VE does not exist.

This experiment demonstrates that there is not a proliferative burst in the VE at the onset of DVE movement, though there exists a tendency for dividing cells to fall into the lateral right quadrant. The biological significance of this observation is not understood but possible implications will be discussed.

3.3. Discussion

This Chapter aimed to assess the levels of proliferation within the embryo at the time of DVE movements. More specifically, proliferation within the VE was analysed to test if differential proliferation along the future A-P axis exists, as had previously been reported (Yamamoto *et al.*, 2004). These experiments demonstrate that at the time of the DVE movements, low levels of cell division are present within the VE. Furthermore, no evidence of differential proliferation between the anterior and posterior quadrants of the VE were observed which argues against a differential proliferation model being responsible for directing DVE movements.

Proliferation levels in this study were assessed in two ways: BrdU incorporation and phospho-Histone-H3 (PH3) staining. The former is incorporated in the S phase of the cell cycle and therefore gives an indication of cycling cells, whilst the latter allows the direct observation of actively dividing cells in M phase. This distinction is important in light of the Srinivas *et al* (2004) study that used time lapse imaging of DVE movement to show anterior movement of the DVE to occur within a 4-5 hr period (Srinivas *et al.* 2004). Despite 70-80% of the VE cycling at the time of DVE movements as demonstrated by BrdU incorporation, only mitotic cells dividing in this time frame could feasibly contribute to a passive displacement by providing a mechanical force within the VE.

The VE was the least mitotically active tissue in the embryo at the time of DVE movements. In fact the proportion of mitotic nuclei actually decreased as the DVE was induced, and this low level was then maintained when the DVE movements

began. Considering the low mitotic index of the VE described here, as well as the long estimated cell cycle length of the VE in the literature (Snow, 1977; Lawson *et al*., 1991), cell division would have to be regionalised to contribute to the movement of the DVE.

BrdU-incorporation analysis suggested that the distribution of cycling cells in the VE did not show a marked or consistent regional difference between the anterior and posterior regions during the DVE movement. Analysis of the distribution of mitotic cells confirmed this finding; whilst a slightly greater proportion of dividing cells were distributed along the A-P axis, both sides displayed an almost identical mitotic index. To test if this static analysis had missed a transient proliferative burst, dividing cells were accumulated by treating embryos with a short pulse of nocodazole. This analysis demonstrated that not only did anterior and posterior VE possess a similar mitotic index, but that both populations cycled at similar rates. Taken together these results suggest that at the time of DVE movements, differential proliferation between the anterior and posterior VE does not exist.

In the literature a lack of regional bias within the VE can also be inferred by looking at clone doubling time in the endoderm at the time of DVE movements. When single cells from different regions of the VE were labelled and embryos cultured for 18-28.5 hrs, no significant difference in the number of clonal descendants between the injected regions could be found, further suggesting that no regional bias of proliferation within the VE exists at this stage (Perea-Gomez *et al.* 2001a).

These findings seemingly contradict with Yamamoto *et al*'s proposal that proliferation levels are greater in the posterior VE relative to the anterior VE at 5.7

dpc (Yamamoto *et al*., 2004). Embryos at 5.7 dpc correspond to the tilted group in this study, where BrdU-incorporation and the distribution of mitotic cells are shown not to exhibit a regional A-P bias. However, before DVE movements, Yamamoto *et al* describe BrdU-incorporation levels to be uniform throughout the VE (Yamamoto *et al*., 2004). Indeed 5.5 dpc embryos correspond to embryos in the distal group in this study where levels of BrdU-incorporated nuclei are similar in the DVE and flanking VE. Similarly, the percentage of mitotic nuclei throughout the VE is maintained to within 1% in a proximal-distal orientation; supporting the assertion that no regional proliferative bias exists prior to DVE movements. Reasons for this discrepancy at later stages between this work and that of Yamamoto *et al* (2004) have been addressed in the next Chapter.

Interestingly, although evidence of differential proliferation in an A-P orientation was not found, at later stages there did appear to be differential levels of dividing cells between the left and right VE quadrants. Analysis of mitotic nuclei distribution demonstrated that the lateral left quadrant had the smallest mitotic index compared to the lateral right quadrant. This difference was statistically significant, and was observed both in freshly dissected embryos, and those cultured in nocodazole suggesting that the observation might reflect a *bona fide* biological phenomenon.

Mechanistically, during the DVE movements, the radially symmetrical egg cylinder is converted to a bilaterally symmetrical egg cylinder (Perea-Gomez *et al.*, 2004; Mesnard *et al*., 2004). Perhaps the differential growth of these lateral regions of the VE is a consequence of the shifting morphology of the embryo.

This Chapter reports that during the initiation of DVE movements, no evidence for differential proliferation between the anterior and posterior VE could be found. It is therefore unlikely that the movement of the DVE can be attributed to a passive displacement mechanism.

Chapter 4 – The role of proliferation at 6.25 dpc

4.1. Introduction

Time lapse studies of DVE movements have shown that a pioneering population of cells reach the boundary between the epiblast and extra-embryonic ectoderm within 4-5 hrs (Srinivas *et al*., 2004). However much of the DVE remains distally localised over this period (Fig. 1A). This observation seems to be at odds with a passive displacement mechanism as the DVE/AVE does not appear to be moving as a coherent epithelial sheet. Yamamoto proposed that Nodal signalling is required in the VE, and the asymmetric inhibition of *Nodal* results in an imbalance in cell proliferation in the posterior versus anterior VE (Yamamoto *et al*., 2004). The previous Chapter could find no evidence for differential proliferation between anterior and posterior VE at the time of DVE movement. Moreover levels of cell division were simply not great enough to account for the passive displacement of these DVE cells.

It is clear that by 6.5 dpc, these distally located DVE cells have caught up with the pioneer cells, and the AVE forms a continuous tissue (Fig1. A). Is it possible that differential proliferation is the mechanism that drives the later movement of the DVE? This hypothesis is supported by the observations that; (a) movement of these cells occur over a longer time period (approximately 12 hrs), which considering the long cell cycle lengths is a more plausible time frame; (b) Yamamoto observed absence of BrdU incorporation in a large patch of the anterior VE between 6.0-6.5 dpc (Yamamoto *et al*., 2004). The overall process of DVE movement might therefore combine an initial, relatively fast migration of a pioneering DVE population, followed by a slower passive movement of the remaining DVE (Fig. 1B).

This Chapter aims to test this hypothesis in two ways. Firstly a detailed characterisation of proliferation levels in the VE of 6.25 dpc embryos will be assessed using BrdU incorporation and PH3 staining as markers of proliferation. If the hypothesis is robust then one would predict a decrease in proliferation within the anterior VE versus the rest of the VE. Secondly, the functional requirements of cell division, and in particular Nodal on the process of AVE movements will be tested. Embryo culture experiments will utilise a variety of cell cycle inhibitors and the Nodal inhibitor, SB-431542 to perturb proliferation. If the AVE fails to position appropriately during culture this will strengthen the hypothesis that differential proliferation might have a role in this process.

Figure 1 – Model of AVE movement incorporating active migration and differential proliferation

(A) Longitudinal confocal sections of three *Hex*GFP embryos at different stages of AVE movement. DVE/AVE is expressing GFP (green) and nuclei are in blue. The DVE initially tilts and migrates (5.5 dpc), although at 5.75 dpc some DVE cells persist at the distal tip. By 6.25 dpc, all DVE cells have moved to the anterior. (B) A schematic representation of a two wave model of DVE/AVE movement: At 5.5 dpc a pioneering population of DVE cells move anteriorwards in an active migratory process that is completed within 4-5 hrs. By 6.25 dpc all of the AVE is now situated on the anterior side of the embryo in a process involving passive displacement of the DVE cells by differential proliferation in the VE along the A-P axis.

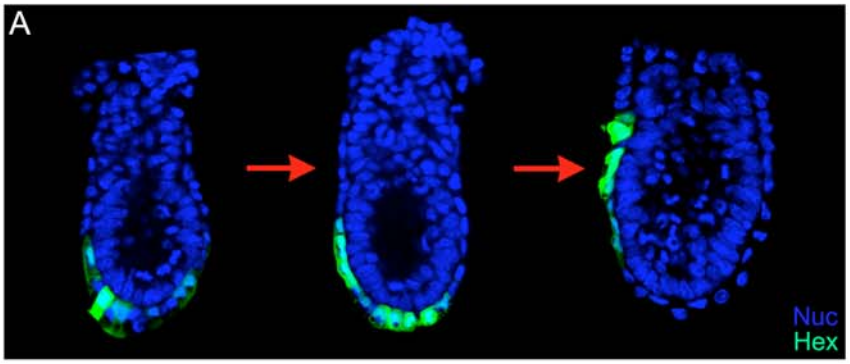
A
Nuc
Hex

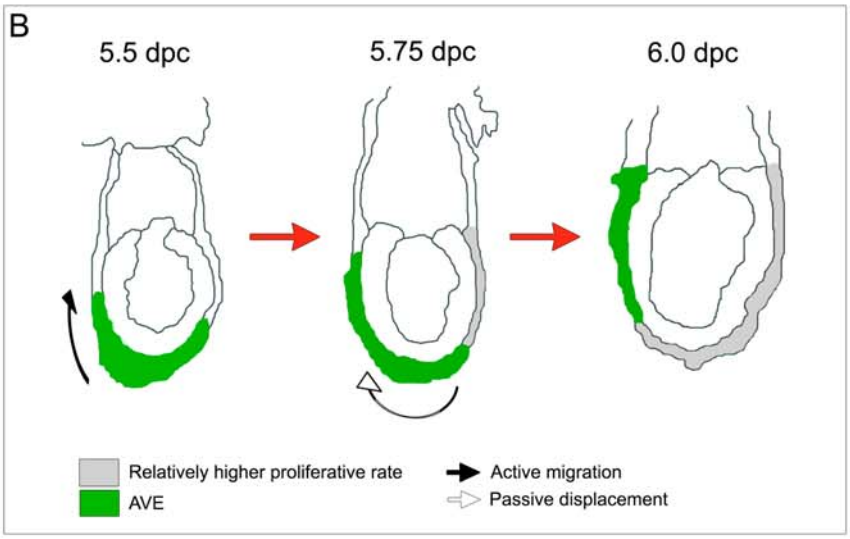
B
5.5 dpc
5.75 dpc
6.0 dpc
Relatively higher proliferative rate
AVE
Active migration
Passive displacement

4.2. Results

4.2.1. The AVE shows a similar incorporation index to the rest of the VE, but the success of BrdU detection is sensitive to the protocol used

To test for the presence of a non-BrdU incorporating patch of anterior VE cells, 6.25 dpc *Hex*GFP embryos were administered BrdU, which was subsequently detected immunofluorescently. Two different BrdU-labelling protocols were used.

Initially embryos were cultured in 20 μM BrdU for 1 hr. Culturing embryos was favoured over *in utero* administration as exposure time could be more accurately and reproducibly regulated. Whilst embryos cultured in the absence of BrdU produced no detectable signal (0/4 embryos, Fig. 2A+A'), those exposed to BrdU clearly showed nuclear staining within the VE, but was excluded from the bulk of the GFP-positive AVE (6/7 embryos, Fig. 2B+B'). One embryo displayed no BrdU-positive nuclei. This result supported Yamamoto's observations that no proliferation in the anterior VE exists, although the absence of any epiblast staining was cause for concern.

In an attempt to recapitulate this result using Yamamoto's reported protocol, pregnant *Hex*GFP mice were injected intraperitonealy with BrdU (50 mg/kg) and dissected 1 or 3 hrs thereafter. The staining protocol was exactly the same as before so the only difference was the method of BrdU administration. As expected, no staining was detected in non-injected mice (0/4 embryos, Fig. 2C+C'). In treated mice dissected after 1 hr BrdU staining could be detected in VE, but not AVE as seen in the previous culture experiment (3/3 embryos, Fig. 2D+D'). Surprisingly, when treated mice were dissected after 3 hrs, BrdU-positive nuclei were distributed throughout the VE including the AVE (10/10 embryos, Fig. 2E+E').

Figure 2 – BrdU incorporation at 6.25 dpc

*Hex*GFP embryos underwent three different BrdU staining protocols. All protocols involved immunofluorescent staining for BrdU (red) and GFP (green). Longitudinal sections were acquired on the confocal microscope at multiple levels. Nuclei are stained in blue and representative embryo sections are presented. (A-B') BrdU Culture - Protocol 1. Freshly dissected *Hex*GFP embryos were cultured in the absence of BrdU (A+A') or 20 μM BrdU for 1 hr (B+B'). (C-E') BrdU injection protocol. Pregnant *Hex*GFP mice were injected i.p. with BrdU at 50 mg/kg and dissected 1 or 3 hrs thereafter. Embryos underwent the same BrdU staining protocol as Protocol 1. (C+C') Negative control embryos dissected from a mother injected with PBS vehicle alone. (D+D') Treated embryos dissected 1 hr after BrdU injection. (E+E') Treated embryos dissected 3 hrs after BrdU injection. (F+F') BrdU Culture - Protocol 2. Freshly dissected *Hex*GFP embryos were cultured in 20 μM BrdU for 30 mins. (G) The number of BrdU-positive nuclei in the AVE and VE were counted and expressed as a percentage of the total cell number, referred to as the incorporation index. Three confocal sections were quantified per embryo (n=11), and mean values have been presented. Error bar = ± SEM. Scale bar 40 μm.

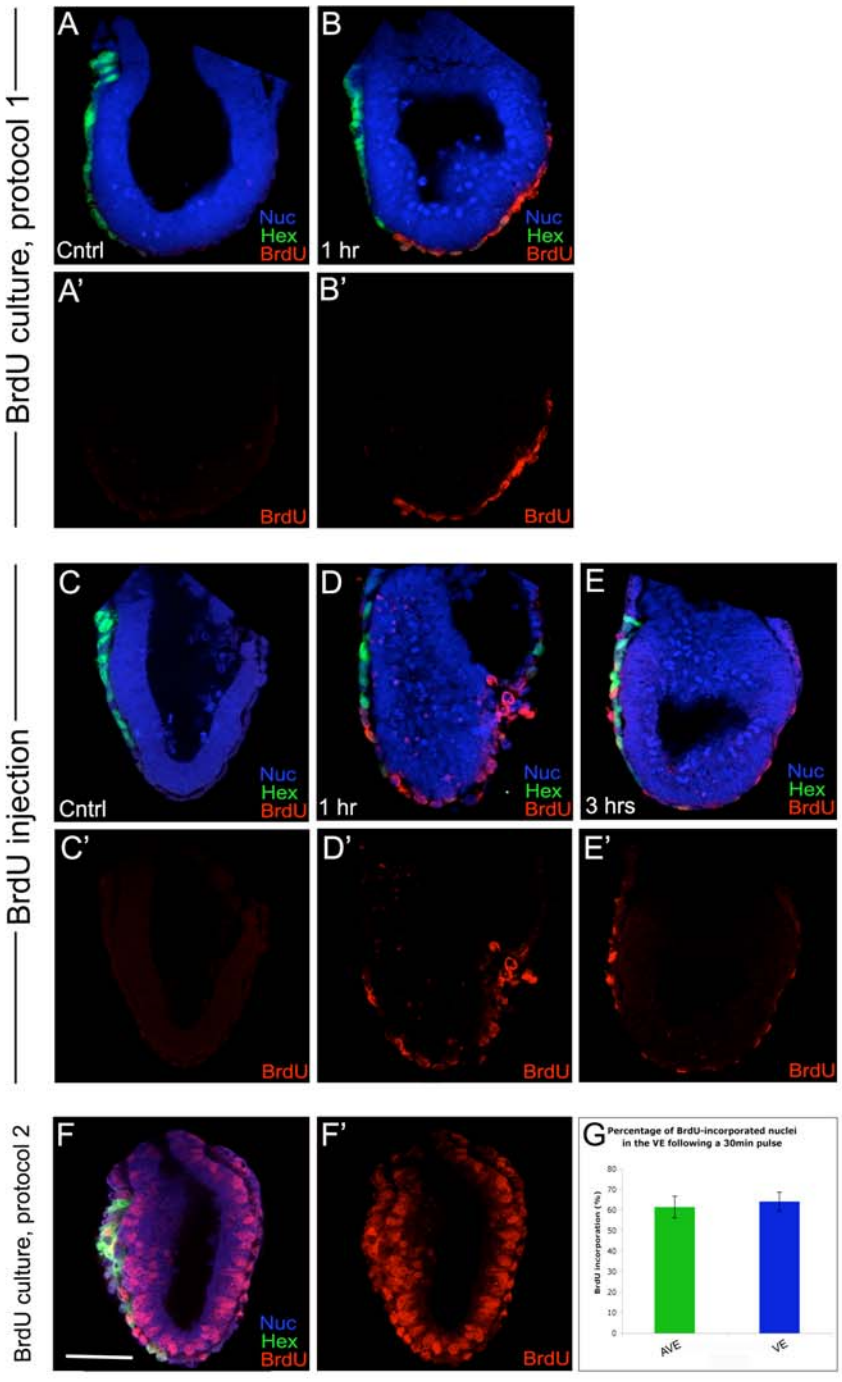
BrdU culture, protocol 1
A
Cntrl
Nuc
Hex
BrdU
B
1 hr
A'
B'
BrdU injection
C
D
E
3 hrs
C'
D'
E'
BrdU culture, protocol 2
F
F'
G
Percentage of BrdU-incorporated nuclei in the VE following a 30min pulse
BrdU incorporation (%)
AVE
VE

Again the epiblast failed to stain in any of the treated embryos strongly suggesting there were problems with this protocol. These might have consisted of a failure of the antibody to bind the BrdU epitope due to insufficient HCl treatment, insufficient permeabilisation of the tissue, a failure of BrdU incorporation into the underlying epiblast or a combination of these factors. Therefore another staining protocol was used; adapted from the Wholemount BrdU staining protocol found on the Rossant web page (www.sickkids.ca/rossant/protocols), and differing from the previous protocol in the BrdU antibody used, recipe of the permeabilisation solution and method of DNA denaturation.

Embryos were cultured in 20 μM BrdU for 30 mins. This time robust staining was detected throughout the epiblast and VE including the AVE (11/11 embryos, Fig. 2F+F'). As all nuclei had been counterstained it was possible to calculate the incorporation index, or the number of BrdU-positive nuclei expressed as a percentage of the total cell number. Several longitudinal sections were acquired at different levels for each embryo and BrdU-positive versus negative nuclei were quantified (Fig. 2G). The AVE had a mean incorporation index of 61.44% (n=11, SEM ± 5.25%), a similar value to the 64.13% obtained in the rest of the VE (n=11, SEM ± 4.61%) (Fig. 2G). This result does not support the differential proliferation model.

4.2.2. At 6.25 dpc the VE displays low levels of randomly distributed mitotic nuclei

The anterior and posterior VE display similar levels of proliferation at 6.25 dpc, with both VE populations having in excess of 60% of its cells in S phase. To confirm this finding it was necessary to use a different cell cycle marker. For this purpose an antibody against phospho-Histone-H3 (PH3) was used to mark M phase nuclei. If the

BrdU result was correct then it could be presumed that anterior VE would exhibit similar levels of mitotic nuclei as the rest of the VE.

Eleven *Hex*GFP embryos were dissected at 6.25 dpc and mitotic nuclei were stained. Complete stacks were taken through each embryo and reconstructed. The number of dividing cells within the epiblast and VE were calculated and the mean number expected to be found in each tissue expressed graphically (Fig. 3A+B). The epiblast had a mean value of 20.91 mitotic cells per embryo (n=11, SEM ± 2.23) whilst the VE had a total number of 3.91 mitotic cells per embryo (n=11, SEM ± 0.69). At this stage the epiblast contained 5-fold more dividing cells than the VE. However looking at the actual numbers of dividing cells is not useful as the numbers are not directly comparable. In order to directly compare the mitotic capacity of these two tissues it was necessary to determine what proportion of the total number in each tissue compartment were dividing, ie the mitotic index.

To calculate the mitotic index, 4-5 non-overlapping longitudinal sections from five randomly selected embryos were quantified with respect to the total number of cells and mitotic nuclei in the VE and epiblast. The epiblast had a mean mitotic index of 5.74% (n=5, SEM ± 0.84%) whilst the VE had a mean mitotic index of 1.56% (n=5, SEM ± 0.66%) (Fig. 3C). Despite the low proportion of mitotic cells in the VE it was important to assess their regional distribution within the tissue in relation to AVE position. It was possible that, although the proliferative capacity of the VE was low, synchronised mitotic nuclei could produce passive movement of an intervening tissue.

As *Hex*-expressing cells of the AVE expressed GFP, embryos could easily be divided into anterior, posterior, lateral left and lateral right quadrants.

Figure 3 – Distribution of mitotic nuclei within the VE and epiblast at 6.25 dpc

Freshly dissected *Hex*GFP embryos at 6.25 dpc were immunofluorescently stained with the M phase marker anti-phospho-Histone-H3. Complete stacks of 11 embryos were taken at 4 μm intervals by confocal microscopy. The number of mitotic nuclei were counted allowing the mean number of divisions in each tissue per embryo to be calculated. (A) Confocal section of a stained embryo divided into its tissue compartments: visceral endoderm (VE) and epiblast. Mitotic nuclei (red), all nuclei (blue), AVE domain expressing GFP (green). (B) Mean number of mitotic nuclei in the VE and epiblast were plotted (n=11). (C) Five embryos were randomly picked and the mitotic index was calculated in the epiblast and VE. The mitotic index (MI) was defined as the percentage of mitotic nuclei. 4-6 confocal sections were quantified per embryo and mean values have been presented. Error bar = ± SEM. (D) The VE from eight embryos was divided into anterior, posterior, lateral left and lateral right quadrants. The mitotic index in each quadrant was counted and represented as a percentage of the total number.

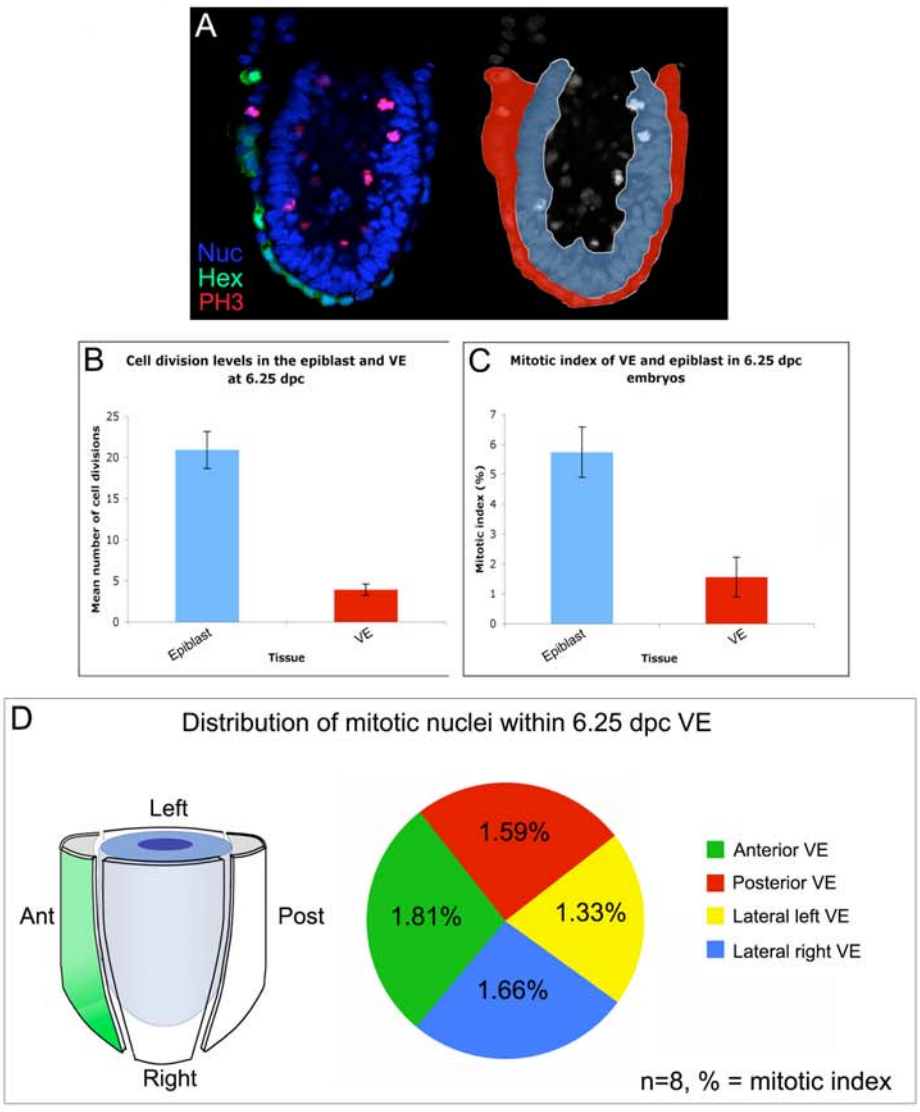
A
Nuc
Hex
PH3
B
Cell division levels in the epiblast and VE at 6.25 dpc
Mean number of cell divisions
25
20
15
10
5
0
Epiblast
VE
Tissue
C
Mitotic index of VE and epiblast in 6.25 dpc embryos
Mitotic index (%)
7
6
5
4
3
2
1
0
Epiblast
VE
Tissue
D
Distribution of mitotic nuclei within 6.25 dpc VE
Left
Ant
Post
Right
1.59%
1.81%
1.33%
1.66%
Anterior VE
Posterior VE
Lateral left VE
Lateral right VE
n=8, % = mitotic index

The number of dividing nuclei within the VE of eight embryos were scored in relation to which quadrant they were situated (Fig. 3D). The anterior quadrant had an MI of 1.81% (n=8, SEM ± 0.82%) compared to 1.59% (n=8, SEM ± 0.67%) in the posterior quadrant. The lateral left quadrant had an MI of 1.33% (n=8, SEM ± 0.65%), and the lateral right quadrant had an MI of 1.66% (n=8, SEM ± 1.12%) (Fig. 3D). The small variation in MI values between the quadrants was not statistically significant as assessed using a χ^2 test (P=0.756), and therefore suggested that the low levels of cell division within the VE show no regional bias. This finding conflicts with the differential proliferation model.

4.2.3. At 6.25 dpc the AVE and VE cycle at a similar rate

Phospho-Histone-H3 (PH3) staining on fixed embryos indicated that less than 2% of the VE population were mitotic. What could not be assessed using this 'molecular snapshot' approach was the dynamics of cell division within the VE. The increase in mitotic index over time during nocodazole-induced mitotic arrest was analysed to determine whether there was an identifiable difference between the cycling rates of AVE and VE. *Hex*GFP embryos were cultured in nocodazole from 0-5 hrs, and embryos were periodically removed and stained for PH3 (Fig. 4A). The mitotic index was calculated for each embryo at each time point by taking an average of 2-4 longitudinal sections per embryo acquired at different non-overlapping planes. The VE was divided into two populations: GFP-positive AVE and GFP-negative cells that constituted the rest of the VE. The percentage of cells in mitosis for both populations was plotted as a function of time in the presence of nocodazole (Fig. 4B).

Figure 4 – Testing for cell cycle differences in AVE and VE

Freshly dissected 6.25 dpc *Hex*GFP embryos were cultured in 200 nM nocodazole for 0, 0.5, 1, 1.5, 2, 3, 4 and 5 hrs (n=11, 6, 11, 8, 9, 10, 6 and 4 respectively). Cultured embryos were immunofluorescently stained withan anti-PH3 antibody and stacks taken at 5 μm intervals were acquired on the confocal microscope. (A) Representative longitudinal confocal sections of stained embryos at each time point. Mitotic nuclei (red), all nuclei (blue), AVE expressing GFP (green). (B) Accumulated mitotic nuclei in the AVE and VE were quantified in each embryo and the mean mitotic indices in both tissues were plotted as a function of length of nocodazole exposure. Error bars = ± SEM.

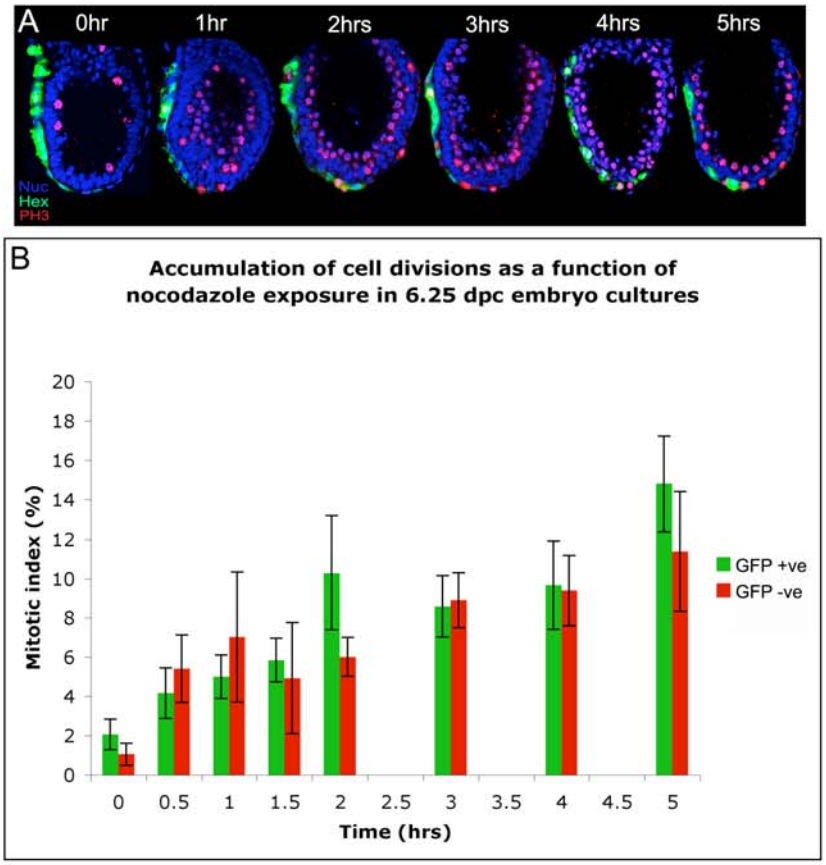
A
0hr
1hr
2hrs
3hrs
4hrs
5hrs
Nuc
Hex
PH3
B
Accumulation of cell divisions as a function of nocodazole exposure in 6.25 dpc embryo cultures
Mitotic index (%)
0
2
4
6
8
10
12
14
16
18
20
0
0.5
1
1.5
2
2.5
3
3.5
4
4.5
5
Time (hrs)
GFP +ve
GFP -ve

Non-cultured embryos had a mean basal mitotic index of 2.06% (n=11, SEM ± 0.77%) in the AVE compared to 1.06% (n=11, SEM ± 0.56%) in the rest of the VE. These values were similar to those obtained previously (Fig. 3C). Accumulation of mitotic nuclei was observed after only 30 mins. This initial mitotic arrest constituted the largest fold difference between the basal mitotic index, with 4.17% (n=6, SEM ± 1.29) of cells in the AVE dividing compared to 5.41% (n=6, SEM ± 1.71) in the remaining VE. The percentage of mitotic cells continued to increase modestly with nocodazole exposure up to the 5 hr timepoint.

The most important point to be derived from these results is that at no time did the mitotic index between the two populations significantly deviate from one another, and therefore the AVE cycles at a similar rate to cells in the rest of the VE.

4.2.4. *Nodal* is not required for proliferation in the VE, but is required for AVE movement

Taking together the BrdU-labelling experiments and PH3 staining, approximately 63% of the VE is either in S- or M-phase of the cell cycle. Yamamoto proposed that Nodal signalling was responsible for promoting cell proliferation in the VE and demonstrated that Nodal null embryos displayed a markedly impaired BrdU uptake in the VE and epiblast compared to wild type patterns of incorporation (Yamamoto *et al*., 2004). To test this hypothesis in our culture system, the potent inhibitor of the Nodal signalling pathway, SB-431542, was used to block Nodal signalling. Proliferation was assessed by BrdU uptake, whilst the position of the AVE was determined by using *Hex*GFP embryos.

Embryos were subdivided into three regions for analysis: the GFP-positive AVE, the GFP-negative VE and the epiblast.

Figure 5 – The effect of *Nodal* inhibition on proliferation and AVE movement

Freshly dissected 5.5 dpc embryos were cultured for 16 hrs in the chemical inhibitor of activin/nodal, SB-431542 at a concentration of 20 μM. 30 mins before fixation, embryos were transferred to another drop containing both SB-431542 and 20 μM BrdU and cultured for a further 30 mins. Embryos were immunofluorescently stained for BrdU and GFP and longitudinal sections were acquired on the confocal microscope at multiple levels. (A-B') Representative untreated embryos in longitudinal (A+A') and transverse (B+B') section showing robust BrdU incorporation (red) and correct AVE movement (green). All nuclei are labelled blue. (C-E') Treated embryos in longitudinal (C+C', E+E') and transverse (D+D') section. Notice the low number of BrdU-positive nuclei within the epiblast compared to the VE and ExE. (E+E') Approximately one third of treated embryos had VE detaching from the epiblast. (F) Treated (n=14) and non-treated (n=11) embryos were divided into three populations: epiblast, AVE and VE. The number of BrdU-positive nuclei in each population was quantified and expressed as a percentage of the total cell number, referred to as the incorporation index. Bars = ± SEM. Scale bar 40 μm.

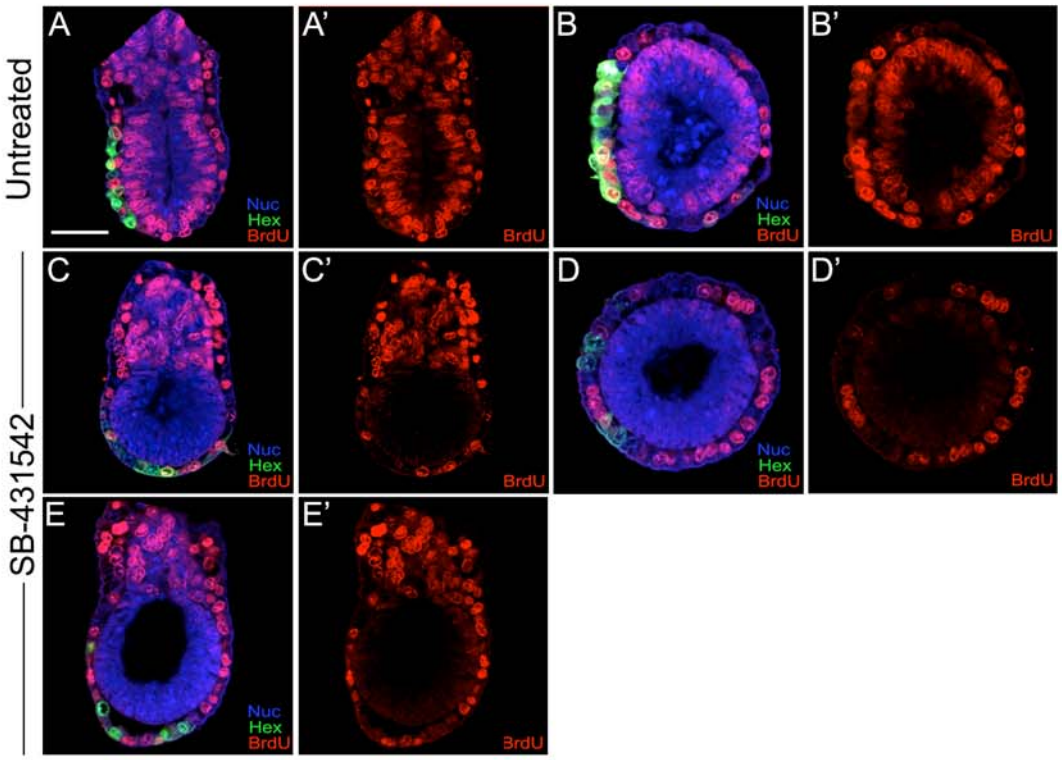
Untreated
SB-431542
A
A'
B
B'
C
C'
D
D'
E
E'
Nuc
Hex
BrdU
BrdU

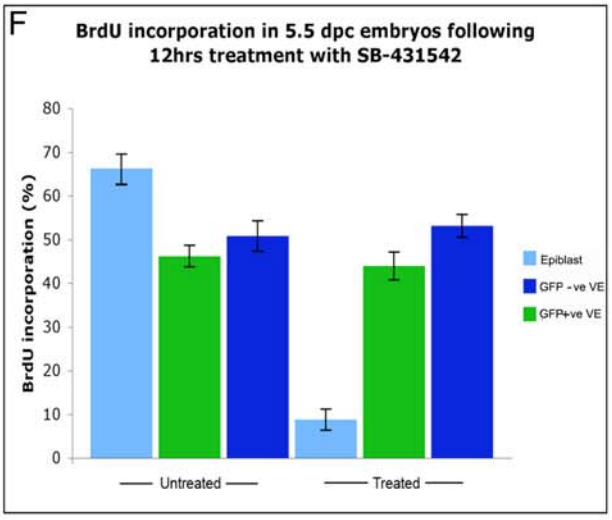
F
BrdU incorporation in 5.5 dpc embryos following 12hrs treatment with SB-431542
BrdU incorporation (%)
80
70
60
50
40
30
20
10
0
Untreated
Treated
Epiblast
GFP - ve VE
GFP+ve VE

An incorporation index was calculated for each sub-population per embryo and these were pooled together. Untreated embryos consistently displayed staining throughout all of its tissues including the epiblast and VE as previously observed (compare Fig. 5 A-B' with Fig. 2F+F'). The AVE had moved anteriorly in all embryos (11/11), with GFP-positive cells reaching the boundary between the epiblast and extra-embryonic ectoderm. The mean incorporation index of the AVE was 46.23% (n=11, SEM ± 2.49%), similar to the rest of the VE at 50.85% (n=11, SEM ± 3.47%). The epiblast displayed the greatest incorporation index at 66.26% (n=11, SEM ± 3.25%) reflecting the shorter cell cycle length in this tissue (Fig. 5F).

Embryos treated with SB-431542 showed a very striking expression of BrdU incorporation; whilst the extra-embryonic ectoderm and VE displayed staining of a similar intensity and distribution as non-treated controls, the epiblast was almost completely devoid of any BrdU-positive nuclei (Fig. 5C-D'). Furthermore, the AVE failed to move appropriately and was either located at the distal tip of the epiblast (10/14 embryos), or very weakly on one side of the embryo (4/14 embryos). Five embryos also displayed a VE that had detached from the epiblast, presumably a consequence of the non-proliferating epiblast failing to maintain physical contact with the overlying VE (Fig. 5E+E'). This was compounded by the fact that VE was still dividing, with AVE possessing an incorporation index of 43.97% (n=18, SEM ± 3.17%) and the remaining VE, 53.12% (n=14, SEM ± 2.60%) (Fig. 5F). The epiblast had a mean incorporation index of just 8.78% (n=14, SEM ± 2.43)-a huge decrease compared to non-treated controls.

This experiment suggests that proliferation within the VE is *Nodal*-independent, but that Nodal signalling is required for anterior movement of the AVE.

4.2.5. Disrupting cell division throughout the embryo perturbs AVE movement

Low levels of randomly distributed mitotic cells in the VE suggest that differential proliferation is unlikely to play a role in passively displacing the AVE. However the previous experiment demonstrated that by blocking Nodal signalling and consequently proliferation in the epiblast, the AVE was unable to move. This suggests that proliferation in the epiblast may be required for AVE movements. To test this possibility, embryos at the time of DVE movement were cultured overnight in cell cycle inhibitors. Genistein and Okadaic acid were used, previously shown to halt the cell cycle during G_2-M transition (DiPaola, 2002; Alexandre *et al*., 1991). Nocodazole was also used, shown to block cells in M phase. Mitotic arrest was confirmed by staining treated embryos for PH3 and looking for a change in numbers of mitotic nuclei compared to non-treated controls.

Embryos cultured without (Fig. 6A+A'), or in the presence of 15 nM Okadaic acid (Fig. 6B+B') displayed a typical distribution of PH3-positive nuclei. Furthermore the AVE had moved to an anteriorwards position in the vast majority of embryos (23/23 control embryos; 10/13 15 nM Okadaic acid-treated embryos). However, embryos cultured in 20 nM Okadaic acid showed a loss of dividing nuclei (Fig. 6C+C'). Furthermore, GFP-expressing AVE cells remained in a distal position (5/24 20 nM Okadaic acid-treated embryos had a correctly positioned AVE), despite embryos maintaining a grossly normal morphology. A similar outcome was found when embryos were cultured in the cell cycle inhibitor, Genistein. Non-treated control embryos (Fig. 6 D+D') and embryos treated with 50 μM Genistein (Fig. 6E+E') displayed indistinguishable PH3 staining, and the AVE had moved anteriorwards in the vast majority of embryos (19/20 control embryos; 9/11 15 nM 50 μM Genistein-treated embryos).

Figure 6 – The effects of blocking cell division on AVE movements

Freshly dissected 5.5 dpc *Hex*GFP embryos were cultured for 16 hrs in the cell cycle inhibitors Okadaic acid (15/20 nM), Genistein (50/100 μM) and Nocodazole (50/200 nM). Pictures of embryos were acquired on a fluorescent microscope post-culture and then immunofluorescently stained for mitotic nuclei using an anti-PH3 antibody. Stained embryos were re-acquired on the confocal microscope, with longitudinal sections captured at multiple levels. Mitotic nuclei (red), AVE (green), all nuclei (blue).

(A-C') Okadaic acid culture: (A) Non-treated control embryos after culture, (A') and PH3 staining; (B) Embryos treated with 15 nM Okadaic acid after culture, (B') and PH3 staining; (C) Embryos treated with 20 nM Okadaic acid after culture, (C') and PH3 staining. Notice the absence of PH3-positive nuclei and distal AVE at this concentration. (D-F') Genistein culture: (D) Non-treated control embryos after culture, (D') and PH3 staining; (E) Embryos treated with 50 μM Genistein after culture, (E') and PH3 staining; (F) Embryos treated with 100 μM Genistein after culture, (F') and PH3 staining. Notice the reduction of PH3-positive nuclei and distal AVE at this concentration. (G-I) Nocodazole culture: (G) Non-treated embryos after culture; (H) Embryos treated with 50 nM Nocodazole; (I) Embryos treated with 200 nM Nocodazole. Notice the distal AVE in embryos cultured at 200 nM Nocodazole. Scale bar 50 μm for A,B,C,D,E,F,G,H, and I; 35 μm for A',B', C' D' E' and F'.

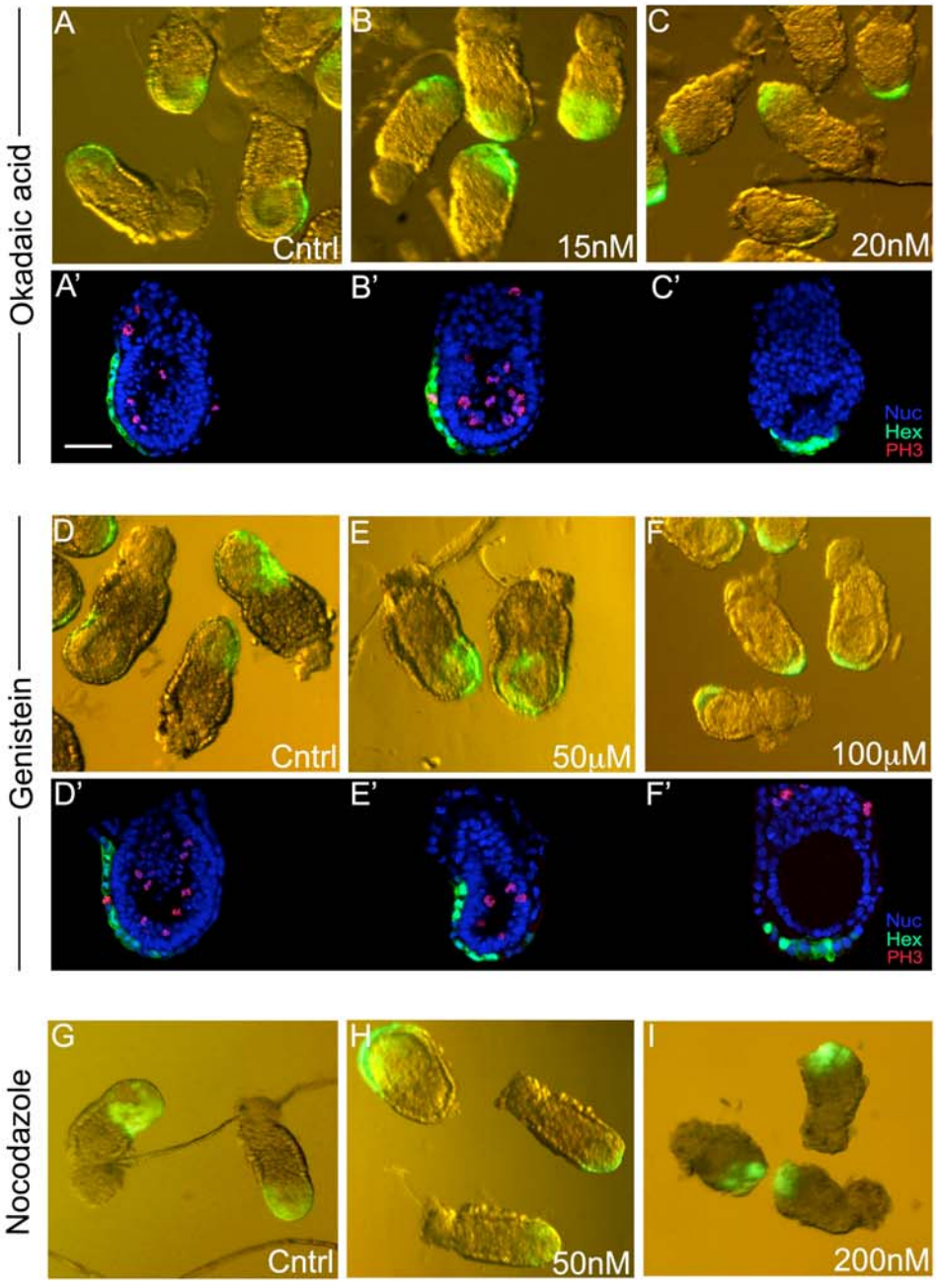
Okadaic acid
A
Cntrl
B
15nM
C
20nM
A'
B'
C'
Nuc
Hex
PH3
Genistein
D
Cntrl
E
50μM
F
100μM
D'
E'
F'
Nuc
Hex
PH3
Nocodazole
G
Cntrl
H
50nM
I
200nM

When the concentration of Genistein was increased to 100 μM, embryos not only displayed a sharp decrease in the levels of mitotic cells, but the AVE failed to move in 17/18 embryos analysed (Fig. 6F+F'). Once again post-cultured embryos displayed a grossly normal morphology compared to non-treated cultured controls.

Finally embryos were treated overnight in nocodazole. Embryos treated with 50 nM nocodazole appeared indistinguishable from non-treated control embryos, with the AVE moving appropriately in all embryos (12/12 control embryos; 7/7 50 nM nocodazole-treated embryos). (Fig. 6G+H). However at a concentration of 200 nM the AVE failed to move in 16/18 treated embryos (Fig. 6I), as previously described (Section 3.2.4, Fig. 4). At this concentration the number of mitotic nuclei increased by approximately 3-fold compared to non-treated controls.

Unlike embryos cultured in either Okadaic acid or Genistein, embryos cultured overnight in 200 nM nocodazole appeared morphologically atypical, with the absence of a well defined pro-amniotic cavity and a rough-looking VE. This suggested that 200 nM nocodazole treatment had other secondary effects on embryo development, most likely affecting such processes as intracellular transport and cell movement due to the static nature of the microtubule network. Nevertheless, it appears that by inhibiting cell division throughout the embryo, AVE movements were perturbed. This strengthens the argument that division within the epiblast is necessary for these movements to be successfully completed.

4.3. Discussion

This Chapter aimed to test the hypothesis that differential proliferation in the VE could contribute in later AVE movements by passive displacement. Two approaches were used to address this possibility. Firstly, a detailed analysis of proliferation within the VE was undertaken, using BrdU incorporation and PH3 staining as cell cycle markers. *Hex*GFP embryos allowed visualisation of the AVE, thus the proliferative capacity of the AVE versus the rest of the VE could be compared. Secondly a variety of embryo culture experiments were performed to demonstrate the functional significance of perturbing cell division on AVE movements.

Initially, BrdU incorporation was used to assess differences in the proliferative capacity of the AVE and surrounding VE. When Protocol 1 was used, the AVE was initially shown to be unable to incorporate BrdU 1 hour after BrdU administration. Staining using this protocol was restricted to the VE and excluded from the epiblast which was surprising as the epiblast was shown by PH3 staining to comprise a 3-fold greater mitotic index than its surrounding VE. When the length of time between BrdU exposure and fixation was increased to 3 hours the AVE became stained, but still no staining was observed in the epiblast, suggesting that the uptake of BrdU may vary between cell types. Furthermore, the published staining pattern of a 6.5 dpc transverse section, using the same protocol, showed no AVE staining and weak or no epiblast staining (Yamamoto *et al*., 2004). These observations suggest that when using Protocol 1, certain cell types may be refractory to the uptake of BrdU.

When Protocol 2 was used, BrdU incorporation was found throughout all tissues of the embryo, including the epiblast. Furthermore the AVE was shown to have a similar percentage of BrdU-incorporated nuclei compared to the rest of the VE. This observation conflicted with the differential proliferation model and indicated that by altering the protocol, BrdU incorporation could be detected in all cell types of the early post-implantation embryo.

The lack of differential proliferation between the AVE and the rest of the VE as assessed by BrdU incorporation, was confirmed by examining the distribution of mitotic nuclei. Analysis of mitotic cells in 6.25 dpc embryos was reminiscent to the levels and distribution observed in tilted embryos, 18 hrs earlier (see previous Chapter). The mitotic index continued to remain at under 2%, whilst the proportion of mitotic nuclei in the VE between all quadrants displayed no regional bias, further contradicting the differential proliferation hypothesis, and adding strength to the validity of the refined BrdU staining protocol.

Further evidence that the AVE and VE display no differences in their relative cell cycle rates comes from taking a stathmokinetic approach using nocodazole. The rate of mitotic arrest between the AVE and the VE did not significantly deviate from one another at any length of nocodazole exposure, suggesting that the two populations contained similar numbers of mitotic cells, with comparable cell cycle lengths.

Yamamoto and colleagues proposed that Nodal signalling promotes cell proliferation in the VE and differential proliferation within this tissue is due to differential Nodal signalling (Yamamoto *et al*., 2004). They demonstrated that by injecting embryos with a *Nodal* expression vector, cell proliferation was stimulated, whilst injection of

the Nodal antagonists *Lefty1* and *Cerl* resulted in the inhibition of proliferation. Moreover the DVE tended to move away from the side where proliferation was stimulated and towards the side where proliferation had been inhibited (Yamamoto *et al*., 2004).

Although differential proliferation was not observed in this study between the anterior and posterior VE, it is still possible that Nodal signalling is required for the migration of AVE cells. To investigate this, Nodal signalling was blocked in embryos by treating with the small molecular inhibitor SB-431542. When this was done, two interesting observations could be made. Firstly whilst levels of proliferation were maintained in the VE and ExE compared to non-treated controls, levels in the epiblast were drastically reduced. Secondly, the AVE failed to move to the anterior of the embryo in SB-431542 treated embryos. These results suggest that (a) Proliferation within the VE and ExE occurs through a Nodal-independent mechanism, whilst proliferation in the epiblast requires Nodal signalling; (b) Nodal signalling is required for the movement of the AVE.

If AVE movement does require an interaction with the epiblast in a *Nodal*-dependant manner what could be the possible mechanism? The epiblast is always closely apposed to the overlying VE during AVE movements and presumably the epiblast must proliferate to maintain this contact. If this contact is disrupted, for example by blocking proliferation in the epiblast, this tissue interaction will be affected. The epiblast might be responsible for ‘stretching’ the VE to allow room for migratory behaviour. Indeed in a proportion of the SB-431542 treated embryos the VE could be

seen to detach from the epiblast. Furthermore, if the epiblast failed to maintain contact with the VE then reciprocal signalling interactions could be perturbed.

The failure of AVE to move as a result of decreased Nodal signalling is recapitulated in a number of mutants. Loss of the Nodal co-factor *Cripto* causes a failure of the AVE to rotate at 6.0 dpc (Ding *et al*., 1998). A similar phenotype is seen in some $Nodal^{\Delta 600/-}$ embryos where the autoregulatory enhancer (ASE) is removed (Norris *et al*., 2002). The ASE is essential for transcription of *Nodal* in the VE and epiblast. However this paper demonstrated it was the strength of Nodal signalling in the epiblast specifically that was crucial in activating *Nodal* targets in the VE, resulting in normal morphogenesis including AVE rotation (Norris *et al*., 2002).

The results presented here suggest that one of the roles of Nodal in the epiblast is to promote proliferation, and thereby maintain contact with the VE necessary to activate *Nodal* targets in the VE. Mesnard *et al*. (2006) proposed that Nodal signalling is required to promote the growth of the egg cylinder by increasing cell division in the epiblast. Our finding are consistent with this hypothesis, although the fact that levels of proliferation within the VE are unaffected when Nodal signalling is inhibited does not agree with Yamamoto *et al*'s observations. Why are these findings at odds with one another?

One possible explanation could come from the method used in the Yamamoto *et al* (2004) manuscript to modulate the levels of Nodal signalling in the 5.5 dpc embryo. In the study, Nodal or its antagonists were transfected into embryos by injecting liposomes into the VE that containing the appropriate vectors and Lipofectamine 2000. It is possible that these liposomes also transfected epiblast cells and therefore affected Nodal signalling in this tissue. Alternatively, it is possible that

changing the levels of Nodal expression in the VE at 5.5 dpc might have affected the fate of these VE cells, and this in turn altered their migratory behaviour.

To understand if proliferation in the epiblast is necessary for AVE movements, embryos were cultured in three different cell cycle inhibitors: Okadaic acid, Genistein and Nocodazole. The AVE failed to move when proliferation was inhibited with all three inhibitors, suggesting that reducing cell division throughout the embryo can affect AVE positioning. Due to the different mechanisms of action of the inhibitors it seems unlikely that the inability to affect AVE movement is attributable to secondary effects. Moreover, considering the difference between levels of proliferation in the epiblast compared to the VE, it seems reasonable to assume that the failure of AVE movements could be due specifically to the lack of division in the epiblast. For example, by impairing the interactions with the juxtaposed VE. This observation strengthens the argument that one of the roles of Nodal is to promote proliferation in the epiblast and thus maintain contact with the VE.

This report indicates that differential proliferation within the VE is unlikely to be the mechanism used by the embryo to contribute to later AVE movements. However evidence presented here suggests that *Nodal*-dependant proliferation in the epiblast might be implicated in AVE movements by maintaining contact with the closely apposed VE.

Chapter 5 – Creation of the Hexd mouse line

5.1. Introduction

The AVE is an essential extraembryonic tissue required for the correct specification of the A-P axis. Its secretion of various Wnt and Nodal antagonists are responsible for restricting these signalling molecules towards the posterior of the embryo, thereby determining the site of primitive streak formation (reviewed in Perea-Gomez *et al.*, 2001b; Beddington and Robertson, 1999). Furthermore, its role in initiating anterior character to the underlying ectoderm has been confirmed genetically and embryologically as discussed in the Introduction (reviewed in Martinez-Barbera and Beddington, 2001). However does this tissue, or that of its precursor, the DVE, have additional roles? Using the very methods that have enabled us to understand its function, they have also hindered the ability to completely answer the question. This statement seems counterintuitive, but both microsurgical ablation studies and analysis of mutant embryos carry with them inherent drawbacks.

To date, two studies have used microsurgical ablation to address the function of the AVE (Thomas and Beddington, 1996) and DVE (Miura and Mishina, 2007). The latter study reported that DVE ablation was successful in 50% of the embryos, with an additional 10% failing to grow when cultured due to damage of the epiblast (Miura and Mishina, 2007). Microsurgical ablation experiments require that embryos be cultured *in vitro*, meaning embryos are able to recapitulate their *in vivo* situation for a limited period of time. Additionally, it is difficult to accurately remove just AVE tissue, resulting in either partial ablation and/or the mechanical disruption of surrounding tissue, not to mention the presumable regeneration of the ablated tissue. These factors make results difficult to interpret and subtle functions unable to detect.

Gene targeting studies in mice has allowed the identification of many genes and signalling molecules required for head formation (Beddington and Robertson, 1999). Although this approach enables the role of a particular gene to be identified, it does not address the role of the tissue as a whole. Furthermore, genetic compensation by other genes may complicate the analysis of gene knock-out experiments. For example when *Lefty1*, *Cerl* or *Dkk1* are knocked-out, correctly patterned embryos still develop (Meno *et al.*, 1998; Shawlot *et al.*, 2000; Mukhopadhyay *et al.*, 2001). Even in *Cerl* and *Lefty1* compound mutants, only a proportion show patterning defects (Perea-Gomez *et al.*, 2002), while the others are rescued, possibly due to ectopic expression of *Lefty2* functionally compensating (Yamamoto *et al.*, 2004). This indicates that a degree of redundancy exists within the AVE, and that any residual AVE function in a mutant embryo might not be revealed using this approach.

This Chapter describes a novel approach aimed to find additional functions of the AVE and DVE precursors. In an attempt to circumvent the problems associated with microsurgical ablation experiments, the strategy involves the generation of a mouse line in which diphtheria toxin A (DTA) has been knocked-in to the *Hex* locus by homologous recombination. DTA is activated by Cre-mediated recombination, causing *Hex*-expressing cells, such as those in the AVE/DVE, to be genetically ablated *in vivo*. The generation of this mouse line, and a primary characterisation of genetically ablated mutants is described.

5.2. Results

5.2.1. A genetic strategy for AVE/DVE ablation

To address the function of the AVE as a whole and *in vivo*, this project aimed to carry out a targeted ablation of the AVE. Diphtheria toxin A (DTA) was knocked-in to the *Hex* locus by homologous recombination in embryonic stem (ES) cells. DTA catalyses the inactivation of elongation factor 2, resulting in termination of protein synthesis and apoptosis of the target cell (Collier, 1975; 2001). In positively targeted ES cells, DTA is under the control of the endogenous *Hex* regulatory sequence. However, the toxin is initially rendered inactive due to the presence of a sequence rich in termination codons, the reversed *Pgk-neo* gene, between its ATG codon and the rest of the DTA open reading frame (a similar strategy is described by Lee *et al.*, 2000). This sequence is flanked by *loxP* sites and can therefore be deleted by Cre-mediated recombination (Nagy, 2000). When these mice (*Hex-XneoX*-DTA) are crossed with mice harbouring Cre recombinase, *Pgk-neo* is excised and DTA can be translated resulting in the death of *Hex*-expressing cells (Figure 1).

5.2.2. Characterisation of positively targeted clones

The *Hex-XneoX*-DTA targeting construct produced two positively targeted ES cell clones, named HDS118 and Hexd32. A probe 5' external to the site of recombination was used to confirm integration into the *Hex* locus (Fig. 2A). In addition, a DTA probe confirmed the targeting vector had integrated once, excluding the possibility of the random integration of multiple copies (Fig. 2B). To functionally test the efficiency of the *Hex-XneoX*-DTA ablation, HDS 118 ES cells were transiently transfected with the Cre expression plasmid Turbo-Cre and cultured.

Figure 1 - Strategy for ablation of the AVE.

The first line represents genomic organization in the *Hex* locus. The boxes represent the 4 *Hex* exons. The second line is the targeting vector that will be used to generate the knock-in of the diphtheria toxin (DTA) into the *Hex* locus. The first ATG is the *Hex* ATG. The second ATG is the DTA's ATG. This ATG is separated from the rest of the DTA coding region by the positive selection cassette (the neomycin gene driven by the pgk promoter-*Neo*) flanked by LoxP sites (black triangles). The orientation of transcription of the selection cassette is inverse to the orientation of the transcription of DTA. This cassette contains translational stop codons in all reading frames. An IRES sequence is present upstream of the DTA ATG to ensure correct initiation of the translation of the DTA. The third line represents the locus of the knock-in allele after homologous recombination of the targeting vector. ES cells containing this recombination event will be used to generate mice that carry this *Hex* allele. The fourth line represents the result of excising the selection cassette (containing the translational stop codons) by Cre recombination. This event will place the DTA under the control of the *Hex* regulatory sequences and will therefore allow the activation of the DTA in the *Hex* expressing cells of the AVE. The approximate position of the 5' probe for Southern blot analysis has been indicated.

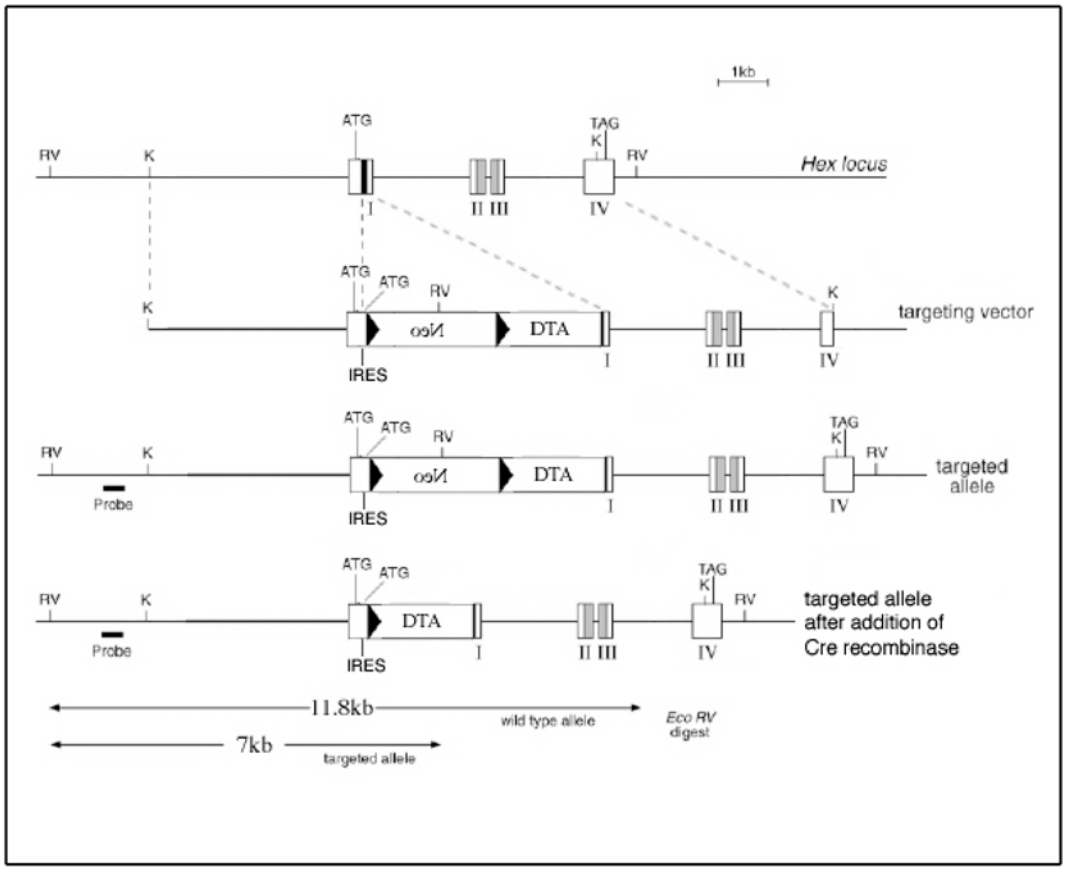
1kb
ATG
TAG
K
RV
K
RV
Hex locus
I
II III
IV
ATG
ATG
RV
K
K
targeting vector
Neo
DTA
IRES
I
II III
IV
ATG
ATG
RV
TAG
K
RV
RV
K
targeted
allele
Probe
Neo
DTA
IRES
I
II III
IV
ATG
ATG
TAG
K
RV
RV
K
targeted allele
after addition of
Cre recombinase
Probe
DTA
IRES
I
II III
IV
11.8kb
wild type allele
Eco RV
digest
7kb
targeted allele

Figure 2 – Molecular and functional characterisation of positively targeted ES cell clones

ES cell genomic DNA was digested with *EcoRV* and hybridised with either a 5' probe (A) or DTA probe (B) to confirm the presence of the targeted allele. (C) HDS 118 ES cells were plated at low density in a 6-well plate and transiently transfected with Cre expression plasmid. Negative control wells underwent the transient transfection procedure with a GFP-expressing plasmid. One day after transfection cells were cultured in medium without LIF to encourage differentiation. Scale bar 20 μm (D) Mouse genomic DNA derived from chimeric Hexd32 x 129sv cross was digested with *EcoRV* and hybridised with a 5' probe to confirm germline transmission of the targeted allele. (E) Standard PCR using genomic DNA derived from Hexd32 x β-actin Cre cross demonstrating proof of principal by Cre-mediated excision of the *Pgk-neo* cassette.

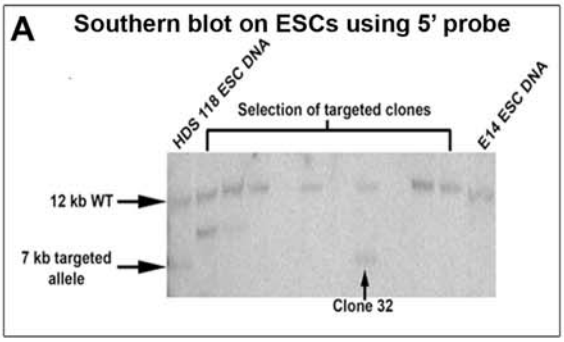
A
Southern blot on ESCs using 5' probe
HDS 118 ESC DNA
Selection of targeted clones
E14 ESC DNA
12 kb WT
7 kb targeted allele
Clone 32

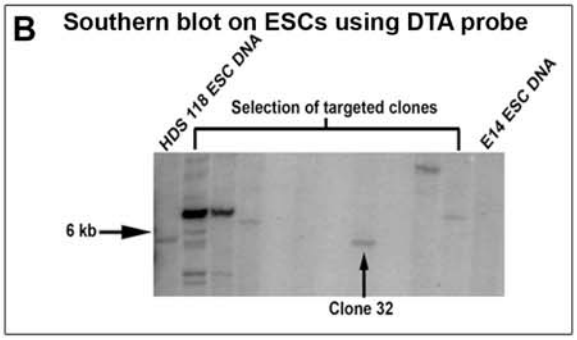
B
Southern blot on ESCs using DTA probe
HDS 118 ESC DNA
Selection of targeted clones
E14 ESC DNA
6 kb
Clone 32

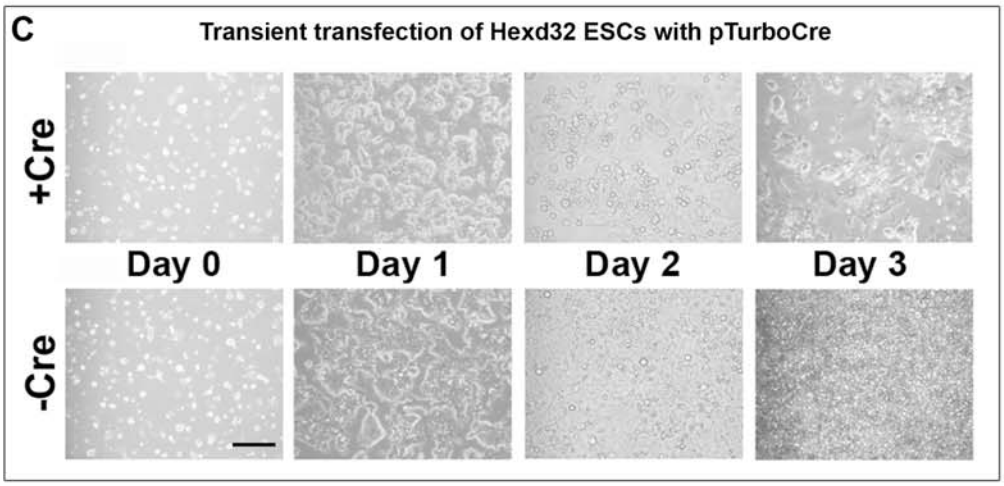
C
Transient transfection of Hexd32 ESCs with pTurboCre
+Cre
-Cre
Day 0
Day 1
Day 2
Day 3

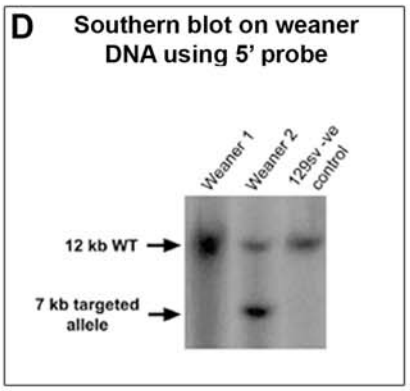
D
Southern blot on weaner DNA using 5' probe
Weaner 1
Weaner 2
129sv -ve control
12 kb WT
7 kb targeted allele

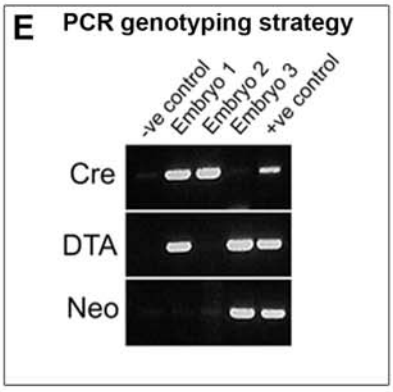
E
PCR genotyping strategy
-ve control
Embryo 1
Embryo 2
Embryo 3
+ve control
Cre
DTA
Neo

Non-Cre transfected cells were transfected with a GFP-expressing plasmid to control for cell death due to the transfection procedure. One day post-transfection there appeared to be little difference between the Cre-treated and non-treated cells, with similar levels of confluency and cell morphology (Fig. 2C). At day 2 the non-Cre transfected control cells were confluent whilst large cell-free patches were apparent in the Cre-treated cells. In addition, there were a greater number of floating dead cells in these wells compared to non-treated wells. On day 3 this pattern continued; non-treated cells were now over-confluent whilst Cre-treated cells continued to show large cell-free patches and increased cell death. Although this experiment used a transient transfection and therefore not all cells would be expected to die, these results indicate that cell death could occur as a result of Cre-mediated recombination, demonstrating that the DTA ablation system was functional *in vitro*.

5.2.3. The ablation system is functional *in vivo*

Both targeted clones were karyotyped, and injected into C57BL6 blastocysts by the CSC Microinjection facility. This resulted in 10 chimeras, 7 of which transmitted the targeted allele through their germline as confirmed by PCR and Southern blot analysis (Fig. 2D). Mice heterozygous for the unrecombined *Hex-XneoX*-DTA allele were viable and fertile (Table 1), and the mouse line was named Hexd32.

To generate embryos expressing the activated *Hex-DTA* allele, Hexd32 mice were crossed to either β-actin Cre or to female Sox2 Cre mice. Both lines express Cre ubiquitously from the 1-2 cell stage enabling recombination in all cells (Lewandoski *et al.*, 1997; Hayashi *et al.*, 2003, Vincent *et al.*, 2003). Standard PCR analysis confirmed that in compound Hexd32/+; β-actin Cre/+ heterozygotes, recombination was successful as demonstrated by excision of the *Pgk-neo* cassette and the

subsequent failure to produce a PCR product (Fig. 2E). To test the timing and efficiency of ablation *in vivo*, the *Hex*-expressing domain was assessed by wholemount *in situ* hybridisation (WISH) and/or *Hex*GFP expression at different embryonic stages. The *Hex*GFP domain of Hexd32/+; β-actin Cre/+ mutants was indistinguishable from non-activated embryos at 5.5 dpc (Fig. 3A+A'). However, one day later at 6.5 dpc, the majority of *Hex* transcript in the AVE had been abolished (Fig. 3B+B'; n=3/4,). This result was confirmed by a large reduction in the *H*exGFP domain in mutants from both Cre lines (Fig. 3C+C'; n=2/2; G+G'), suggesting that ablation was taking place between 5.5-6.5 dpc. Morphologically, activated and non-activated embryos were indistinguishable, although the efficiency of ablation appeared greater in the β-actin Cre cross in which fewer residual GFP-postive cells remained. For this reason, subsequent analysis of mutant embryos was done exclusively from crosses with the β-actin Cre mouse line. A reduction in the *Hex*-expressing domain was not observed in littermate embryos from any other genotype, indicating the specific nature of the genetic ablation.

By 7.5 dpc, the *Hex*-expressing population of the definitive endoderm was observed in DTA-active mutants, with *Hex* transcripts and GFP expression spanning a similar-sized domain and comparable levels to non-activated embryos (Fig. 3D-E'; n=4/4,). The inability to differentiate activated mutants from non-activated embryos by comparing the pattern of *Hex* transcript was also apparent at 9.5 dpc, with all embryos showing robust expression in the liver, thyroid and intersomitic regions (Martinez-Barbera *et al.*, 2000) (Fig. 3F+F'; n=5/5). The failure of the *Hex*-expressing population to diminish between 7.5-9.5 dpc suggested that the efficiency of ablation was in some way impaired.

Figure 3 – *In vivo* characterisation of the genetic ablation system

(A-F') Embryos at various stages derived from Hexd32 x β-actin Cre cross. (A+A') Fluorescence/brightfield overlay of 5.5 dpc mutant and non-mutant embryos. DVE is expressing *Hex*GFP (green) and can be seen in both embryos. (B+B') At 6.5 dpc, mutant embryos display vastly reduced *Hex* transcript domain as assessed by wholemount *in situ* hybridisation (WISH) analysis (red arrow), compared to non-mutant counterparts. (C+C') Ablation of *Hex*-expressing population is confirmed by a reduction in *Hex*GFP (green) domain in mutants at 6.5 dpc (red arrow). (D+D') WISH analysis of *Hex* at 7.5 dpc indicates that the *Hex*-expressing cells of the anterior definitive endoderm (ADE) are present in mutant embryos. (E+E') Fluorescence/brightfield overlay of 7.75 dpc mutant and non-mutant embryos show that *Hex*GFP-expressing cells are present in the ADE and blood islands (BI). (F+F') WISH analysis of *Hex* at 9.5 dpc indicates that the *Hex*-expressing cells of the liver (orange arrow), thyroid (blue arrow) and intersomitic regions (yellow arrow) are present in mutant embryos. (G+G') Fluorescence/brightfield overlay of 6.5 dpc mutant and non-mutant embryos derived from Hexd32 x Sox2 Cre (maternal) cross. Red arrow points to the AVE domain which shows are marked reduction compared to non-mutant littermates. Scale bar 40 μm in A+A'; 60 μm in B-C', G+G'; 80 μm in D+D'; 90 μm in E+E'; 400 μm in F+F'.

Wildtype
Hexd x βactin Cre
HexGFP
Hex
HexGFP
Hex
HexGFP
Hex
HexGFP
A
A'
B
B'
C
C'
D
D'
E
E'
F
F'
G
G'
5.5 dpc
DVE
6.5 dpc
AVE
6.5 dpc
AVE
7.5 dpc
ADE
ADE
7.75 dpc
BI
9.5 dpc
6.5 dpc
Sox2 Cre

Genetic background	Total number of offspring	Genotype				Chi-square test results	
		Expected number of DTA/+	Observed number of DTA/+	Expected number of +/+	Observed number of +/+	χ^2	P value
CD1	28	14	11	14	17	1.29	0.26
129sv[a]	87	43.5	44	43.5	43	0.01	0.91

Table 1. Frequency of genotypes among offspring from Hexd × Wildtype crosses. Distribution of offspring among genotypes does not deviate from the expected Mendelian frequency ($P > 0.05$). [a] indicates that Hexd heterozygotes were backcrossed twice with 129sv mice.

Hexd × β-actin Cre		Genotype				Chi-square test results	
Stage (dpc)	Total	Expected number of mutants	Observed number of mutants	Expected number of non-mutants	Observed number of non-mutants	χ^2	P value
5.5	20	5	6	15	14	0.26	0.60
6.5	180	45	40	135	140	0.74	0.39
7.5	41	10.25	15	30.75	26	2.94	0.09
9.5	81	20.25	17	60.75	64	0.70	0.40
11.5	41	10.25	7	30.75	34	1.37	0.24
Weaning	156	39	18	117	138	**15.08**	**0.0**

Table 2. Genotyping results of Hexd × β-actin Cre crosses at various embryonic stages and weaning age. Observed numbers did not significantly deviate from the expected Mendelian frequencies at any embryonic stage analysed ($P > 0.05$). However, there was a highly significant deviation between observed numbers of weaned mutant mice and the expected number ($P < 0.01$, **bold font**). This indicates that mutants were dying between 11.5 dpc and weaning age.

Hexd × Sox2 Cre		Genotype				Chi-square test results	
Stage (dpc)	Total	Expected number of mutants [a]	Observed number of mutants	Expected number of non-mutants	Observed number of non-mutants	χ^2	P value
6.5	11	5.5	4	5.5	7	0.82	0.37
7.5	18	9	8	9	10	0.22	0.64
9.5	13	6.5	7	6.5	6	0.08	0.78

Table 3. Genotyping results of Hexd × Sox2 Cre crosses at 6.5-9.5 dpc. Observed numbers did not significantly deviate from the expected Mendelian frequencies at any embryonic stage ($P > 0.05$). [a] indicates that when the Sox2 Cre allele is maternally inherited, all progeny possess Sox2 Cre irrespective of the genotype. Therefore mutants are expected at 1:1 instead of the typical 1:3 ratio.

Indeed between 5.5-11.5 dpc, the frequency of mutants did not significantly deviate from the expected Mendelian ratio ($P > 0.05$) when Hexd32 mice were crossed with either Cre line (Table 2+3), indicating that the ablation system was not embryonically lethal between this period. However this analysis would not detect the loss of a small number of mutants that might die in this period due to the ablation system.

Interestingly, the frequency of observed mutants at weaning age from the β-actin Cre cross did significantly deviate from expected Mendelian ratios ($P < 0.01$, Table 2). The ablation system was responsible for embryonic death in approximately 54% of mutant embryos between 11.5 dpc and weaning age. The significance of the surviving mutants will be discussed in Section 6.1.

5.2.4. The decrease in *Hex*-expressing cells is accompanied by a reduction in other AVE markers

The onset of *Hex* expression in the DVE at 5.0 dpc, followed by its disappearance by 6.5 dpc, suggests the ablation system *in vivo* was taking no longer than 36 hours to kill *Hex*-expressing cells. To test how the loss of *Hex*-expressing cells of the AVE affected the expression of other AVE genes, DTA-activated mutants were characterised by *in situ* hybridisation analysis at 6.5 dpc.

Five markers were used to characterise the AVE; *Cerl*, *Sfrp5*, *Lefty1/2*, *Lim1* and *Dkk1*. With the exception of *Dkk1*, in a proportion of mutants the expression domains of these markers showed variable degrees of reduction, ranging from a total absence of transcript (*Cerl*, n=1/11; *Lefty1/2*, n=2/5; *Lim1*, n=1/10), to partial reduction in both intensity of transcript and the size of expression domain (*Cerl*, n=2/11; *Sfrp5*, n=1/3; *Lim1*, n=4/10) (Fig. 4A-D').

Figure 4 – Characterisation of the AVE domain in 6.5 dpc mutant embryos

The expression of a selection of AVE markers was assessed in DTA-activated mutant embryos derived from the Hexd32 x β-actin Cre cross. (A+A') *Cerl*, (B+B') *Sfrp5*, (C+C') *Lefty1/2* (*Lefty1* expression in AVE, *Lefty2* expression in primitive streak (PS)), (D+D') *Lim1* (in AVE and PS), (E+E') *Dkk1*. Red arrows point to reduction of transcript expression in AVE. (F-G') TUNEL staining showing variation in apoptotic nuclei irrespective of genotype. Scale bar 60 μm.

Wildtype
Hexd x βactin Cre
Cerberus
Sfrp5
Lefty1/2
Lim1
Dkk1
TUNEL
A
A'
B
B'
C
C'
D
D'
E
E'
F
F'
G
G'
AVE
PS

The remaining mutants showed normal transcript expression as compared to non-activated littermates, which equated to approximately 56% of the mutants showing an absence or perturbed patterning of the AVE. Interestingly, there was a tendency for a small patch of expression to remain in the anterior region of the AVE (Fig. 4B'+C'). This observation was supported by analysis of the anterior AVE marker *Dkk1*, whose domain was unaffected in all mutants observed (Fig. 4E+E'; n=7/7). This suggests that after 5.5 dpc, *Dkk1*-expressing cells do not co-express with *Hex*-expressing cells of the AVE, unlike the other markers analysed whose co-expression can be inferred by the variable reduction in their expression patterns.

To test if the anterior portion of the AVE was recalcitrant to ablation, mutants were TUNEL stained, as DTA-induced death had been previously shown to go through an apoptotic pathway (Collier, 2001). The prediction was that AVE would be distinguishable by a high density of apoptotic nuclei, whilst the anterior portion would show a relative reduction. In fact levels of apoptosis varied so much throughout the embryonic ectoderm and VE, irrespective of genotype, that this experiment was unable to address the specific question, though intriguingly in all embryos apoptosis was almost exclusively absent from the extra-embryonic ectoderm (Fig. 4F-G'; n=31).

5.2.5. The ability to correctly position the primitive streak is impaired in a proportion of mutants

It is well documented that one of the roles of the AVE is to correctly position the site of primitive streak formation (reviewed in Perea-Gomez *et al.*, 2001b; Beddington and Robertson, 1999). To test the ability of DTA-activated mutants to establish a primitive streak, markers of this tissue were analysed by WISH analysis at 6.5-7.5

dpc. At 6.5 dpc over half of the mutants showed some form of AVE patterning defect as described in the previous section. Despite this fact, the *Lefty2* expression domain in *Lefty1/2 in situs* was always present in mutants towards one side of the proximal epiblast as expected, albeit at a reduced intensity compared to non-activated littermates (Fig. 4C+C'; Fig. 5A+A'; n=4/5). When *Lim1* transcript was absent from the AVE at 6.5 dpc, a reduced and/or patchy expression domain in the epiblast was still evident (Fig. 4D+D'; n=5/10). This indicates that the AVE still has partial function and is able to restrict the site of primitive streak formation; although the reduced epiblast expression suggests the AVE might be further responsible for enhancing expression of primitive streak genes once their position has been determined.

One day later at 7.5 dpc, robust expression of *T* and *Lim1* within the primitive streak was clear in the vast majority of embryos (Fig. 5B+B'; C+C'). In 1/6 mutant embryos the expression of *T* was absent from the anterior of the primitive streak (Fig. 5B''). A further 10% (n=2/20) of mutant embryos displayed a severely retarded phenotype characterised by a much smaller, rounder morphology than non-mutant counterparts and the inability to form a primitive streak as judged by the absence of either *T* or Lim1 expression (Fig. 5B'''+C''). This suggests that ablating the AVE results in variable patterning defects of the primitive streak in a proportion of mutant embryos.

Figure 5 – Characterisation of primitive streak formation in mutant embryos

The expression of a selection of primitive streak markers was assessed in DTA-activated mutant embryos derived from the Hexd32 x β-actin Cre cross. (A+A') *Lefty1/2* expression at 6.5 dpc appears to be lost in the AVE (*Lefty1*) but detected in the PS (*Lefty2*, red arrow) at low levels compared to non-mutant embryos. (B-B''') *T* expression at 7.5 dpc showing either no change in primitive streak formation (B'), absence of anterior primitive streak domain (B'', orange arrows), or failure to induce any *T* expression (B'''). (C-C'') *Lim1* expression at 7.5 dpc showing either no change in primitive streak formation (C'), or a failure to induce *Lim1* expression (C''). Scale bar 50 μm in A+A'; 60 μm in B-C''.

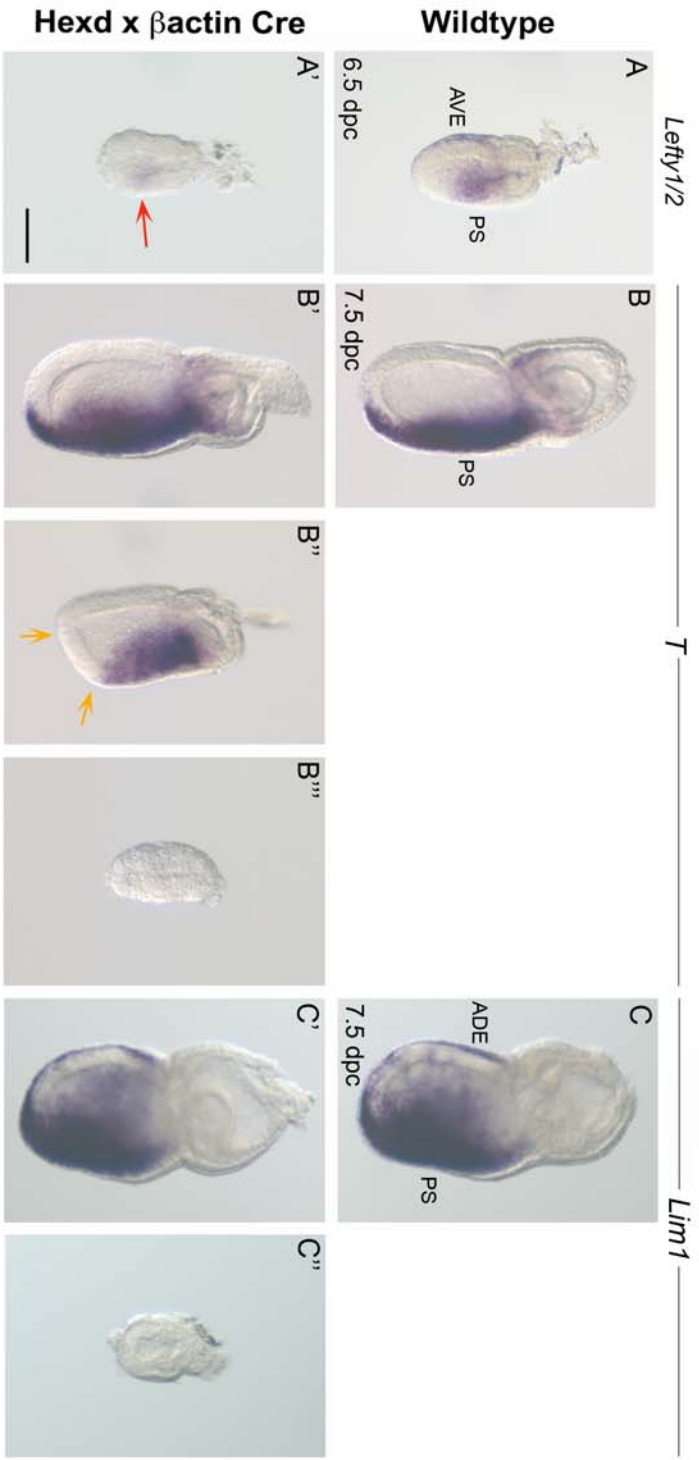
Wildtype
Hexd x βactin Cre
Lefty1/2
T
Lim1
A
A'
6.5 dpc
AVE
PS
B
B'
B''
B'''
7.5 dpc
PS
C
C'
C''
7.5 dpc
ADE
PS

5.3. Discussion

This Chapter described a novel approach to address the function of the AVE. To achieve this, a Cre inducible form of Diphtheria toxin fragment A (DTA) was targeted to the *Hex* locus, one of the earliest expressed AVE genes, by homologous recombination in ES cells. The timing of this ablation system was tested by crossing mice harbouring the targeted allele to mouse lines ubiquitously carrying Cre recombinase, allowing the kinetics and efficiency of *in vivo* ablation to be determined.

Ablation of *Hex*-expressing cells was evident by 6.5 dpc using both Sox2 Cre and β-actin Cre lines, as determined by the loss of *Hex* transcript and/or a *Hex*GFP domain in mutant embryos. By 7.5 dpc the *Hex*-expressing domain was re-established in the anterior visceral endoderm although it is unclear whether this corresponded to *Hex*-expressing cells of the AVE, ADE or both populations. Nevertheless, by 11.5 dpc the frequency of observed mutants significantly deviated from the expected Mendelian ratio (Table 2). Interestingly the 56% of mutants at 6.5 dpc exhibiting an absence or mispatterning of the AVE corresponds nicely to the 54% of mutants that fail to survive to weaning age. This suggests that the ablation system is effective at reducing or abolishing the AVE in over half of the mutants at 6.5 dpc, and that these mutants die by 11.5 dpc.

Given that *Hex* is expressed in the primitive endoderm of the blastocyst (Thomas *et al*, 1996; Chazaud and Rossant, 2006; Mesnard *et al*., 2006), and that both Cre mouse lines used should induce recombination in all cells of the embryo at or before the blastocyst stage (Lewandoski *et al*., 1997; Hayashi *et al*., 2003, Vincent *et al*., 2003), perhaps it seems surprising that *Hex*-expressing cells are not ablated even before DVE

induction. Furthermore, the fact that mutants are not dying by 11.5 dpc, and are actually indistinguishable from non-mutant littermates, indicates that not all *Hex*-expressing cells are being ablated as one would expect a phenotype at least as severe as that observed in *Hex* null mice (Martinez-Barbera *et al*., 2000b). Both of these points suggest that the efficiency of the ablation system is in some way compromised.

This ablation system relies firstly on the Cre-mediated recombination of *loxP* sites, followed by the transcription, translation and cytotoxic action of DTA in *Hex*-expressing cells. Therefore the onset of ablation is dependant on multiple steps that are likely to be influenced by factors such as the type of Cre line used, and the nature of the cells type to be ablated. Certainly a variation in the time taken for ablation to occur is evident in the literature; Ivanova proposed a minimum time lapse of around 16-20 hours between the onset of *Cre* expression and cell ablation in their system (Ivanova *et al*, 2005) whilst Brockschneider reported a longer time lapse in their system of 36-48 hours (Brockschneider *et al*, 2005). The efficiency of our system seems to be partially dependant on the type of Cre line used. Specifically the proportion of *Hex*-expressing cells that remained in 6.5 dpc mutants using Sox2 Cre was greater than when β-actin Cre was utilised.

Moreover, despite β-actin Cre being reportedly a ubiquitous deleter from the 1-2 cell stage (Lewandowski *et al*., 1997), in our hands this appears not to be the case. When β-actin Cre mice were crossed to the ROSA26 LacZ reporter line (Soriano, 1999), double heterozygous blastocysts at 3.5 and 4.5 dpc displayed salt and pepper distribution of blue and white cells throughout their tissues, indicating that ubiquitous recombination was not achieved at this stage (see Appendix II). This might impair the

efficiency of the ablation system if these non-recombined cells happened to express *Hex*.

It is also likely that the time taken for ablation to take place can be overcome in a rapidly dividing cell population. This factor is unlikely to apply to cells of the AVE which divide very slowly (this thesis; Snow, 1977; Lawson and Pederson, 1987) but will could in the *Hex*-expressing population of the ADE which divide more rapidly (Lawson *et al.*, 1991; Snow, 1977). Another possibility is that the targeting of DTA into the genome has induced some form of silencing of this allele. The ability of a genome to epigenetically silence an allele which harbours foreign DNA is well documented and includes methylation of the affected region (Doerfler *et al*., 2001; Muller *et al*., 2001). This might account for those mutants that are born with a seemingly 'activated' DTA allele.

Despite impairment in the efficiency of the ablation system, the loss of *Hex*-expressing cells was associated with a reduction or absence of AVE markers in approximately 56% of mutant mice at 6.5 dpc. Intriguingly the expression of *Dkk1* was unaffected in all mutant embryos, suggesting that *Hex*- and *Dkk1*-expressing cells comprise discrete cell populations. Variation in the expression of other AVE markers following ablation indicates transient overlap of *Cerl*, *Lefty1*, *Lim1* and *Sfrp5* in *Hex*-expressing cells, supporting the idea that the AVE comprises a mixed population of cells.

The ability of a mispatterned/ablated AVE to correctly position the primitive streak was tested by analysing the expression of posterior genes between 6.5-7.5 dpc. In 10% (2/20) of mutants at 7.5 dpc a primitive streak was unable to form. This

corroborated to the 11% (4/36) of mutants that showed a complete absence of AVE expression at 6.5 dpc, suggesting that the whole AVE is required to initiate primitive streak formation. Other mutants showed reduced expression levels of primitive streak markers or a loss of its anterior portion. Together these results indicate that ablation of the AVE is responsible for a variety of primitive streak patterning defects; reiterating the importance of this tissue in A-P axis establishment. The relationship between the AVE and primitive streak formation has been further explored in the next Results chapter.

Chapter 6 – Characterisation of Hexd^{act} embryos

6.1. Introduction

The previous Chapter described the creation and primary characterisation of a mouse line in which DTA had been knocked-in to the *Hex* locus. This approach of Cre-mediated activation of DTA has been extensively utilised to address the *in vivo* function of specific cell lineages or tissues. Tissue-specific promoters have been used to drive DTA expression for the ablation of skeletal muscle (Grieshammer *et al*, 1998), cardiac myocytes (Lee *et al*, 1998), lens fibre cells in the ocular lens (Breitman *et al*, 1990) and the neural roof plate (Lee *et al*, 2000). Alternatively, DTA has been knocked into the ubiquitously expressed ROSA26 locus allowing the ablation of specific cell populations depending upon tissue-specific Cre expression (Ivanova *et al*., 2005; Wu *et al*., 2005; Brockschnieder *et al*., 2004).

In the context of the Hexd32 knock-in mouse line, this system allowed Cre-inducible expression of DTA in cells that express *Hex*, therefore allowing specific ablation of this cell population. In mutants harbouring the knock-in allele and Cre recombinase, 56% displayed patterning defects in the AVE, 11% of which showed a total loss of AVE markers. This corresponded to a similar percentage of mutants that were unable to initiate gastrulation. A further proportion of mutants displayed patchy and/or weak expression of primitive streak markers. Despite this fact, about half of the mutants survived and were born. These mice presumably possess the recombined allele (Hexd^{act}), but for some reason were not susceptible to the effects of ablation. This Chapter describes the phenotypic analysis of embryos derived from Hexd^{act} mice.

6.2. Results

6.2.1. Hexd^{act} embryos display two Classes of phenotype depending on the time of ablation

Hexd^{act} embryos were divided into two classes of phenotype by virtue of their morphology and timing of the loss of *Hex* and/or *Hex*GFP expression. Class I mutants were grossly morphologically normal at 5.5 dpc (Fig. 1A+A'), but by 6.5 dpc confocal analysis indicated a disorganised epiblast structure and a failure of complete proamniotic cavitation (Fig. 1B-B''). Class I mutants at 6.5 dpc showed a reduced or absent *Hex*GFP domain (Fig. 1B-B''; n=5/5) and an absence of *Hex* transcript (Fig. 1C+C'; n=6/6) indicating that *Hex*-expressing cells of the AVE are ablated between 5.5-6.5 dpc. However, Class I embryos were able to gastrulate and at 7.5 dpc the *Hex* domain of expression in the anterior definitive endoderm was present and indistinguishable from non-mutants (Fig. 1D-E'). The observed numbers of mutants did not deviate from the expected number between 5.5-8.5 dpc (Table 1+2).

Class II embryos were rare (4.4% of the mutants, n=14), and distinguishable at 5.5 dpc by a small and rounded egg cylinder (Fig. 1A+A''). These mutants had an absence of *Hex*GFP-expressing cells in the DVE at this stage, suggesting that these cells had been ablated prior to 5.5 dpc (Fig. 1A''). Class II mutants were observed at 7.5 dpc (n=8), but were unable to gastrulate. Due to the infrequency of the Class II phenotype, the total observed number of mutants did not significantly deviate from the expected number, however the Class II phenotype was observed in both heterozygous (Hexd^{act}/+) and homozygous (Hexd^{act}/ Hexd^{act}) embryos (Table 1+2).

6.2.2. Class I mutants display severe patterning defects of the AVE

To further characterise the extent of patterning defects in Class I mutants, the expression of five AVE markers were tested at 6.5 dpc.

Hexd^{act} × CD1		**Genotype**				**Chi-square test results**	
Stage	Total	Expected number of mutants	Observed number of mutants	Expected number of non-mutants	Observed number of non-mutants	χ^2	P value
5.5	18	9	7	9	11	0.89	0.35
6.5	36	18	13	18	23	2.78	0.10
7.5	42	21	15	21	27	3.43	0.06
8.5	14	7	4	7	10	2.57	0.11
Weaning	95	47.5	33	47.5	62	**8.85**	**0.0**

Table 1. Genotyping results of Hexd^{act} × CD1 crosses at various embryonic stages and weaning age. Observed numbers did not significantly deviate from the expected Mendelian frequencies at any embryonic stage (P > 0.05). However, there was a highly significant deviation between observed numbers of weaned mutant mice and the expected number (P < 0.01, **bold font**). This indicates that mutants were dying between 8.5 dpc and weaning age.

Hexd^{act} × Hexd^{act}		**Genotype**						**Chi-square test results**	
Stage	Total	Expected number of homozygous mutants	Observed number of homozygous mutants	Expected number of heterozygous mutants	Observed number of heterozygous mutants	Expected number of wildtype	Observed number of wildtype	χ^2	P value
6.5	145	36.25	46	72.5	65	36.25	34	3.54	0.17
7.5	269	67.25	66	134.5	131	67.25	72	0.45	0.80
8.5	38	9.5	6	19	21	9.5	11	1.74	0.42
Weaning	21	5.25	0	10.5	9	5.25	12	**14.14**	**0.0**

Table 2. Genotyping results of Hexd^{act} × Hexd^{act} intercrosses at various embryonic stages and weaning age. Observed numbers did not significantly deviate from the expected Mendelian frequencies at any embryonic stage (P > 0.05). However, there was a highly significant deviation between observed numbers of weaned mutant mice and the expected number (P < 0.01, **bold font**). This indicates that mutants were dying between 8.5 dpc and weaning age.

Figure 1 – Characterisation of the genetic ablation system in Hexd^{act} embryos

(A-B'', D+D') Hexd^{act} embryos staged between 5.5-7.5 dpc were analysed by confocal microscopy. Nuclear stain (blue); F-actin (red). (A) Wildtype embryo at 5.5 dpc. *Hex*GFP cells are present in the DVE (green). (A') Class I embryo at 5.5 dpc showing *Hex*GFP expression in the DVE (cyan arrow). (A'') Class II embryo at 5.5 dpc showing small and rounded morphology and an absence of *Hex*GFP-expressing cells. (B) Wildtype embryo at 6.5 dpc. *Hex*GFP cells are present in the AVE (orange arrow). (B'+B'') Class I embryos at 6.5 dpc showing an absence of *Hex*GFP expression in the AVE. Incomplete proamniotic cavitation shown by yellow arrow in (B''). (C) WISH analysis of *Hex* showing expression in the AVE of a wildtype embryo at 6.5 dpc. (C') WISH analysis of *Hex* in a Class I mutant embryo at 6.5 dpc showing an absence of *Hex* transcript in the AVE. (D) Wildtype embryo at 7.5 dpc showing expression of *Hex*GFP in the anterior definitive endoderm (green). (D') Class I mutant embryo at 7.5 dpc showing expression of *Hex*GFP in the anterior definitive endoderm (green). (E) WISH analysis of *Hex* in the anterior definitive endoderm of a wildtype embryo at 7.5 dpc. (E') WISH analysis of *Hex* in Class I mutant embryo at 7.5 dpc showing expression in the anterior definitive endoderm. Scale bar 40 μm in A-A''; 60 μm in B-B''; 90 μm in C+C'; 100 μm in D-E'.

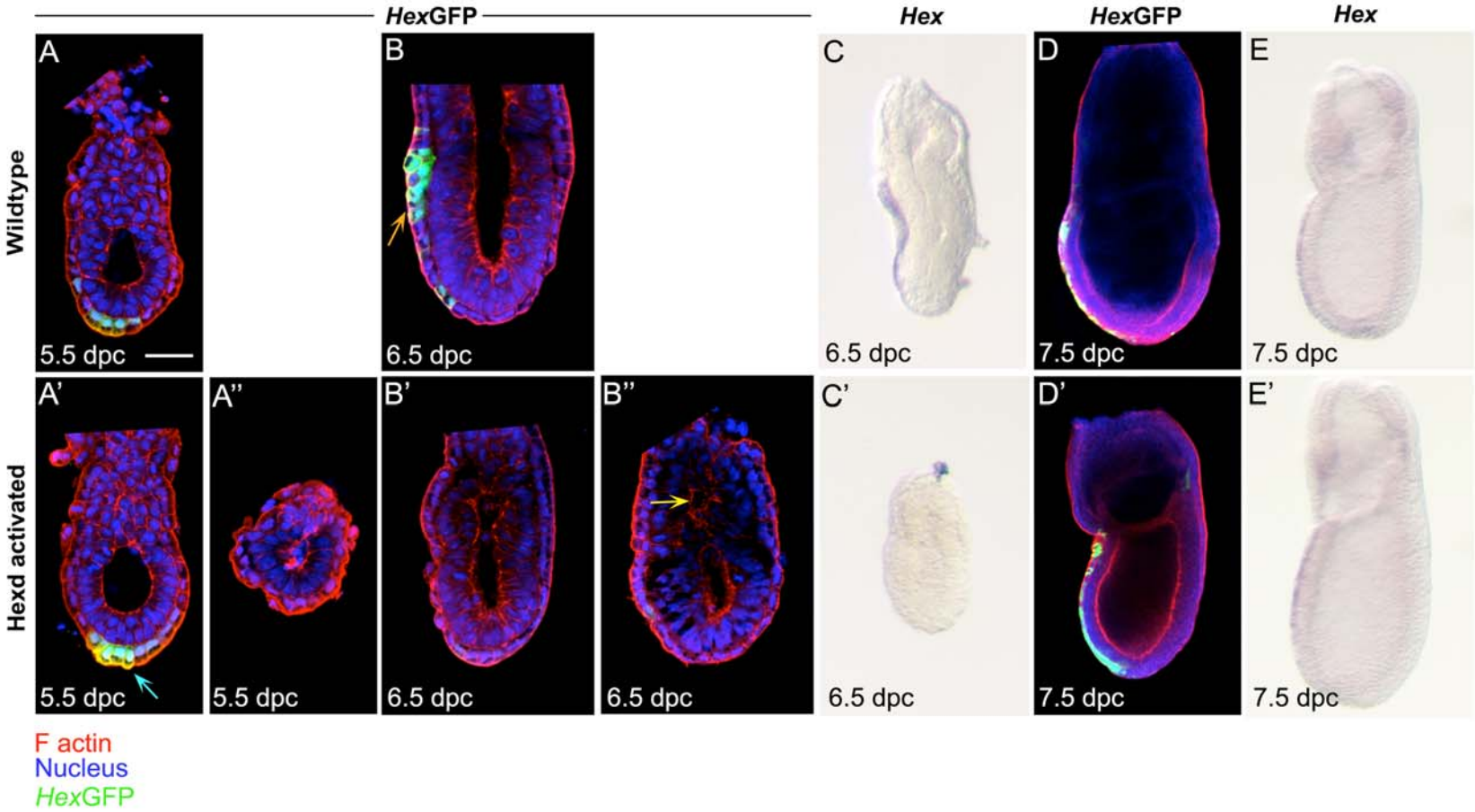
HexGFP
Hex
HexGFP
Hex
Wildtype
Hexd activated
A
B
C
D
E
A'
A''
B'
B''
C'
D'
E'
5.5 dpc
6.5 dpc
6.5 dpc
7.5 dpc
7.5 dpc
5.5 dpc
5.5 dpc
6.5 dpc
6.5 dpc
6.5 dpc
7.5 dpc
7.5 dpc
F actin
Nucleus
HexGFP

Figure 2 – Characterisation of the AVE domain in 6.5 dpc Class I mutants

The expression of a selection of AVE markers was assessed in Hexd^{act} Class I mutant embryos by WISH analysis. (A) Wildtype and (A') mutant embryo showing expression of *Lefty1/2*. L1, *Lefty1* expression in the AVE; L2, *Lefty2* expression in the primitive streak. (B) Wildtype and (B') mutant embryo displaying expression of *Fz8* in the AVE. (C) Wildtype and (C') mutant embryo displaying expression of *Cerl* in the AVE. (D) Wildtype and (D') mutant embryo displaying expression of *Sfrp5* in the AVE. (E) Wildtype and (E') mutant embryo displaying expression of *Dkk1* in the AVE. (F) Wildtype and (F') mutant embryo displaying expression of *Ttr* in the extraembryonic visceral endoderm. Scale bar 90 μm.

Wildtype
Hexd activated
Lefty1/2
Fz8
Cerberus
Sfrp5
Dkk1
Ttr
A
A'
B
B'
C
C'
D
D'
E
E'
F
F'
6.5 dpc
L1
L2

WISH analysis revealed AVE patterning defects in 30% of mutant embryos (n=26/86). This consisted of a vast reduction or total absence of transcript of some markers (*Lefty1/2*, n=13/28; *Fz8*, n=4/13; *Cerl*, n=7/16; *Sfrp5*, n=2/14) (Fig. 2A-D'), but no change in the expression of *Dkk1* and *Sfrp5*, two markers of the anterior portion of the AVE (*Dkk1*, n=15/15; *Sfrp5*, n=12/14). This indicates that cells expressing these genes do not overlap with *Hex*-expressing cells (Fig. 2D-E'). It was apparent that despite the AVE patterning defects caused by genetic ablation system, the visceral endoderm remained intact and showed no evidence of a loss of integrity. Miura and Mishina found that microsurgical ablation of the DVE caused the embryonic visceral endoderm to acquire extraembryonic visceral endoderm character (Miura and Mishina, 2007). To test this possibility the expression of *transthyretin* (*Ttr*) was examined. At 6.5 dpc, *Ttr* is expressed exclusively in extraembryonic visceral endoderm (Makover *et al*., 1988). This was consistent in all of the embryos tested in this study irrespective of genotype, suggesting that the embryonic visceral endoderm does not adopt an extraembryonic character in Class I mutants (Fig. 2F+F'; n=16).

6.2.3. Class I mutants show a failure to specify the anterior primitive streak and exhibit EMT defects

To explore the effect of AVE ablation in Hexd^{act} mice on the formation of the primitive streak, the expression of a selection of primitive streak markers were analysed by WISH. At 6.5 dpc, *Lefty2* is normally expressed in the primitive streak. At this stage the *Lefty2* domain observed in *Lefty1/2 in situs* was absent in a proportion of mutants (Fig. 2A+A', n=7/28). *Eomes* expression, which is normally expressed in the extraembryonic ectoderm and posterior epiblast at this stage, was

also absent in the epiblast in a proportion of mutants (Fig. 3D+D', n=2/11). However, the expression of *T* and *Cripto* were all initiated or restricted (in the case of *Cripto*) to the posterior side of mutant embryos (Fig. 3B+B', F+F', *T*, n=7; *Cripto*, n=9). This suggests the onset of some markers was delayed, possibly due to defects in the initiation of primitive streak formation.

Once the primitive streak is initiated, epiblast cells traverse through the primitive streak and adopt a mesodermal or endodermal fate (Introduction in this thesis, Fig. 3; reviewed in Tam and Behringer, 1997). WISH analysis revealed that whilst mutant embryos displayed robust expression of *T* and *Eomes* in the extraembryonic mesoderm and intermediate primitive streak, a proportion displayed a lack of expression in the mesodermal derivatives of the anterior primitive streak (Fig. 3C+C', E+E'; *T*, n=3/14; *Eomes*, n=3/18). This suggested that mesoderm cells expressing these markers were unable to extend anteriorly or were incorrectly patterned, unlike the expression domains in the wildtype situation (Fig. 3C+E). The node and anterior mesendoderm marker, *HNF3β*, was expressed normally in mutant embryos indicating that these particular anterior primitive streak derivatives were unaffected (Fig. 3A+A', n=8/8). Additionally expression of *Wnt3* and the paraxial mesoderm marker *Tbx6* in mutant embryos was indistinguishable from non-mutant counterparts (Fig. 3G-H'; *Wnt3*, n=11/11; *Tbx6*, n=13/13) further indicating that only a subset of mesoderm cells were affected in a proportion of Class I mutants.

To test if the failure to anteriorly extend *T*- and *Eomes*-expressing cells of the primitive streak was due to defective cell movements, expression of *FGF8* and its downstream target *Snail* were analysed. *FGF8* has been shown to have a crucial role in controlling the morphogenesis of mesoderm at the primitive streak, in part by controlling *Snail* expression (Ciruna and Rossant, 2001; Cano *et al.*, 2000).

Figure 3 – Characterisation of primitive streak formation in Class I mutants

The expression of a selection of primitive streak markers was assessed in Class I mutants by WISH analysis. (A) Wildtype and (A') mutant embryo displaying expression of *HNF3β* in the node at 7.5 dpc. (B) Wildtype and (B') mutant embryo displaying expression of *T* in the primitive streak at 6.5 dpc. (C) Wildtype and (C') mutant embryo displaying expression of *T* in the primitive streak and axial mesendoderm at 7.5 dpc. The mutant embryo shows an absence of *T* expression in the anterior primitive streak (orange arrowheads). (D) Wildtype and (D') mutant embryo displaying expression of *Eomes* in the extraembryonic ectoderm and primitive streak at 6.5 dpc. Green arrow signifies absence of epiblast expression. (E) Wildtype and (E') mutant embryo displaying expression of *Eomes* in the extraembryonic ectoderm and primitive streak at 7.5 dpc. The mutant embryo shows an absence of *Eomes* expression in the anterior primitive streak (yellow arrow). (F) Wildtype and (F') mutant embryo displaying expression of *Cripto* in the primitive streak at 6.5 dpc. (G) Wildtype and (G') mutant embryo displaying expression of *Wnt3* in the intermediate and extraembryonic mesoderm at 7.5 dpc. (H) Wildtype and (H') mutant embryo displaying expression of *Tbx6* in the paraxial mesoderm at 7.5 dpc. (I) Wildtype and (I') mutant embryo displaying expression of *FGF8* in the mesoderm at 7.5 dpc. Mutants embryos show reduced expression in the intermediate mesoderm compartment (cyan arrow). (J) Wildtype and (J') mutant embryo displaying expression of *Snail* throughout the primitive streak at 7.5 dpc. Mutants show reduced expression in the primitive streak (red arrow). (K) Wildtype and (K') mutant embryos derived from a Hexd x Sox2Cre (male) cross. Expression of *T* observed throughout the mesoderm at 7.5 dpc in both wildtype and mutant embryos. Scale bar 90 μm.

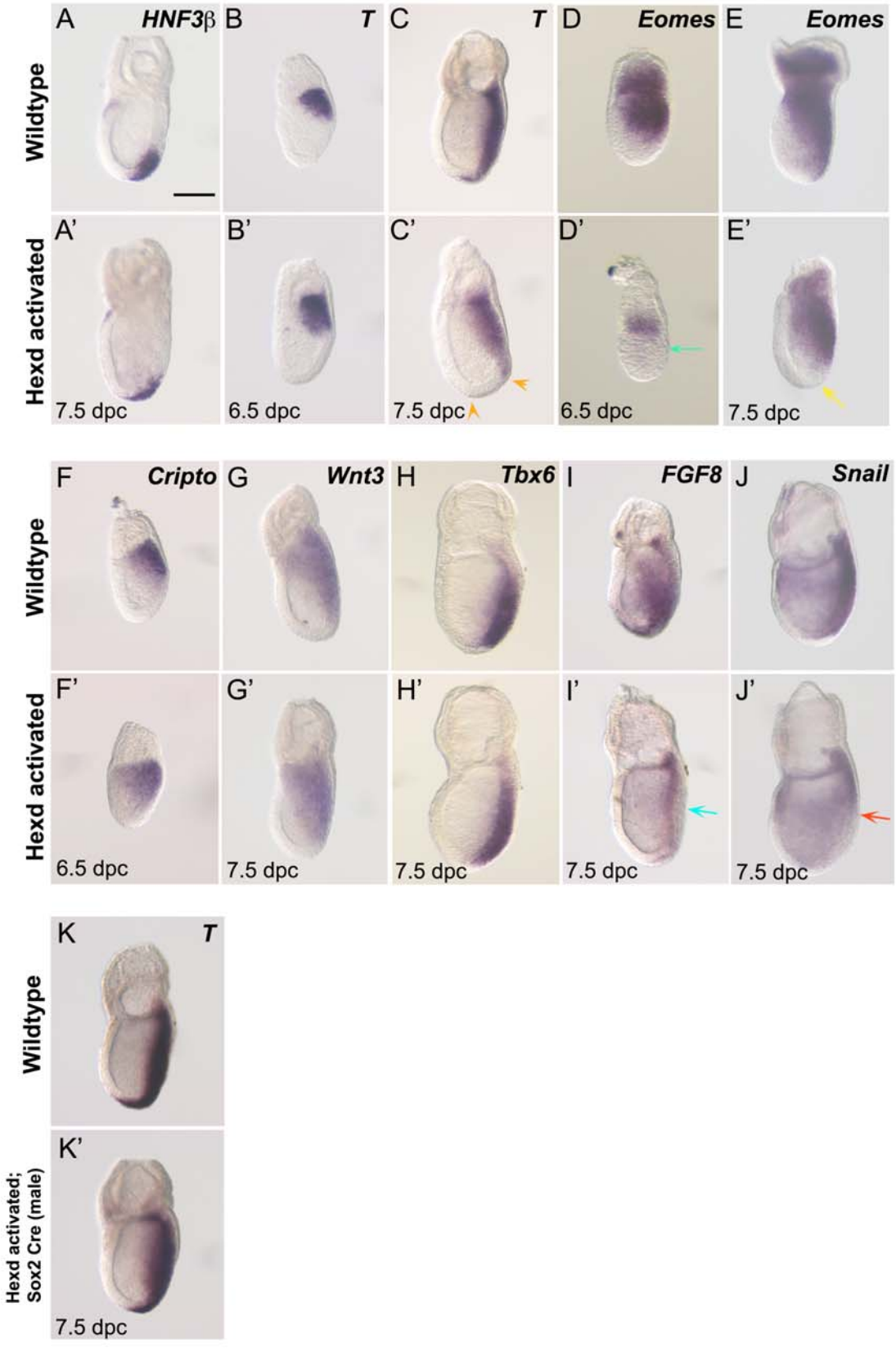
Wildtype
Hexd activated
A HNF3β
B T
C T
D Eomes
E Eomes
A'
B'
C'
D'
E'
7.5 dpc
6.5 dpc
7.5 dpc
6.5 dpc
7.5 dpc
Wildtype
Hexd activated
F Cripto
G Wnt3
H Tbx6
I FGF8
J Snail
F'
G'
H'
I'
J'
6.5 dpc
7.5 dpc
7.5 dpc
7.5 dpc
7.5 dpc
Wildtype
Hexd activated; Sox2 Cre (male)
K T
K'
7.5 dpc

Indeed, a proportion of Class I Hexd^{act} mutants exhibited reduced expression of both *FGF8* and *Snail* throughout the primitive streak (Fig. 3I-J'; *FGF8, n=5/17; Snail*, n=3/15). Interestingly, the extraembryonic mesoderm expression of both markers appeared unaffected in all mutants as in wildtype embryos, indicating that any morphogenetic defects of the primitive streak were unlikely to affect this mesoderm compartment (Fig. 3I-J'). It appears that ablating the *Hex*-expressing population of AVE cells affects the patterning/correct placement of the anterior primitive streak, possibly as a result of inappropriately regulating cell movements.

6.2.4. There are no apparent defects in the anterior definitive endoderm of Class I mutants

The expression of the definitive endoderm markers *Cerl* and *Sox17* were analysed in Class I Hexd^{act} mutants and found to be present and indistinguishable from wildtype embryos at 7.25-7.5 dpc, suggesting that the anterior definitive endoderm is not ablated in these mutants (Fig. 4A-E'; *Cerl*, n=14; *Sox17*, n=14). To rule out the possibility that patterning defects in the anterior primitive streak were not simply due to ablation of *Hex*-expressing cells of the ADE, Hexd mice were crossed to male Sox2Cre mice. This allowed the ablation system to be activated in epiblast-derived *Hex*-expressing cells, but not extraembryonic tissues such as the AVE (Hayashi *et al.*, 2002). Any anterior primitive streak defects would be a result of ablation of the ADE and not as a consequence of AVE ablation. Embryos were dissected at 7.5 dpc and *T* expression was examined. Unlike the anterior primitive streak patterning defects observed in a proportion of Hexd^{act} mutants, all mutants resulting from Sox2Cre activation had complete *T* expression domains (Fig. 3K+K'; n=9/9).

Figure 4 - Characterisation of the definitive endoderm and anterior neurectoderm in Class I mutants

The expression of a selection of definitive endoderm and neurectoderm markers were assessed in Class I mutants by WISH analysis. (A) Wildtype and (A') mutant embryos showing expression of *Cerl* in the AVE and definitive endoderm (DE) at 7.25 dpc. (B) Wildtype and (B') mutant embryos showing expression of *Cerl* at 7.5 dpc. (C) Wildtype and (C') mutant embryos showing expression of *Sox17* in the AVE and definitive endoderm (DE) at 7.25 dpc. (D) Wildtype and (D') mutant embryos showing expression of *Sox17* at 7.5 dpc. Red arrow points to expression in the definitive endoderm (E+E') Anterior view of the same embryos are shown. Red arrow points to expression in the definitive endoderm. (F) Wildtype and (F') mutant embryos showing expression of *Otx2* in the anterior neurectoderm at 7.5 dpc. (G) Wildtype and (G') mutant embryos showing expression of *Hesx1* in the anterior neurectoderm at 7.5 dpc. (H) Wildtype and (H') mutant embryos showing expression of *Hesx1* in the forebrain at 8.5 dpc. (I+I') Anterior view of the same embryos are shown. (J) Wildtype and (J') mutant embryos showing expression of *Six3* in the forebrain at 8.5 dpc. (K+K') Anterior view of the same embryos are shown. (L) Wildtype and (L') mutant embryos showing expression of *FGF8* in the isthmus (green arrowhead) and commissural plate (magenta arrowhead) at 9.5 dpc. The mutant embryo has the genotype $Hexd^{act}$/Hexd;β-actin Cre/+, and shows an anterior truncation of the forebrain, reminiscent of the *Hex* null phenotype. Scale bar 90 μm in A-G'; 250 μm in H-K'; 500 μm in L+L'.

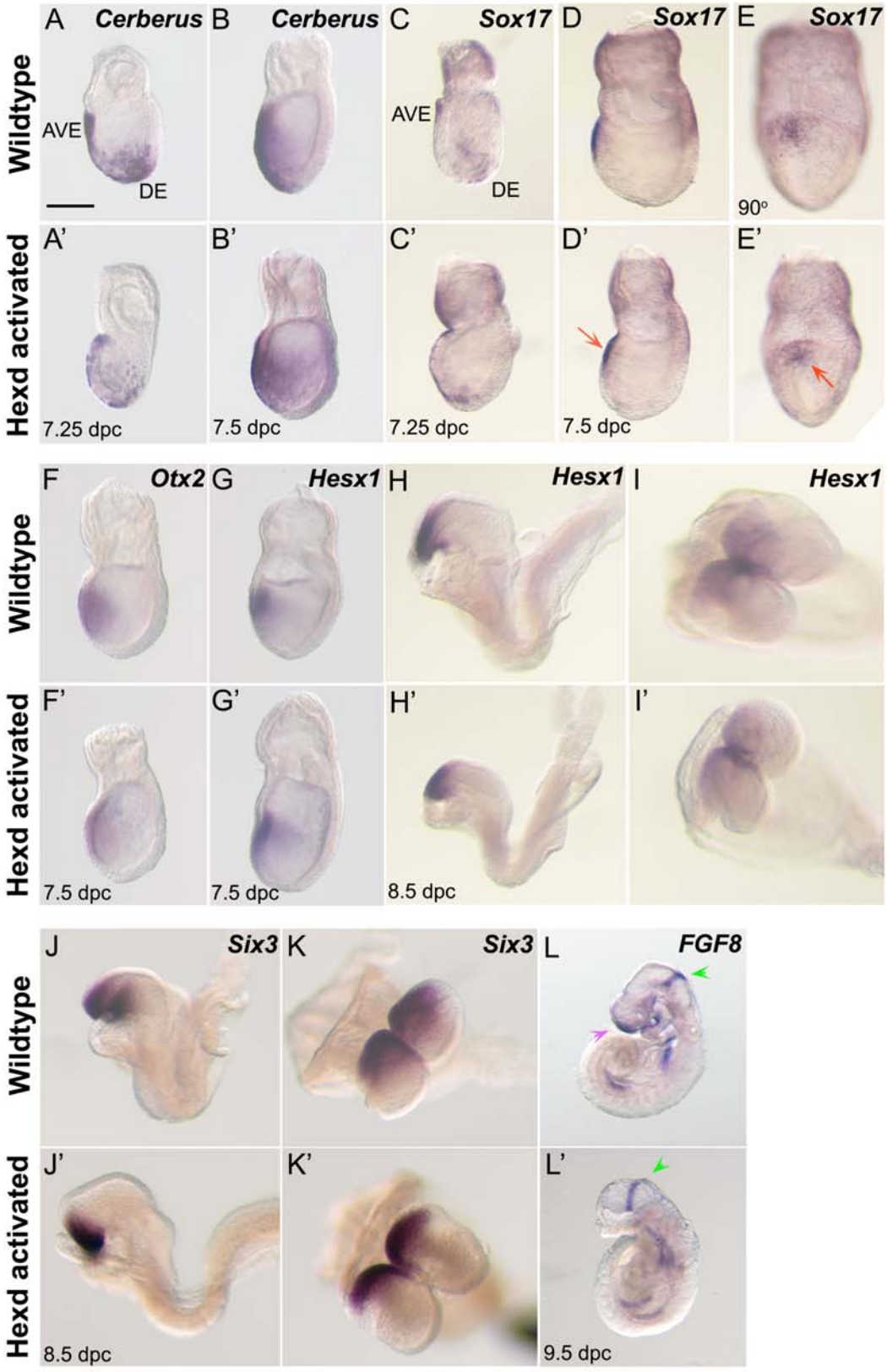
Wildtype
Hexd activated
A Cerberus
B Cerberus
C Sox17
D Sox17
E Sox17
AVE
DE
90°
A'
B'
C'
D'
E'
7.25 dpc
7.5 dpc
7.25 dpc
7.5 dpc
F Otx2
G Hesx1
H Hesx1
I Hesx1
F'
G'
H'
I'
7.5 dpc
7.5 dpc
8.5 dpc
J Six3
K Six3
L FGF8
J'
K'
L'
8.5 dpc
9.5 dpc

This strongly suggested that the observed primitive streak defects were a consequence of AVE ablation.

6.2.5. There are no apparent defects in the anterior neurectoderm of Class I mutants

To determine how the anterior neurectoderm is patterned in Class I mutants the expression of *Otx2* and *Hesx1* were analysed. At 7.5 dpc both genes were correctly expressed in the anterior ectoderm of Class I mutants (Fig. 4F-G'; *Otx2*, n=11; *Hesx1*, n=12). This anterior neurectoderm patterning is maintained in Class I embryos at 8.5 dpc as indicated by the expression of *Hesx1* and *Six3* in the forebrain of all mutants examined (Fig. 4H-K'; *Hesx1*, n=13; *Six3*, n=14). The absence of forebrain defects at this early headfold stage indicates that the ADE is continuing to pattern the underlying ectoderm. This is the stage when *Hex* null embryos start exhibiting forebrain defects (Martinez-Barbera *et al.*, 2000a), and normal forebrain patterning in Class I mutants suggests the efficiency of the ablation system is impaired. The only instance when forebrain truncations were observed was at 9.5 dpc in homozygous Hexd^{act} mutants. In this situation an absence of endogenous *Hex* phenocopies the null mutant as indicated by an absence of *FGF8* expression in the commissural plate (Fig. 4L+L'). In summary, Class I mutants can correctly specify the definitive endoderm and are able to correctly pattern the anterior neurectoderm suggesting that the ADE is only ablated after it has patterned this tissue.

6.2.6. Class II mutants are unable to gastrulate

Class II mutants comprised 4.4% of the total mutants analysed, which hindered characterisation of the phenotype. Morphologically, embryos are small and round, and

could be detected up to 7.5 dpc. Ablation of *Hex*-expressing cells occurs prior to 5.5 dpc as indicated by a loss of *Hex*GFP expression in the DVE (Fig. 5A+A', n=1), and therefore constitutes an earlier ablation than that seen in Class I mutants. At 6.5 dpc, the *Cerl* expression domain is absent in the AVE signifying the loss of this tissue (Fig. 5B+B', n=1). One out of two Class II embryos displayed an expansion of expression of *Ttr* into the embryonic visceral endoderm (Fig. 5C+C', n=1/2). This supports the finding of Miura and Mishina (2007) who found that when DVE was ablated at/prior to 5.5 dpc, ectopic expression of extraembryonic visceral endoderm markers was observed. At 6.5 dpc, *Eomes* transcript is normally detected in the extraembryonic ectoderm (ExE) and the site of primitive streak formation. However, despite the Class II mutant analysed showing robust expression in the ExE, there was a failure to induce epiblast expression (Fig. 5D+D', n=1). This was not due to cells prematurely differentiating down a different lineage as the pluripotency marker *Oct4* was robustly expressed throughout the epiblast at 7.5 dpc in mutant and control embryos (Fig. 5E+E', n=1).

Wnt3 is normally expressed before gastrulation in the proximal epiblast of the egg cylinder, before being restricted to the posterior proximal epiblast and eventually the primitive streak (Liu *et al*., 1999). At 7.5 dpc, Class II mutants expressed *Wnt3* in the proximal epiblast, but showed no sign of any posterior restriction (Fig. 5F+F', n=2). Additionally both *T*, which marks the primitive streak and axial mesoderm, and *HNF3β*, which is expressed in the node, were both absent at 7.5 dpc indicating the lack of primitive streak and node tissue formation (Fig. 5G-H'; *T*, n=2; *HNF3β*, n=2). The inability of Class II mutants to gastrulate results in their reabsorption as they are not detected later than 7.5 dpc.

Figure 5 - Characterisation of Class II mutants

The expression of a selection of markers was assessed in Class II mutants. (A) Confocal slices of wildtype and (A') mutant embryos at 5.5 dpc. *Hex*GFP is expressed in the DVE of the wildtype embryo (green), but is absent from the mutant (A'). Nuclear stain (blue); F-actin (red). (B) Wildtype and (B') mutant embryo showing expression of *Cerl* in the AVE at 6.5 dpc. *Cerl* is absent from the mutant embryo (B'). (C) Wildtype and (C') mutant embryo showing expression of *Ttr* in the extraembryonic visceral endoderm at 6.5 dpc. One out of two Class II embryos analysed showed ectopic expression in the embryonic visceral endoderm (red arrowhead). (D) Wildtype and (D') mutant embryo showing expression of *Eomes* in the extraembryonic ectoderm (green arrow) and primitive streak (blue arrow) at 6.5 dpc. Primitive streak expression is absent in the Class II mutant (D'). (E) Wildtype and (E') mutant embryo showing expression of *Oct4* in the epiblast at 7.5 dpc. (F) Wildtype and (F') mutant embryo showing expression of *Wnt3* at 7.5 dpc. Class II mutants show expression of *Wnt3* in a ring around the proximal epiblast (F'). (G) Expression of *T* at 7.5 dpc in a wildtype embryo is throughout the primitive streak. (G') *T* expression is not observed in Class II mutants. (H) Wildtype expression of *HNF3β* at 7.5 dpc is in the node. (H') *HNF3β* expression is not observed in Class II mutants. Scale bar 40 μm in A+A'; 60 μm in B-D'; 70 μm in E-H'.

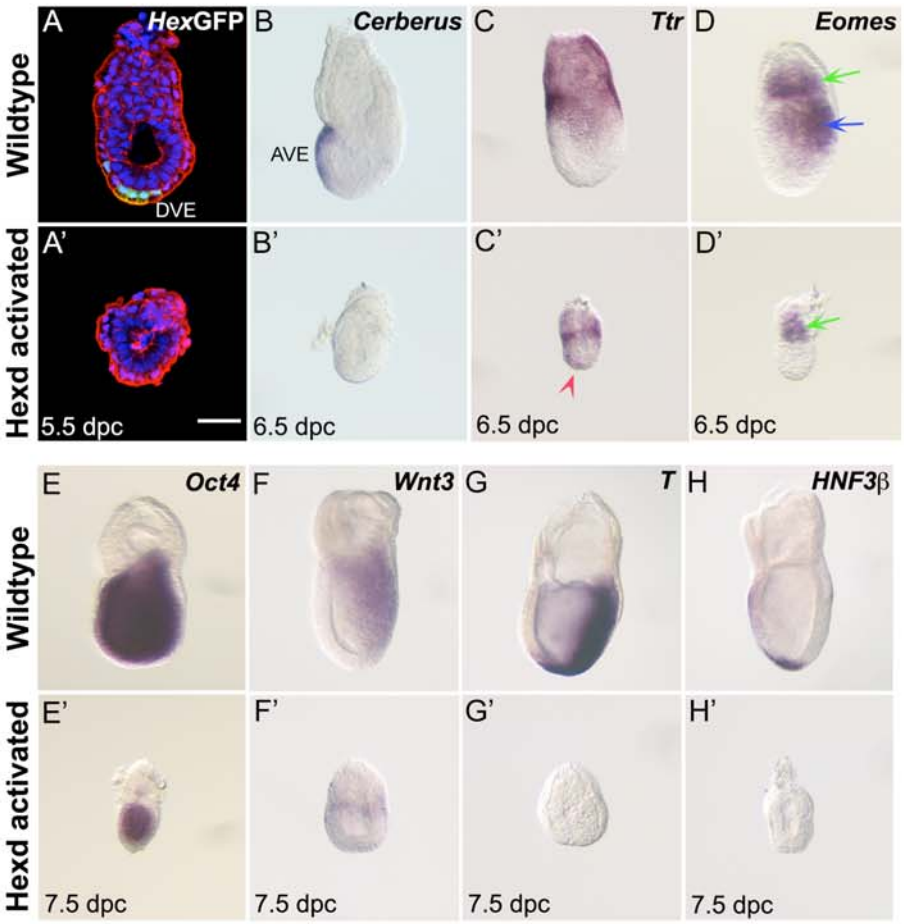
Wildtype
Hexd activated
A
HexGFP
DVE
B
Cerberus
AVE
C
Ttr
D
Eomes
A'
5.5 dpc
B'
6.5 dpc
C'
6.5 dpc
D'
6.5 dpc
E
Oct4
F
Wnt3
G
T
H
HNF3β
E'
7.5 dpc
F'
7.5 dpc
G'
7.5 dpc
H'
7.5 dpc

6.2.7. Nodal signalling is aberrant in both Classes of mutant

The AVE and DVE secrete antagonists of Nodal signalling that restrict its activity to the proximal, then posterior epiblast where it can impart primitive streak-inducing activity (reviewed in Beddington and Robertson, 1999; Perea-Gomez *et al.*, 2001b). To test the consequence of tissue ablation of the AVE on Nodal signalling, $Hexd^{act}$ mutants underwent WISH analysis. At 6.5 dpc, Nodal transcript should be restricted to the posterior epiblast (Fig. 6A). However, 29% of Class I mutants showed proximal but not posterior restriction of Nodal transcript and the level of expression was weak (Fig. 6A', n=8/28). The Class II mutant analysed also displayed weak expression but throughout the epiblast (Fig. 6A'', n=1). This suggested that Class I mutants in which the AVE had been ablated were unable to effectively restrict Nodal to the posterior of the epiblast, whilst Class II mutants that showed an earlier ablation were not capable of restricting Nodal expression at all.

It was curious that Nodal transcripts appeared weaker in activated mutants compared to non-mutants. Was it possible that the AVE not only restricts the site of Nodal expression but also regulates its expression levels? To test this possibility, $Hexd^{act}$ mutants were crossed to $Nodal^{LacZ/+}$ mice. This cross would halve the levels of endogenous Nodal. In heterozygous $Nodal^{LacZ/+}$ embryos the site of β-Gal staining is correctly positioned and the A-P axis is correctly established (Norris *et al.*, 2002; Fig. 6B). If the AVE was involved in increasing the activity of Nodal signalling, then one might expect a greater proportion of $Hexd^{act}$; $Nodal^{LacZ/+}$ mutants to exhibit defects in Nodal restriction and/or expression levels.

Of the eight $Hexd^{act}$; $Nodal^{LacZ/+}$ mutants examined at 6.5 dpc, six showed low-level β-Gal staining in the proximal but not posterior epiblast (Fig. 6B', n=6/8). This indicated that halving the levels of Nodal within the epiblast of ablated mutants

caused an increase in the incidence of proximally restricted *Nodal*. A further two displayed β-Gal staining throughout the epiblast-a defect not observed in Class I mutants with two copies of *Nodal* (Fig. 6B'', n=2/8). The consequence of this observation on primitive streak formation was tested by examining the expression of *T* in these mutants at 7.5 dpc.

Previously, an absence of *T* expression in the anterior primitive streak had been observed in Class I mutants (Fig. 3B+B', n=3/14). In six $Hexd^{act}$; $Nodal^{LacZ/+}$ mutants analysed, one showed a lack of *T* expression in the anterior primitive streak consistent with this phenotype (Fig. 6C', n=1/6). Another mutant showed expression throughout the proximal epiblast which had not been seen before (Fig. 6C'', n=1/6). These results suggest that the combination of ablation in a reduced Nodal background increases the frequency and severity of patterning defects in the primitive streak (33% of mutants display defects when *Nodal* is halved versus 20% of mutants when two copies of *Nodal* are present). This implies that in addition to the role of the AVE in restricting Nodal expression, this tissue also assists in augmenting Nodal activity prior to primitive streak formation.

Figure 6 – Nodal signalling is affected in both Classes of mutant

(A-A’’’) *In situ* analysis of *Nodal* expression at 6.5 dpc. (A) Wildtype embryo displaying posterior restriction of *Nodal* transcript. Green line demarcates anterior (A) and posterior (P) boundary. (A’) Class I mutants display proximal restriction of *Nodal* transcript as indicated by the green line. P and D corresponds to proximal and distal respectively. (A’’) The Class II mutant displays *Nodal* transcript throughout the epiblast. (B-B’’) Embryos derived from $Hexd^{act/+}$ x $Nodal^{LacZ/+}$ cross at 6.5 dpc. (B) Wildtype embryo displaying posterior restriction of β-Galactosidase (*b-Gal*) activity. (B’) Compound mutant showing a smaller proximal domain of β-Galactosidase activity. (B’’) Compound mutant showing β-Galactosidase activity throughout the epiblast. (C-C’’) Embryos derived from $Hexd^{act/+}$ x $Nodal^{LacZ/+}$ cross at 7.5 dpc. (C) Wildtype embryo showing expression of *T* throughout the primitive streak. (C’) Compound mutant showing an absence of *T* in the anterior portion of the primitive streak (red arrowheads). (C’’) Compound mutant showing expression of *T* in the proximal epiblast as indicated by the orange line. Scale bar 100 μm in A-B’’; 120 μm in C-C’’.

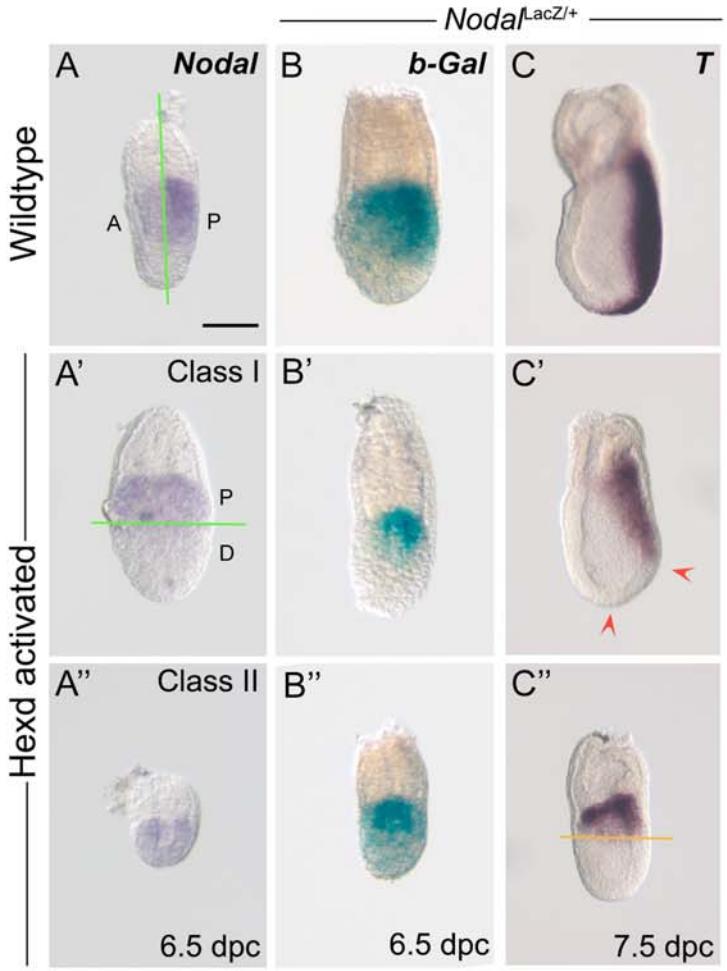
Nodal LacZ/+
Wildtype
Hexd activated
A
Nodal
A
P
B
b-Gal
C
T
A'
Class I
P
D
B'
C'
A''
Class II
6.5 dpc
B''
6.5 dpc
C''
7.5 dpc

6.3. Discussion

This Chapter characterised Hexd^{act} embryos derived from mice that possess the activated DTA allele but survive and are fertile. The most likely reason for their survival is the epigenetic silencing of the knocked-in allele, thereby circumventing cell death caused by the ablation system. During germ-cell development, epigenetic marks such as DNA methylation are generally erased by a currently unknown mechanism (reviewed in Reik, 2007). This meant that in the context of this ablation system, the Hexd^{act} allele should be re-activated and have the capacity to kill *Hex*-expressing cells.

This indeed was the case. Two classes of mutant were observed depending on the timing of the genetic ablation. Class I embryos were morphologically normal but 30% exhibited a loss or severe reduction of AVE markers between 5.5 and 6.5 dpc. A similar proportion of Class I mutants were unable to restrict Nodal expression to the posterior of the embryo, suggesting that this was a functional consequence of an absence of AVE tissue. Class II mutants were observed at a frequency of 4.4%. In these mutants, *Hex*-expressing cells were lost before 5.5 dpc as determined by an absence of the *Hex*GFP domain. Accordingly, Nodal expression at 6.5 dpc was observed throughout the epiblast, consistent with an absence of DVE tissue. The exact timing of ablation in Class II mutants was not precisely determined. As the DVE was not present at 5.5 dpc, it is possible that ablation might have occurred in *Hex*-expressing cells in the primitive endoderm. Considering the widespread expression of *Hex* transcript in the primitive endoderm of 4.5-4.75 dpc embryos (Chazaud *et al*., 2006b; Mesnard *et al*., 2006), it is unlikely the whole population was ablated without recapitulating the peri-implantation defects of mutants where primitive endoderm fails

to form (examples include *Grb2* and *Fgfr2* null embryos (Chazaud *et al*., 2006b; Arman *et al*., 1998)).

It is worth noting that both phenotypic classes were present when the Hexd allele was activated by Cre recombination, as discussed in Results Chapter 3. This indicated that the $Hexd^{act}$ allele could function in the re-activated context to produce the two classes of mutant observed previously. The advantage of using mice with the activated allele was the increased frequency of mutant embryos due to heterozygous $Hexd^{act/+}$ crosses resulting in 75% mutant embryos instead of the typical 25% from the Hexd x βactin Cre cross.

Almost one fifth (n=6/32) of Class I mutants showed an absence of the anterior primitive streak as determined by loss of *Eomes* or *T* transcript in this region. The possibility that this was due to cell ablation in the *Hex*-expressing population of the anterior definitive endoderm was discounted as (i) other markers of this tissue (*Cerl* and *Sox17*) were correctly localised and (ii) when the ablation system was restricted to epiblast-derived tissues (such as the definitive endoderm) by paternal Sox2Cre activation, *T* was expressed throughout the primitive streak in all mutants analysed. This meant that lack of anterior primitive streak tissue was a result of AVE ablation, but by what mechanism?

Diagnostic *in situ* hybridisation analysis demonstrated that *FGF8* and its target *Snail* were weakly expressed in the middle streak (n=8/32), unlike the strong expression found in non-mutant counterparts. Both of these genes are key regulators in controlling morphogenetic cell movements of mesoderm. FGF signalling has been shown to control *Snail* expression, and *Fgfr1* null mutants are unable to maintain

Snail expression resulting in a mispatterned primitive streak (Ciruna and Rossant, 2001; Cano *et al.*, 2000). *Snail* is required for mesendoderm formation and in *Snail* null embryos, *T* is expressed but does not extend rostrally-as seen in Class I mutants (Carver *et al*., 2001). It is possible that in Class I mutants, mesoderm cells are specified but fail to extend anteriorly due to defective cell movements. Defects in cell movements might also explain the disorganised epiblast morphology at 6.5 dpc detected by confocal analysis. Arnold and colleagues recently reported that *Eomes* expression in the posterior epiblast was essential for epithelial-to-mesenchymal transition in the primitive streak (Arnold *et al.*, 2008). Although *FGF8* and *Snail* expression were unaffected in these mutants, they too showed a lack of *T* expression in the anterior primitive streak.

In the case of the primitive streak defects observed in Class I mutants, a failure to detect anterior mesoderm might be a consequence of the inability of cells to appropriately extend the primitive streak due to EMT defects. However, other anterior streak derivatives such as the node and definitive endoderm were present and correctly located. An alternative possibility is that specific patterning defects within the primitive streak have caused certain cell populations to be mis-specified.

In support of this second possibility, different levels of Nodal activity have previously been shown to specify different cell fates in the mouse embryo (Norris *et al.*, 2002; Vincent *et al*., 2003; Dunn *et al*., 2004). Specifically, specification of the anterior streak derivatives can be curtailed by knocking-out *Smad2* from the epiblast (Vincent *et al*., 2003b), or *FoxH1* (Hoodless *et al*., 2001) or lowering the level of *Nodal* activity in $Nodal^{\Delta 600/+}$ embryos (Norris *et al.*, 2002). Was it possible that the anterior primitive streak defects could be a result of inappropriate levels of Nodal signalling?

Both classes of mutant showed defects in the restriction of *Nodal* transcript. Class II mutants expressed *Nodal* throughout the epiblast-a characteristic also observed when the DVE was microsurgically ablated (Miura and Mishina, 2007). The inability of this class to gastrulate might be a result of them not reaching the required number of cells (Snow, 1977), or levels of *Nodal* not being sufficiently great to initiate target genes. Class I mutants were unable to restrict Nodal expression to the posterior of the epiblast at 6.5 dpc and showed reduced intensity of transcript compared to non-mutants. Furthermore, when crossed to a $Nodal^{LacZ/+}$ background, compound heterozygotes ($Hexd^{act/+}$;$Nodal^{LacZ/+}$) showed an increased frequency of proximal Nodal expression at 6.5 dpc. At 7.5 dpc these mutants displayed an absence of the anterior primitive streak or a failure to rotate the proximodistal axis as determined by proximal *T* expression-a phenotype not previously observed when both copies of *Nodal* were present. As $Nodal^{LacZ/+}$ mutants display no A-P patterning defects, these results suggest that the AVE cooperates with *Nodal* signalling to correctly establish the A-P axis.

Despite a proportion of Class I embryos displaying a loss of AVE at 6.5 dpc and a loss of anterior primitive streak mesoderm at 7.5 dpc, all embryos showed correct localisation of anterior neurectoderm markers at 7.5-8.5 dpc. The current model of establishing anterior identity is that AVE initiates, and as gastrulation proceeds these signals are stabilised and embellished by anterior streak derivatives (Kimura *et al.*, 2000; Perea-Gomez *et al.*, 2002; reviewed in Beddington and Robertson, 1999; Martinez-Barbera and Beddington, 2001). Maybe in the context of this ablation system, any residual AVE that was not ablated (such as *Dkk1*- and *Sfrp5*-expressing cells) was sufficient to initiate neural identity. Alternatively the AVE might have

already performed its initiating function before being ablated at 6.5 dpc. Either way, it is clear that the anterior primitive streak defects observed at 7.5 dpc do not perturb anterior neurectoderm development.

This is contrary to the experiments of Thomas and Beddington who demonstrated microsurgical ablation of the AVE diminished *Hesx1* expression in the anterior neurectoderm (Thomas and Beddington, 1996). Although in this experiment the AVE was ablated at 6.5 dpc, so most likely anterior definitive endoderm was also removed. This would explain the loss or reduction of *Hesx1* expression in the underlying ectoderm as the source of maintenance signals from the definitive endoderm had been removed.

It is perhaps surprising that Class I embryos do not phenocopy *Cerl*$^{-/-}$*;Lefty1*$^{-/-}$ compound mutants, considering that both these gene expression domains are absent from the AVE in Hexd^{act} embryos. In *Cerl*$^{-/-}$*;Lefty1*$^{-/-}$ embryos, the primitive streak can develop ectopically and primitive streak patterning defects are present but can be rescued after removal of one copy of the *Nodal* gene (Perea-Gomez *et al.*, 2002). In Class I mutants, the site of primitive streak formation is specified but *Nodal* is not correctly restricted and is expressed at lower levels. Furthermore, the patterning defects observed in the anterior primitive streak are augmented when one copy of *Nodal* is removed. The differences in phenotype between these two mutants suggest that ablating the whole AVE has revealed an additional function on top of its *Nodal*-antagonising role: not only does the AVE restrict the position of *Nodal* expression, but prior to this it also enhances its activity. The AVE could be increasing the level of *Nodal*, perhaps by secreting activating co-factors or aiding the sorting of *Nodal*-

positive cells to the posterior (Lu and Robertson, 2004). These possibilities need testing.

Chapter 7 - General discussion

The anterior visceral endoderm (AVE) is an extraembryonic tissue required for restricting the site of primitive streak formation (Perea-Gomez *et al.*, 2002) and specifying anterior pattern in the mouse embryo (reviewed by Martinez-Barbera and Beddington, 2001). This thesis has addressed two aspects of AVE function. Firstly, the contribution of proliferation to AVE movements, and secondly a novel approach to genetically ablate this tissue and thereby glean insight into additional roles during A-P axis establishment.

7.1. Proliferation during AVE movements

The AVE is induced at the distal tip of the embryo and at 5.5 dpc migrates to the prospective anterior (Thomas *et al.*, 1998). This movement is essential for converting the existing proximal-distal axis into an anterior-posterior axis (reviewed by Beddington and Robertson, 1999). How these movements take place is still not well understood. One suggestion is that differential proliferation within the visceral endoderm passively displaces the AVE towards the anterior side, which has reportedly lower levels of proliferation than the posterior side (Yamomoto *et al.*, 2004). Another possibility is that the AVE actively migrates to the anterior side, possibly in response to cues inherent to the embryo.

Data presented here show low levels of proliferation within the visceral endoderm throughout the time of AVE movements. Furthermore, no regional differences in the levels of proliferation were observed between the anterior and posterior visceral endoderm, with both cell populations cycling at similar rates. This

finding does not support the differential proliferation model for directing AVE movements.

The most compelling evidence for studying AVE cell movements has come from directly visualising embryos in real time using transgenic lines that express GFP in an AVE-specific manner (Srinivas *et al*., 2004). Movements occur within 4-5 hours, with cells projecting filopodial processes in the direction of movement-indicative of an active migratory process (Srinivas *et al*., 2004). Further evidence for active migration comes from knocking out *Nap1* and showing that polarised cell movements are perturbed (Rakeman and Anderson, 2006). The direction of DVE movements might be determined by guiding these cells towards *Dkk1* (an antagonist of Wnt/β-catenin signalling) expressed in the prospective anterior of the embryo and away from a repellant Wnt3a signal found in the posterior of the embryo, (Kimura-Yoshida *et al*., 2005).

Although proliferation within the visceral endoderm seems not to specifically direct AVE movements, a more general requirement for proliferation was observed in this study. Blocking cell division throughout the embryo prevented AVE migration, as did blocking Nodal signalling (Fig. 1). Interestingly when Nodal signalling was blocked, proliferation levels in the epiblast dramatically fell whilst levels in the visceral endoderm were unaffected. Indeed the role of Nodal in promoting proliferation in the epiblast has previously been inferred (Mesnard *et al*., 2006; Yamamoto *et al*., 2004). Perhaps by reducing proliferation in the epiblast, the physical interaction between this tissue and the overlying visceral endoderm is affected, resulting in AVE movement defects.

Figure 1 – Schematic representation of proliferation in the mouse embryo during AVE movements

(A) At 5.5 dpc, the anterior visceral endoderm precursors (green) are located at the distal tip of the conceptus. Low levels of dividing cells are randomly distributed throughout the visceral endoderm at this stage (red dots). When embryos are cultured for 12 hrs, the anterior visceral endoderm moves anteriorwards until cells reach the embryonic-extraembryonic ectoderm boundary. Cells in the visceral endoderm continue to divide at a low rate and with no regional bias. (B) When 5.5 dpc embryos are cultured for 12 hrs in the cell cycle inhibitor Okadaic acid, cell division throughout the epiblast and visceral endoderm is abolished. The AVE fails to move anteriorwards in these conditions. (C) When 5.5 dpc embryos are cultured for 12 hrs in the Nodal/activin inhibitor SB-431542, proliferation within the epiblast significantly falls. Proliferation throughout the visceral endoderm is unaffected, indicating that cell division within this tissue is independent of Nodal/activin signalling, unlike the epiblast. The anterior visceral endoderm fails to move anteriorwards in cultured embryos, despite the levels of cell division in this tissue remaining unaffected.

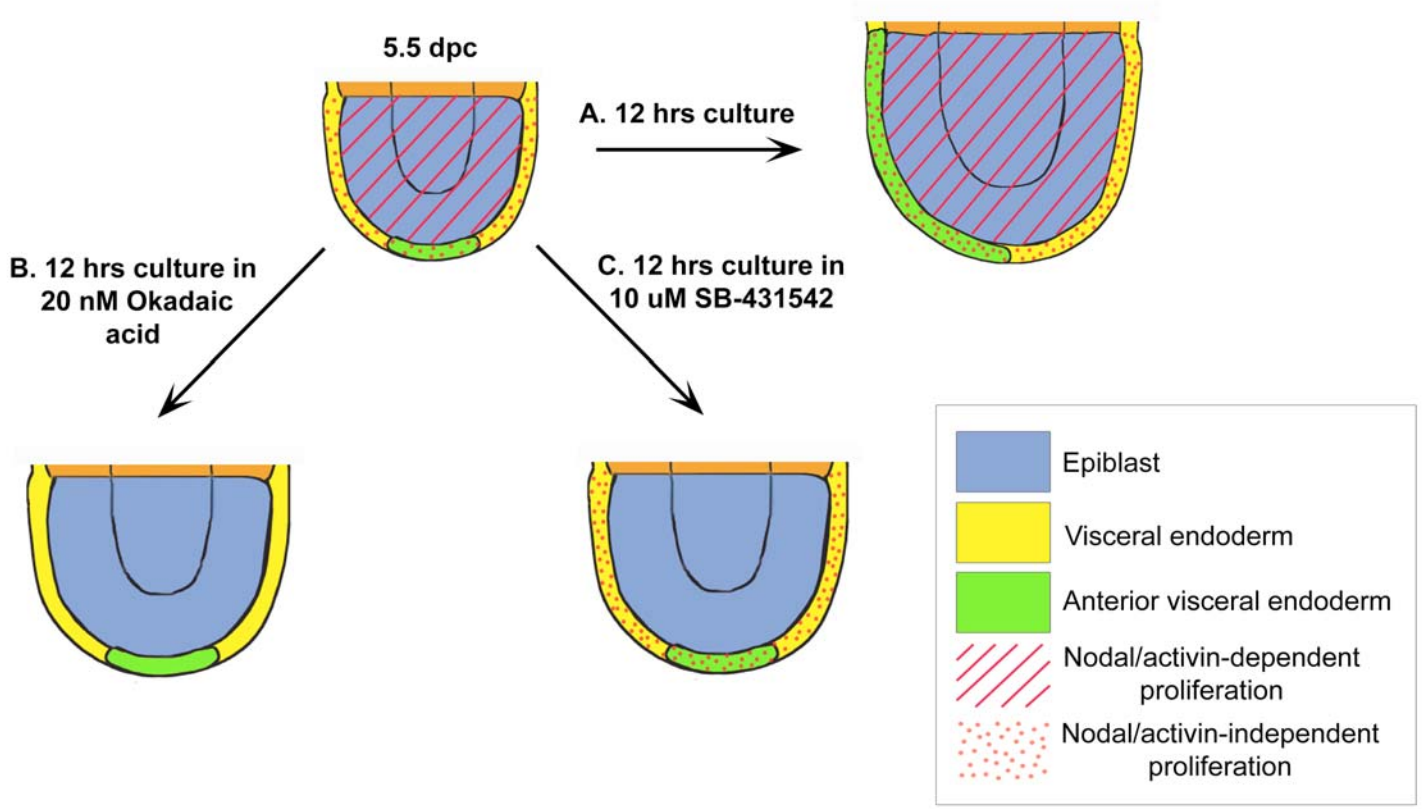
5.5 dpc
A. 12 hrs culture
B. 12 hrs culture in 20 nM Okadaic acid
C. 12 hrs culture in 10 uM SB-431542
Epiblast
Visceral endoderm
Anterior visceral endoderm
Nodal/activin-dependent proliferation
Nodal/activin-independent proliferation

There remain many intriguing questions concerning the nature of AVE movements. For example, what is the exact mechanism behind determining the direction of DVE movements and how does the AVE know when to stop when it reaches the boundary between the epiblast and extraembryonic ectoderm? Recent advances in imaging and genetic techniques are enabling less invasive observations into the cellular basis of AVE movements *ex vivo*. Concurrently, a better understanding of *in vitro* cell differentiation systems have allowed extraembryonic endoderm (XEN) cells to be derived and characterised (Kunath *et al*., 2005), enabling further insight into the developmental program of this lineage.

7.2. Genetic ablation in Hexd embryos

The AVE functions in part by repressing the expression of posterior genes in the anterior epiblast (Kimura *et al*., 2000; Perea-Gomez *et al*., 2001a), resulting in primitive streak formation on the opposite side of the embryo (Perea-Gomez *et al*., 2002). Additionally the AVE, in combination with anterior epiblast tissue, is able to induce ectopic neural structures in non-neural ectoderm (Tam and Steiner, 1999). In an attempt to elucidate further roles of the AVE, this thesis described a genetic ablation system that allowed the inducible expression of DTA in *Hex*-expressing cells, enabling the specific ablation of this cell population.

Depending on the time of cell death, two distinct classes of phenotype were observed. Embryos in which the ablation had occurred prior to 5.5 dpc displayed a failure to restrict *Nodal* transcript, which was expressed weakly throughout the epiblast. When the AVE was ablated between 5.5-6.5 dpc, *Nodal* was restricted proximally but not posteriorly.

Figure 2 – Schematic representation of the defects in Hexd embryos from 5.5 to 7.5 dpc

(A) At 5.5 dpc, anterior visceral endoderm precursors (green) are located at the distal tip of the conceptus. These cells express antagonists of Nodal signalling (red antagonist arrows). At the onset of gastrulation at 6.5 dpc, anterior visceral endoderm cells have moved anteriorwards, reaching the boundary between the epiblast and extraembryonic ectoderm. These cells continue to secrete Nodal antagonists resulting in the restriction of *Nodal* transcript (olive green) to the posterior of the epiblast cup. This marks the site of primitive streak formation. During gastrulation the primitive streak elongates and two new germ layers are formed: the mesoderm (purple) and definitive endoderm (brown). At 7.5 dpc, the definitive endoderm displaces the anterior visceral endoderm and signals to the underlying ectoderm, which becomes anterior neurectoderm (turquoise). (B) Class I Hexd mutants have anterior visceral endoderm precursors at 5.5 dpc, but not anterior visceral endoderm at 6.5 dpc. *Nodal* is therefore restricted proximally but not posteriorly, and at a lower intensity than in the wildtype situation. During gastrulation at 7.5 dpc, definitive endoderm is formed and anterior neurectoderm develops, but the anterior primitive streak is absent. (C) Class II Hexd mutants do not have anterior visceral endoderm precursors at 5.5 dpc, or any signs of anterior visceral endoderm at 6.5 dpc. *Nodal* transcript is found throughout the epiblast at this stage. Class II mutants do not initiate a primitive streak and fail to gastrulate.

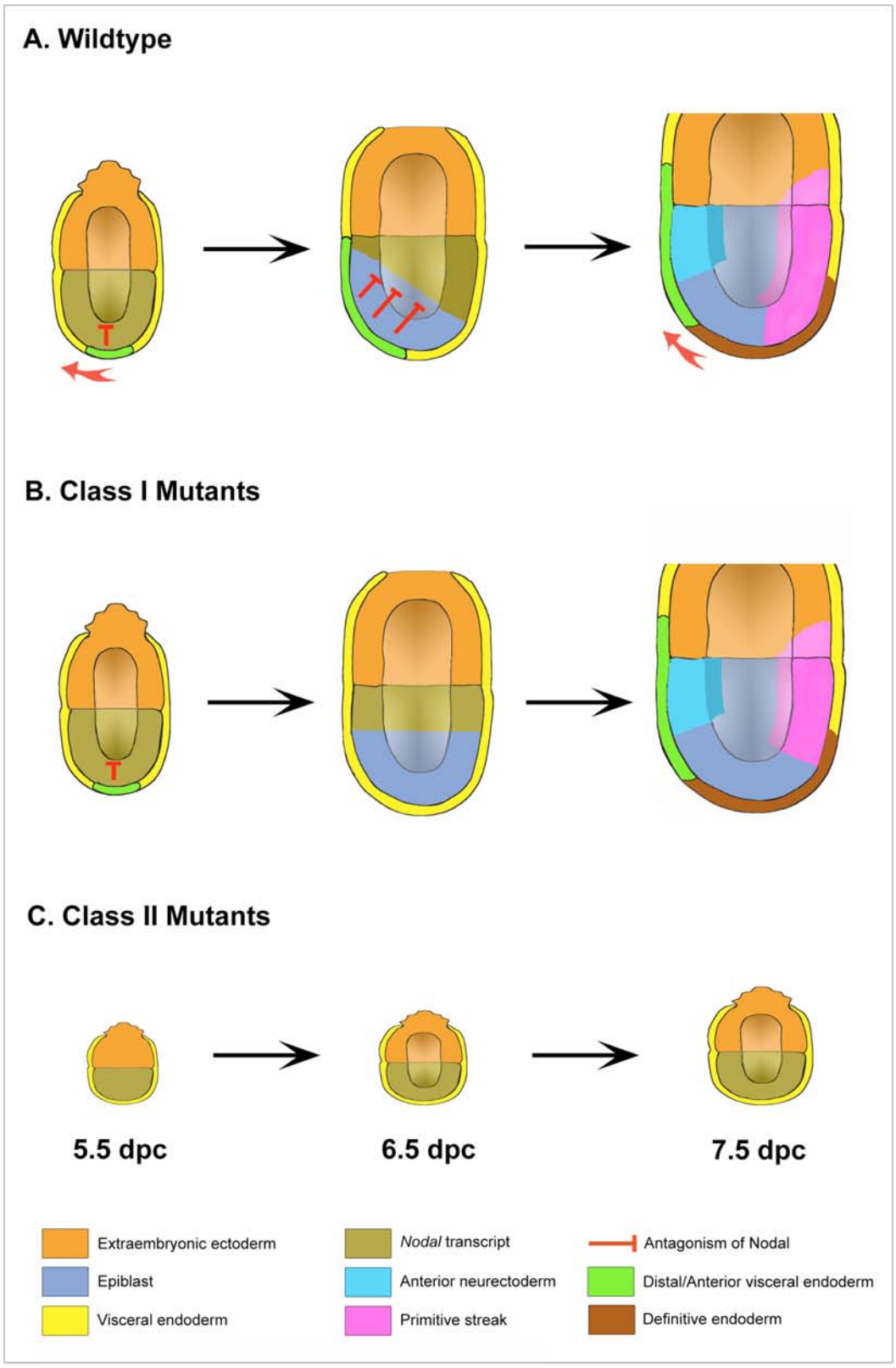
A. Wildtype
T
B. Class I Mutants
T
C. Class II Mutants
5.5 dpc
6.5 dpc
7.5 dpc
Extraembryonic ectoderm
Epiblast
Visceral endoderm
Nodal transcript
Anterior neurectoderm
Primitive streak
Antagonism of Nodal
Distal/Anterior visceral endoderm
Definitive endoderm

This is consistent with the idea that the AVE is a signalling centre that restricts the expression of Nodal to the posterior of the embryo by secreting Lefty1 and Cerl (Meno *et al*., 1997; Belo *et al*., 1997; Perea-Gomez *et al*., 2002). Therefore in the absence of this antagonism, *Nodal* is inappropriately restricted (Fig. 2).

In addition to the role of the AVE in suppressing signalling molecules to the anterior epiblast, results from this thesis suggest an additional role is to increase the activity of Nodal signalling in the epiblast. Firstly, a proportion of ablated embryos formed a primitive streak that was missing its anterior portion. This phenotype is reminiscent of the anterior primitive streak patterning defects observed when Nodal activity is reduced in the epiblast (Hoodless *et al*., 2001; Norris *et al*., 2002; Vincent *et al*., 2003b; Dunn *et al*., 2004). This is supported by the fact that by further reducing the levels of Nodal in AVE ablated embryos increased the frequency and severity of the phenotypes observed.

Mechanistically, how is the AVE able to enhance Nodal signalling? Perhaps the AVE secretes a factor that is able to feed into the autoregulatory loop of Nodal. Two candidates might be Nodal itself or BMP2 which have previously been shown to be expressed in the visceral endoderm at the time of DVE induction (Varlet *et* al., 1997; Coucouvanis and Martin, 1999) and also demonstrated to enhance *Nodal* activity in mouse and chick (Saijoh *et al*., 2003; Norris *et al*., 2002; Piedra and Ros, 2002; Fujiwara *et al*., 2002; Schlange *et al*., 2002). It would be interesting to test whether reduced *Nodal* transcript levels equates to a reduction in active signalling. This could be assessed by analysing the expression of pSmad2/3 and pSmad1/5/8 in AVE ablated embryos.

Another possibility is that the AVE facilitates the sorting of Nodal-expressing cells in a posterior direction. A model whereby cells showing higher levels of Nodal signalling will sort to the posterior of the embryo was initially proposed by Lu and Robertson (2004). To test this the position and number of Nodal-expressing cells could be determined in AVE ablated embryos. The prediction would be that if the AVE had a role in directing these movements, the distribution of Nodal-positive cells would be randomly scattered throughout the proximal epiblast in ablated embryos.

Therefore during A-P axis establishment, the DVE/AVE acts in a feedback loop. First it is induced at 5.0 dpc by Nodal signalling from the epiblast (Brennan *et al.*, 2001; Mesnard *et al.*, 2006). Once the DVE/AVE is established, it acts to either increase Nodal signalling levels in the epiblast or to cause a sorting of Nodal-positive cells to the proximal, then posterior epiblast. This would ensure sufficient Nodal expressing cells are found in the posterior for initiation and proper formation of the primitive streak to take place (Conlon *et al.*, 1994; Brennan *et al.*, 2001). During this process the extraembryonic ectoderm also plays a critical role by secreting the convertases that process Nodal and further enhances the activity of this pathway (Beck *et al.*, 2002). Nodal activity is further increased by another feedback loop between the epiblast and the extraembryonic ectoderm whereby Nodal maintains BMP expression in the extraembryonic ectoderm and in turn BMP maintains Nodal expression via Wnt3a in the epiblast (Winnier *et al.*, 1995; Mishina *et al.*, 1995; Beppu *et al.*, 2000; Ben-Haim *et al.*, 2006).

A second role for the AVE, and opposite to the first role, is to secrete Cerl and Lefty1, two antagonists of Nodal signalling that inhibit Nodal activity in the anterior of the embryo (Meno *et al.*, 1997; Belo *et al.*, 1997). This ensures primitive streak

formation occurs only in the posterior of the embryo (Perea-Gomez *et al*., 2002). It is therefore a series of reciprocal interactions between the epiblast, AVE and extraembryonic ectoderm that establishes the A-P axis in the mouse embryo.

Bibliography

Acampora, D., Mazan, S., Lallemand, Y., Avataggiato, V., Maury, M., Simeone, A., and Brulet, P. (1995). Forebrain and midbrain regions are deleted in *Otx2*$^{-/-}$ mutants due to a defective anterior neurectoderm specification during gastrulation. *Development* **121**: 3279-3290.

Acampora, D., Avantaggiato, V., Tuorto, F., Briata, P., Corte, G., and Simeone, A. (1998). Visceral endoderm-restricted translation of *Otx1* mediates recovery of *Otx2* requirements for specification of anterior neural plate and normal gastrulation. *Development* **125**: 5091-5104.

Alexandre, H., Van Cauwenberge, A., Tsukitani, Y., and Mulnard, J. (1991). Pleiotropic effect of okadaic acid on maturing mouse oocytes. *Development* **112**: 971-980.

Alisch, R. S., Jin, P., Epstein, M., Caspary, T., and Warren, S. T. (2007). *Argonaute2* is essential for mammalian gastrulation and proper mesoderm formation. *PLoS Genetics* **3**: 2565-2571.

Ang, S. –L., Wierda, A., Wong, D., Stevens, K. A., Cascio, S., Rossant, J., and Zaret, K. S. (1993). The formation and maintenance of the definitive endoderm lineage in the mouse: involvement of HNF3/forkhead proteins. *Development* **119**: 1301-1315.

Ang, S. –L., and Rossant, J. (1994). HNF-3β is essential for node and notochord formation in mouse development. *Cell* **78**: 561-574.

Ang, S. –L., Jin, O., Rhinn, M., Daigle, N., Stevenson, L., and Rossant, J. (1996). A targeted mouse Otx2 mutation leads to severe defects in gastrulation and formation of axial mesoderm and to deletion of rostral brain. *Development* **122**: 243-252.

Ang, S, -L., and Constam, D. B. (2004). A gene network establishing polarity in the early mouse embryo. *Seminars in Cell & Developmental Biology* **15**: 555-561.

Arman, E., Haffner-Krausz, R., Chen, Y., Heath, J. K., and Lonai, P. (1998). Targeted disruption of fibroblast growth factor (FGF) receptor 2 suggests a role for FGF signalling in pregastrulation mammalian development. *PNAS* **95**: 5082-5087.

Arnold, S. J., Stappert, J., Bauer, A., Kispert, A., Herrmann, B. G., and Kemler, R. (2000). Brachyury is a target gene of the Wnt/beta-catenin signalling pathway. *Mech. Dev.* **91**: 249-258.

Arnold, S. J., Hofmann, U. K., Bikoff, E. K., and Robertson, E. J. (2008). Pivotal roles for eomesodermin during axis formation, epithelial-mesenchymal transition and endoderm specification in the mouse. *Development* **135**: 501-511.

Baena-Lopez., L. A., Baonza, A., and Garcia-Bellido, A. (2005). The orientation of cell divisions determines the shape of *Drosophila* organs. *Current Biology* **15**: 1640-1644.

Beck, S., Le Good, J. A., Guzman, M., Ben Haim, N., Roy, K., Beermann, F., and Constam, D. B. (2002). Extraembryonic proteases regulate Nodal signalling during gastrulation. *Nat. Cell Biol.* **4**: 981-985.

Beddington, R. S. P. (1987). Isolation, culture and manipulation of post-implantation mouse embryos. In *Mammalian Development: A Practical Approach,* (ed. M. Monk). Oxford: IRL Press.

Beddington, R. S. P., and Robertson, E. J. (1989). An assessment of the developmental potential of embryonic stem cells in the midgestation mouse embryo. *Development* **105**: 733-737.

Beddington, R. S. (1994). Induction of a second neural axis by the mouse node. *Development* **120:** 613-620.

Beddington, R. S. and Robertson, E. J. (1998). Anterior patterning in mouse. *Trends in Genetics* **14**: 277-284.

Beddington, R. S. and Robertson, E. J. (1999). Axis development and early asymmetry in mammals. *Cell* **96(2):** 195-209.

Bedford, F. K., Ashworth, A., Enver, T., and Wiedemann, L. M. (1993). HEX: a novel homeobox gene expressed during haematopoiesis and conserved between mouse and human. *Nucleic Acids Res.* **21**: 1245-1249.

Belo, J. A., Bouwmeester, T., Leyns, T., Kertesz, L., Gallo, N., Follettie, M., and De Robertis, E. M. (1997). Cerberus-like is a secreted factor with neuralizing activity expressed in the anterior primitive endoderm of the mouse gastrula. *Mech. Dev.* **68**: 45-57.

Ben-Haim, N., Lu, C., Guzman-Ayala, M., Pescatore, L., Mesnard, D., Bischofberger, M., Naef, F., Robertson, E. J., and Constam, D. B. (2006). The Nodal precursor acting via activin receptors induces mesoderm by maintaining a source of its convertases and BMP4. *Dev. Cell* **11**: 313-323.

Beppu, H., Kawabata, M., Hamamoto, T., Chytil, A., Minowa, O., Noda, T., and Miyazono, K. (2000). BMP Type II receptor is required for gastrulation and early development of mouse embryos. *Dev. Biol.* **221**: 249-258.

Breitman, M. L., Rombola, H., Maxwell, I. H., Klintworth, G. K., and Bernstein, A. (1990). Genetic ablation in transgenic mice with an attenuated diphtheria toxin A gene. *Molecular and Cellular Biology* **10**: 474-479.

Brennan, J., Lu, C. C., Norris, D. P., Rodriguez, T. A., Beddington, R. S., and Robertson, E. J. (2001). *Nodal* signalling in the epiblast patterns the early mouse embryo. *Nature* **411**:965-969.

Brewer, A., Nemer, G., Gove, C., Rawlins, F., Nemer, M., Patient, R., and Pizzey, J. (2002). Widespread expression of an extended peptide sequence of GATA-6 during

murine embryogenesis and non-equivalence of RNA and protein expression domains. *Mechanisms of Development* **119**: 121-129.

Brockschneider, D., Lappe-Siefke, C., Goebbels, S., Boesl, M. R., Nave, K-A., and Riethmacher, D. (2004). Cell depletion due to diphtheria toxin fragment A after Cre-mediated recombination. *Molecular and Cellular Biology* **24**: 7636-7642.

Camus, A., Perea-Gomez, A., Moreau, A., and Collignon, J. (2006). Absence of Nodal signalling promotes precocious neural differentiation in the mouse embryo. *Dev. Biol.* **295**: 743-755.

Cano, A., Perez-Morena, M. A., Rodrigo, I., Locascio, A., Blanco, M. J., del Barrio, M. G., Portillo, F., and Nieto, M. A. (2000). The transcription factor snail controls epithelial-mesenchymal transitions by repressing E-cadherin expression. *Nat. Cell Biol.* **2**: 76-83.

Carver, E. A., Jiang, R., Lan, Y., Oram, K. F., and Gridley, T. (2001). The mouse Snail gene encodes a key regulator of the epithelial-mesenchymal transition. *MCB* **21**: 8184-8188.

Chazaurd, C., Yamanaka, Y., Pawson, T., and Rossant, J. (2006a). Early lineage segregation between epiblast and primitive endoderm in mouse blastocysts through the Grb2-MAPK pathway. *Developmental Cell* **10**: 615-624.

Chazaud, C., and Rossant, J. (2006b). Disruption of early proximodistal patterning and AVE formation in *Apc* mutants. *Development* **133**: 3379-3387.

Chapman, D. L., Aguinik, I., Hancock, S., Silver, L. M., and Papaioannou, V. E. (1996). Tbx6, a mouse T-Box gene implicated in paraxial mesoderm formation at gastrulation. *Dev. Biol.* **180**: 534-542.

Ciruna, B., Rossant, J. (1999). Expression of the T-box gene *Eomesodermin* during early mouse development. *Mechanism of Development* **81**: 199-203.

Ciruna, B., Rossant, J. (2001). FGF signalling regulates mesoderm cell fate specification and morphogenetic movement at the primitive streak. *Dev Cell* **1**: 37-49.

Collier, R. J. (1975). Diphtheria Toxin: Mode of action and structure. *Bacteriological Reviews* **39**: 54-85.

Collier, R. J. (2001). Understanding the mode of action of diphtheria toxin: a perspective on progress during the 20th century. *Toxicon* **39**: 1793-1803.

Conlon, F. L., Lyons, K. M., Takaesu, N., Barth, K. S., Kispert, A., Herrmann, B., and Robertson, E. J. (1994). A primary requirement for *nodal* in the formation and maintenance of the primitive streak in the mouse. *Development* **120**: 1919-1928.

Constam, D. B., and Robertson, E. J. (2000). SPC4/PACE4 regulates a TGFβ signalling network during axis formation. *Genes & Development* **14**: 1146-1155.

Coucouvanis, E., and Martin, G. R. (1995). Signals for death and survival: A two-step mechanism for cavitation in the vertebrate embryo. *Cell* **83**: 279-287.

Coucouvanis, E., and Martin, G. R. (1999). BMP signalling plays a role in visceral endoderm differentiation and cavitation in the early mouse embryo. *Development* **126**: 535-546.

Dattani, M. T., Martinez-Barbera, J. P., Thomas, P. Q., Brickman, J. M., Gupta, R., Martensson, I. –L., Toresson, H., Fox, M., Wales, J. K. H., Hindmarsh, P. C., Krauss, S., Beddington, R. P. S., and Robinson, I. C. A. F. (1998). Mutations in the homeobox gene *HESX1/Hesx1* associated with septo-optic dysplasia in human and mouse. *Nature Genetics* **19**: 125-133.

Deng, C, -X., Wynshaw-Boris, A., Shen, M. M., Daugherty, C., Ornitz, D. M., and Leder, P. (1994). Murine FGFR-1 is required for early postimplantation growth and axial organization. *Genes & Dev.* **8**: 3045-3057.

Di-Gregorio, A., Sancho, M, Stuckey, D. W., Crompton, L. A., Godwin, J., Mishina, Y., and Rodriguez, T. A. (2007). BMP signalling inhibits premature neural differentiation in the mouse embryo. *Development* **134**: 3359-3369.

Ding, J., Yang, L., Yam, Y, -T., Chen, A., Desai, N., Wynshaw-Boris, A., and Shen, M. M. (1998). *Cripto* is required for correct orientation of the anterior-posterior axis in the mouse embryo. *Nature* **395**: 702-707.

DiPaola, R. S. (2002). To arrest or not to G_2-M cell-cycle arrest. *Clinical Cancer Research* **8**: 3311-3314.

Doerfler, W., Hohlweg, U., Muller, K., Remus, R., Heller, H., and Hertz, J. (2001). Foreign DNA integration- perturbations of the genome-oncogenesis. *Ann. N.Y. Acad. Sci.* **945**: 276-288.

Donnison, M., Beaton, A., Davey, H. W., Broadhurst, R., L'Huillier, P., and Pfeffer, P. L. (2005). Loss of the extraembryonic ectoderm in *Elf5* mutants leads to defects in embryonic patterning. *Development* **132**: 2299-2308.

Dufort, D., Schwartz, L., Harpal, K., and Rossant, J. (1998). The transcription factor HNF3β is required in visceral endoderm for normal primitive streak morphogenesis. *Development* **125**: 3015-3025.

Dunn, N. R., Vincent, S. D., Oxburgh, L., Robertson, E. J., and Bikoff, E. K. (2004). Combinatorial activities of Smad2 and Smad3 regulate mesoderm formation and patterning in the mouse embryo. *Development* **131**: 1717-1728.

Episkopou, V., Arkell, R., Timmons, P. M., Walsh, J. J., Andrew, R, L., and Swan, D. (2001). Induction of the mammalian node requires Arkadia function in the extraembryonic lineages. *Nature* **410**: 825-830.

Finley, K. R., Tennessen, J., and Shawlot, W. (2003). The mouse secreted frizzled-related protein 5 gene is expressed in the anterior visceral endoderm and foregut endoderm during early post-implantation development. *Gen Expression Patterns* **3**: 681-684.

Fujiwara, T., Dehart, D. B., Sulik, K. K., and Hogan, B. L. (2002). Distinct requirements for extra-embryonic and embryonic bone morphogenetic protein 4 in the formation of the node and primitive streak and coordination of left-right asymmetry in the mouse. *Development* **129**: 4685-4696.

Gardner, R. L., Meredith, M. R., and Altman, D. G. (1992). Is the anterior-posterior axis of the fetus specified before implantation in the mouse? *J. Exp. Zool.* **264**: 437-443.

Glinka, A., Wu, W., Delius, H., Monaghan, P. A., Blumenstcok, C., and Niehrs, C. (1998). Dickkopf-1 is a member of a new family of secreted proteins and functions in head induction. *Nature* **391**: 357-362.

Grieshammer, U., Lewandoski, M., Prevette, D., Oppenheim, R. W., and Martin, G. R. (1998). Muscle-specific cell ablation conditional upon Cre-mediated DNA

recombination in transgenic mice leads to massive spinal and cranial motoneuron loss. *Developmental Biology* **197**: 234-247.

Hayashi, S., Lewis, P., Pevny, L and McMahon, A. P. (2002). Efficient gene modulation in mouse epiblast using *Sox2Cre* transgenic mouse strain. *Mechanisms of Development* **119**: 97-101.

Hayashi, S., Tenzen, T, and Mc Mahon, A. P. (2003). Maternal inheritance of Cre activity in a *Sox2Cre* deleter strain. *Genesis* **37**: 51-53.

Hermesz, E., Mackem, S., and Mahon, K. A. (1996). *Rpx*: a novel anterior-restricted homeobox gene progressively activated in the prechordal plate, anterior neural plate and Rathke's pouch of the mouse embryo. *Development* **122**: 41-52.

Hoodless, P. A., Pye, M., Chazaud, C., Labbe, E., Attisano, L., Rossant, J., and Wrana, J. L. (2001). FoxH1 (Fast) functions to specify the anterior primitive streak in the mouse. *Genes & Dev.* **15**: 1257-1271.

Huelsken, J., Vogel, R., Brinkmann, V., Erdmann, B., Birchmeier, C., and Birchmeier, W. (2000). Requirement for β-Catenin in anterior-posterior axis formation in mice. *JCB* **148**: 567-578.

Ivanova, A., Signore, M., Caro, N., Greene, N. D. E., Copp, A. J., and Martinez-Barbera, J. P. (2005). In vivo genetic ablation by Cre-mediated expression of diphtheria toxin fragment A. *Genesis* **43**: 129-135.

Kanai, Y., Kanai-Azuma, M., Noce, T., Saido, T. C., Shiroishi, T., Hayashi, Y., and Yazaki, K. (1996). Identification of two Sox17 messenger RNA isoforms, with and without the high mobility group box region, and their differential expression in mouse spermatogenesis. *J Cell Biol* **133**: 667-681.

Kelly, O. G., Pinson, K. I., and Skarnes, W. C. (2004). The Wnt co-receptors Lrp5 and Lrp6 are essential for gastrulation in mice. *Development* **131**: 2803-2815.

Kemp, C., Willems, E., Abdo, S., Lambiv, L., and Leyns, L. (2005). Expression of all Wnt genes and their secreted antagonists during mouse blastocyst and postimplantation development. *Dev. Dyn.* **233**: 1064-1075.

Kimura, C., Yoshinaga, K., Tian, E., Suzuki, M., Aizawa, S., and Matsuo, I. (2000). Visceral endoderm mediates forebrain development by suppressing posteriorizing signals. *Dev. Biol.* **225**:304-321.

Kimura-Yoshida, C., Nakano, H., Okamura, D., Nakao, K., Yonemura, S., Belo, J. A., Aizawa, S., Matsui, Y., and Matsuo, I. (2005). Canonical Wnt signalling and its antagonist regulate Anterior-Posterior axis polarization by guiding cell migration in mouse visceral endoderm. *Developmental Cell.* **9**:639-650.

Kunath, T., Arnaud, D., Uy, G. D., Okamoto, I., Chureau, C., Yamanaka, Y., Heard, E., Gardner, R. L., Avner, P., and Rossant, J. (2005). Imprinted X-inactivation in

extra-embryonic endoderm cell lines from mouse blastocysts. *Development* **132**: 1649-1661.

Lawson, K. A., and Pederson, R. A. (1987). Cell fate, morphogenetic movement and population kinetics of embryonic endoderm at the time of germ layer formation in the mouse. *Development* **101**: 627-652.

Lawson, K. A., Meneses, J. J., and Pederson, R. A. (1991). Clonal analysis of epiblast fate during germ layer formation in the mouse embryo. *Development* **113**: 891-911.

Leaf, I., Tennessen, J., Mukhopadhyay, M., Westphal, H., and Shawlot, W. (2006). *Sfrp5* is not essential for axis formation in the mouse. *Genesis* **44**: 573-578.

Lee, J. J., Warburton, D., and Robertson, E. J. (1990). Cytogenetic methods for the mouse: preparation of chromosomes, karyotyping, and *in situ* hybridization. *Anal Biochem* **189**: 1-17.

Lee, P., Morley, G., Huang, Q., Fischer, A., Seiler, S., Horner, J. W., Factor, S., Vaidya, D., Jalife, J., and Fishman, G. I. (1998). Conditional lineage ablation to model human diseases. *Proc. Natl. Sci.* **95**: 11371-11376.

Lee, K. J., Dietrich, P., and Jessell, T. M. (2000). Genetic ablation reveals that the roof plate is essential for dorsal interneuron specification. *Nature* **403**: 734-740.

Lewandoski, M., Meyers, E. N., and Martin, G. R. (1997). Analysis of *Fgf8* gene function in vertebrate development. *CSHSQB* **62**: 2070-2077.

Lewis, N. E., and Rossant, J. (1982). Mechanism of size regulation in mouse embryo aggregates. *J Embryol Exp Morphol* **72**: 169-181.

Liu, P., Wakamiya, M., Shea, M. J., Albrecht, U., Behringer, R. R., and Bradley, A. (1999). Requirement for *Wnt3* in vertebrate axis formation. *Nature* **22**: 361-365.

Logan, C. Y., and Nusse, R. (2004). The Wnt signalling pathway in development and disease. *Annu. Rev. Cell Dev. Biol.* **20**: 781-810.

Lu, C. C., Robertson, E. J., and Brennan, J. (2004a). The mouse frizzled 8 receptor is expressed in anterior organizer tissues. *Gene Expression Patterns* **4**: 569-572.

Lu, C. C., and Robertson, E. J. (2004b). Multiple roles for *Nodal* in the epiblast of the mouse embryo in the establishment of anterior-posterior patterning. *Developmental biology* **273**: 149-159.

Mac Auley, A., Werb, Z and Mirkes, P. E. (1993). Characterization of the unusually rapid cell cycles during rat gastrulation. *Development* **117**: 873-883.

Mahmood, R., Bresnick, J., Hornbruch, A., Mahony, C., Morton, N., Colquhoun, K., Martin, P., Lumsden, A., Dickson, C., and Mason, I. (1995). A role for FGF-8 in the initiation and maintenance of vertebrate limb bud outgrowth. *Curr Biol* **5**: 797-806.

Makover, A., Moriwaki, H., Ramakrishnan, R., Saraiva, M. J., Blaner, W. S., and Goodman, D. S. (1998). Plasma transthyretin. Tissue sites of degradation and turnover in the rat. *J. Biol. Chem* **263**: 8598-8603.

Martinez-Barbera, J. P., Rodriguez, T. A., and Beddington, R. S. P. (2000a). The homeobox gene *Hesx1* is required in the anterior neural ectoderm for normal forebrain formation. *Developmental Biology* **223**: 422-430.

Martinez-Barbera, J. P., Clements, M., Thomas, P., Rodriguez, T., Meloy, D., Kioussis, D., and Beddington, R. S. P. (2000b). The homeobox gene *Hex* is required in definitive endodermal tissues for normal forebrain, liver and thyroid formation. *Development* **127**: 2433-2445.

Martinez-Barbera, J. P., and Beddington, R. S. P. (2001). Getting your head around *Hex* and *Hesx1*: forebrain formation in mouse. *Int. J. Dev. Biol.* **45**: 327-336.

Massague, J., Blain, S. W., and Lo, R. S. (2000). TGFbeta signalling in growth control, cancer, and heritable disorders. *Cell* **103**: 295-309.

Meno, C., Ito, Y., Saijoh, Y., Matsuda, Y., Tashiro, K., Kuhara, S., and Hamada, H. (1997). Two closely-related left-right asymmetrically expressed genes, lefty-1 and lefty-2: their distinct expression domains, chromosomal linkage and direct neuralizing activity in Xenopus embryos. *Genes Cells* **2**: 513-524.

Meno, C., Shimono, A., Saijoh, Y., Yashiro, K., Ohishi, S., Noji, S., Kondoh, H., Hamada, H. (1998). Lefty-1 is required for left-right determination as a regulator of lefty-2 and nodal. *Cell* **94**: 287-297.

Meno, C., Gritsman, K., Ohishi, S., Ogfuji, Y., Heckscher, E., Mochida, K., Shimono, A., Kondoh, H., Talbot, W. S., Robertson, E. J., Schier, A., and Hamada, H. (1999). Mouse Lefty2 and zebrafish antivin are feedback inhibitors of nodal signalling during vertebrate gastrulation. *Molecular Cell* **4**: 287-298.

Mesnard, D., Filipe, M., Belo, J. A., and Zernicka-Goetz, M. (2004). The anterior-posterior axis emerges respecting the morphology of the mouse embryo that changes and aligns with the uterus before gastrulation. *Current Biology* **14**: 184-196.

Mesnard, D., Guzman-Ayala, M., and Constam, D. B. (2006). Nodal specifies embryonic visceral endoderm and sustains pluripotent cells in the epiblast before overt axial patterning. *Development* **133**: 2497-2505.

Miura, S., and Mishina, Y. (2007). The DVE changes distal epiblast fate from definitive endoderm to neurectoderm by antagonizing Nodal signalling. *Developmental Dynamics* **236**: 1602-1610.

Mishina, Y., Suzuki, A., Ueno, N., and Behringer, R. R. (1995). *Bmpr* encodes a type I bone morphogenetic protein receptor that is essential for gastrulation during mouse embryogenesis. *Genes Dev.* **9**: 3027-3037.

Mohamed, O. A., Clarke, H. J., and Dufort, D. (2004). β-catenin signalling marks the prospective site of primitive streak formation in the mouse embryo. *Dev. Dynamics* **231**: 416-424.

Mukhopadhyay, M., Shtrom, S., Rodriguez-Esteban, C., Chen, L., Tsukui, T., Gomer, L., Dorward, D. W., Glinka, A., Grinberg, A., Huang, S-P., Niehrs, C., Belmonte, J, C, I., and Westphal, H. (2001). *Dickkopf1* is required for embryonic head induction and limb morphogenesis in the mouse. *Developmental Cell* **1**: 423-434.

Muller, K., Heller, H., and Doerfler, W. (2001). Foreign DNA integration. Genome-wide perturbations of methylation and transcription in the recipient genomes. *JBC* **276**: 14271-14278.

Murray, P., and Edgar, D. (2000). Regulation of programmed cell death by basement membranes in embryonic development. *JCB* **150**: 1215-1221.

Nagy, A. (2000). Cre Recombinase: The universal reagent for genome tailoring. *Genesis* **26**: 99-109.

Nichols, J., Zevnik, B., Anastassiadis, K., Niwa, H., Klewe-Nebenius, D., Chambers, I., Scholer, H., and Smith, A. (1998). Formation of pluripotent stem cells in the mammalian embryo depends on the POU transcription factor Oct4. *Cell* **95**: 379-391.

Nieto, M. A., Bennett, M. F., Sargent, M. G., and Wilkinson, D. G. (1992). Cloning and developmental expression of Sna, a murine homologue of the Drosophila snail gene. *Development* **116**: 227-237.

Norris, D. P., and Robertson, E. J. (1999). Asymmetric and node-specific *nodal* expression patterns are controlled by two distinct *cis*-acting regulatory elements. *Genes & Development* **13**: 1575-1588.

Norris, D. P., Brennan, J., Bikoff, E. K., and Robertson, E. J. (2002). The Foxh1-dependant autoregulatory enhancer controls the levels of Nodal signals in the mouse embryo. *Development* **129**: 3455-3468.

Nothias, J-Y., Majunder, S., Kaneko, K. J., and DePamphilis, M. L. (1995). Regulation of gene expression at the beginning of mammalian development. *The Journal of Biological Chemistry* **270**: 22077-22080.

Oliver, G., Mailhos, A., Wehr, R., Copeland, N. G., Jenkins, N. A., and Gruss, P. (1995). Six3, a murine homologue of the sine oculis gene, demarcates the most anterior border of the developing neural plate and is expressed during eye development. *Development* **121**: 4045-4055.

Perea-Gomez, A., Shawlot, W., Sasaki, H., Behringer, R. R., and Ang, Siew-Lan. (1999). *HNF3β* and *Lim1* interact in the visceral endoderm to regulate primitive streak formation and anterior-posterior polarity in the mouse embryo. *Development* **126**: 4499-4511.

Perea-Gomez, A., Lawson, K. A., Rhinn, M., Zakin, L., Brulet, P., Mazan, S., and Ang, S. -L. (2001a). Otx2 is required for visceral endoderm movement and for the restriction of posterior signals in the epiblast of the mouse embryo. *Development* **128**: 753-765.

Perea-Gomez, A., Rhinn, M., and Ang, S. –L. (2001b). Role of the anterior visceral endoderm in restricting posterior signals in the mouse embryo. *Int. J. Dev. Biol.* **45**: 311-320.

Perea-Gomez, A., Vella, F. D. J., Shawlot, W., Oulad-Abdelghani, Chazaud, C., Meno, C., Pfister, V., Chen, L., Robertson, E., Hamada, H., Behringer, R. R., and Ang, S. –L. (2002). Nodal antagonists in the anterior visceral endoderm prevent the formation of multiple primitive streak. *Developmental Cell* **3**: 745-756.

Perea-Gomez, A., Camus, A., Moreau, A., Grieve, K., Moneron, G, Dubois, A., Cibert, C., and Collignon, J. (2004). Initiation of gastrulation in the mouse embryo is preceded by an apparent shift in the orientation of the Anterior-Posterior axis. *Current Biology* **14**: 197-207.

Pfister, S., Steiner, K. A., and Tam, P. P. L. (2007). Gene expression pattern and progression of embryogenesis in the immediate post-implantation period of mouse development. *Gene Expression Patterns* **7**: 558-573.

Piedra, M. E., and Ros, M. A. (2002). BMP signalling positively regulates Nodal expression during left right specification in the chick embryo. *Development* **129**: 3431-3440.

Poelmann, R. E. (1980). Differential mitosis and degeneration patterns in relation to the alterations in the shape of the embryonic ectoderm of early post-implantation mouse embryos. *J. Embryol. Exp. Morph.* **55**: 33-51.

Power, M. A., and Tam, P. P. L. (1993). Onset of gastrulation, morphogenesis and somitogenesis in mouse embryos displaying compensatory growth. *Anat. Embryol. (Berl).* **187**: 493-504.

Rakeman, A. S., and Anderson, K. V. (2006). Axis specification and morphogenesis in the mouse embryo require *Nap1*, a regulator of WAVE-mediated actin branching. *Development* **133**: 3075-3083.

Reik, W. (2007). Stability and flexibility of epigenetic gene regulation in mammalian devclopment. *Nature* **447**: 425-432.

Rhinn, M., Dierich, A., Shawlot, W., Behringer, R. R., Le Meur, M., and Ang, S. –L. (1998). Sequential roles of *Otx2* in visceral endoderm and neurectoderm for forebrain and midbrain induction and specification. *Development* **125**: 845-856.

Richardson, L., Torres-Padilla, M., and Zernicka-Goetz, M. (2006). Regionalized signalling within the extra-embryonic ectoderm regulates anterior visceral endoderm positioning in the mouse embryo. *Mech Dev* **123**: 288-296.

Rivera-Perez, J. A., Mager, J., and Magnuson, T. (2003). Dynamic morphogenetic events characterize the mouse visceral endoderm. *Developmental Biology* **261**: 470-487.

Rivera-Perez, J. A., and Magnuson, T. (2005). Primitive streak formation in mice is preceded by localized activation of *Brachyury* and *Wnt3*. *Developmental Biology* **288**: 363-371.

Robertson, E. J., Norris, D. P., Brennan, J., and Bikoff, E. K. (2003). Control of early anterior-posterior patterning in the mouse embryo by TGF-beta signalling. *Philos. Trans. R. Soc. Lond. B. Biol. Sci.* **29**: 1351-1357.

Rodriguez, T. A., Casey, E. S., Harland, R. M., Smith, J. C. and Beddington, R. S. (2001). Distinct enhancer elements control Hex expression during gastrulation and early organogenesis. *Dev Biol* **234,** 304-16.

Rodriguez, T. A., Srinivas, S., Clements, M. P., Smith, J. C., and Beddington, R. S. (2005). Initiation and migration of the anterior visceral endoderm is regulated by the extra-embryonic ectoderm. *Development* **132**: 2513-2520.

Roelink, H., Wagenaar, E., Lopes da Silva, S., and Nusse R. (1990). Wnt-3, a gene activated by proviral insertion in mouse mammary tumours, is homologous to int-1/Wnt-1 and is normally expressed in mouse embryos and adult brain. *PNAS* **87**: 4519-4523.

Rossant, J., and Tam, P. P. L., (2004). Emerging asymmetry and embryonic patterning in early mouse development. *Developmental Cell* **7**: 155-164.

Rosner, M. H., Vigano, M. A., Ozato, K., Timmons, P. M., Poirier, F., Rigby, P. W., and Staudt, L. M. (1990). A POU-domain transcription factor in early stem cells and germ cells of the mammalian embryo. *Nature* **21**: 686-692.

Saijoh, Y., Oki, S., Ohishi, S., and Hamada, H. (2003). Left-right patterning of the mouse lateral plate requires Nodal produced in the node. *Developmental Biology* **256**: 160-172.

Schier, A. F., and Shen, M. M. (2000). Nodal signalling in vertebrate development. *Nature* **403**: 385-389.

Schlange, T., Arnold, H-H., and Brand, T. (2002). BMP2 is a positive regulator of Nodal signalling during left-right axis formation in the chicken embryo. *Development* **129**: 3421-3429.

Schmahl, J., and Capel, B. (2003). Cell proliferation is necessary for the determination of male fate in the gonad. *Developmental Biology* **256**: 1-13.

Shawlot, W., and Behringer, R. R. (1995). Requirement for Lim1 in head-organizer function. *Nature* **374**: 425-430.

Shawlot, W., Deng, J. M., and Behringer, R. R. (1998). Expression of the mouse *cerberus*-related gene, *Cerr1*, suggests a role in anterior neural induction and somitogenesis. *PNAS* **95**: 6198-6203.

Shawlot, W., Wakamiya, M., Kwan, K. M., Kania, A., Jessell, T. M., and Behringer, R. R. (1999). *Lim1* is required in both primitive streak-derived tissues and visceral endoderm for head formation in the mouse. *Development* **126**: 4925-4932.

Shawlot, W., Deng, J. M., Wakamiya, M., and Behringer, R. R. (2000). The *Cerberus-Related* gene, *Cerr1*, is not essential for mouse head formation. *Genesis* **26**: 253-258.

Shook, D., and Keller, R. (2003). Mechanisms, mechanics and function of epithelial-mesenchymal transitions in early development. *Mechanisms of Development* **120**: 1351-1383.

Smith, L. J. (1980). Embryonic axis orientation in the mouse and its correlation with blastocyst relationships to the uterus. Part 1. Relationships between 82 hours and 4.25 days. *J. Embryol. Exp. Morph* **55**: 257-277.

Smith, L. J. (1985). Embryonic axis orientation in the mouse and its correlation with blastocyst relationships to the uterus. II. Relationships from 4.25 to 9.5 days. *J. Embryol. Exp. Morph* **89**: 15-35.

Snow, M. H. L. (1977). Gastrulation in the mouse: Growth and regionalization of the epiblast. *J. Embryol. Exp. Morph.* **42**: 293-303.

Snow, M. H. L., and Bennett, D. (1978). Gastrulation in the mouse: assessment of cell populations in the epiblast of tw18/tw18 embryos. *J Embryol Exp Morphol* **47**: 39-52.

Soriano, P. (1999). Generalised *lacZ* expression with the ROSA26 Cre reporter strain. *Nature Genetics* **21**: 70-71.

Srinivas, S., Rodriguez, T., Clements, M., Smith, J. C., and Beddington, R. S. P. (2004). Active cell migration drives the unilateral movements of the anterior visceral endoderm. *Development* **131**: 1157-1164.

Srinivas, S., (2006). The anterior visceral endoderm-Turning heads. *Genesis* **44**: 565-572.

Strumpf, D., Mao, C-A., Yamanaka, Y., Ralston, A., Chawengsaksophak, K., Beck, F., and Rossant, J. (2005). Cdx2 is required for correct cell fate specification and differentiation of trophectoderm in the mouse blastocyst. *Development* **132**: 2093-2102.

Sun, X., Meyers, E. N., Lewandoski, M., and Martin, G. R. (1999). Targeted disruption of *Fgf8* causes failure of cell migration in the gastrulating mouse embryo. *Genes & Dev*. **13**: 1834-1846.

Takaoka, K., Yamamoto, Y., Shiratori, H., Meno, C., Rossant, J., Saijoh, Y., and Hamada, H. (2006). The mouse embryo autonomously acquires anterior-posterior polarity at implantation. *Developmental Cell* **10**: 451-459.

Takaoka, K., Yamamoto, M., and Hamada, H. (2007). Origin of body axes in the mouse embryo. *Current Opinions in Genetics & Development* **17**: 1-7.

Takito, J., and Al-Awqati, Q. (2004). Conversion of ES cells to columnar epithelia by hensin and to squamous epithelia by laminin. *The Journal of Cell Biology* **166**: 1093-1102.

Tam, P. P. L., and Beddington, R. S. P. (1987). The formation of mesodermal tissues in the mouse embryo during gastrulation and early organogenesis. *Development* **99**: 109-126.

Tam, P. P. L., Williams, E. A., and Chan, W. Y. (1993). Gastrulation in the mouse embryo: Ultrastructural and molecular aspects of germ layer morphogenesis. *Microscopy Research and Technique* **26**: 301-328.

Tam, P. P. L, and Behringer, R. R. (1997). Mouse gastrulation: the formation of a mammalian body plan. *Mechanisms of Development* **68**: 3-25.

Tam, P. P., and Steiner, K. A. (1999). Anterior patterning by synergistic activity of the early gastrula organiser and the anterior germ layer tissues of the mouse embryo. *Development* **126**: 5171-5179.

Tam, P. P. L., and Loebel, D. A. F. (2007). Gene function in mouse embryogenesis: get set for gastrulation. *Nature* **8**: 368-381.

Tanaka, S., Kunath, T., Hadjantonakis, A. K., Nagy, A., and Rossant, J. (1998). Promotion of trophoblast stem cell proliferation by FGF4. *Science* **282**: 2072-2075.

Thomas, P. Q., Johnson, B. V., Rathjen, J., and Rathjen, P. D. (1995). Sequence, genome organization, and expression of the novel homeobox gene Hesx1. *J Biol Chem* **270**: 3869-3875.

Thomas, P., and Beddington, R. S. P. (1996). Anterior primitive endoderm may be responsible for patterning the anterior neural plate in the mouse embryo. *Curr. Biol* **6**: 1487-1496.

Thomas, P., Brown, A., and Beddington, R. S. P. (1998). Hex: a homeobox gene revealing peri-implantation asymmetry in the mouse embryo and an early transient marker of endothelial cell precursors. *Development* **125**: 85-94.

Torres-Padilla, M-E., Richardson, L., Kolasinska, P., Meilhac, S. M., Luetke-Eversloh, M. V., and Zernicka-Goetz, M. (2007). The anterior visceral endoderm of the mouse embryo is established from both preimplantation precursor cells and by de novo gene expression after implantation. *Developmental Biology* **309**: 97-112.

Varlet, I., Collignon, J., and Robertson, E. J. (1997). Nodal expression in the primitive endoderm is required for specification of the anterior axis during mouse gastrulation. *Development* **124**: 1033-1044.

Vasquez, R. J., Howell, B., Yvon, A-M. C., Wadsworth, P., and Cassimeris, L. (1997). Nanomolar concentrations of nocodazole alter microtubule instability *in vivo* and *in vitro*. *Molecular Biology of the Cell* **8**:973-985.

Vincent, S. D., and Robertson, E. J. (2003a). Highly efficient transgene-independent recombination directed by a maternally derived *Sox2Cre* transgene. *Genesis* **37**: 54-56.

Vincent, S. D., Dunn, R. N., Hayashi, S., Norris, D. P., and Robertson, E. J. (2003b). Cell fate decisions within the mouse organizer are governed by graded Nodal signals. *Genes & Development* **17**: 1646-1662.

Waldrip, W. R., Bikoff, E. K., Hoodless, P. A., Wrana, J. L., and Robertson, E. J. (1998). *Smad2* signalling in extraembryonic tissues determines anterior-posterior polarity of the early mouse embryo. *Cell* **92**: 797-808.

Wang, H., and Dey, S. K. (2006). Roadmap to embryo implantation: clues from mouse models. *Nature Genetics* **7**: 185-199.

Weber, R. J., Pederson, R. A., Wianny, F., Evans, M. J, and Zernicka-Goetz, M. (1999). Polarity of the mouse embryo is anticipated before implantation. *Development* **126**: 5591-5598.

Whitman, M. (2001). Nodal signalling in early vertebrate embryos. Themes and variations. *Dev. Cell* **1**: 605-617.

Wilkinson, D. G., Bhatt, S and Herrmann, B. G. (1990). Expression pattern of the mouse *T gene* and its role in mesoderm formation. *Nature* **343**: 657-659.

Wilson, V., Manson, L., Skarnes, W. C., and Beddington, R. S. P. (1995). The *T* gene is necessary for normal mesodermal morphogenetic cell movements during gastrulation. *Development* **121**: 877-886.

Winnier, G., Blessing, M., Labosky, P. A., and Hogan, B. L. M. (1995). Bone morphogenetic protein-4 is required for mesoderm formation and patterning in the mouse. *Genes Dev.* **9**: 2105-2116.

Wotton, D., and Massague, J. (2001). Smad transcriptional corepressors in TGF beta family signalling. *Curr. Top. Microbiol. Immunol.* **254**: 145-164.

Wu, S., Wu, Y., and Capecchi, M. R. (2005). Motoneurons and oligodendrocytes are sequentially generated from neural stem cells but do not appear to share common lineage-restricted progenitors *in vivo*. *Development* **133**: 581-590.

Yamaguchi, T. P., Harpal, K., Henkemeyer, M., and Rossant, J. (1994). *Fgfr-1* is required for embryonic growth and mesodermal patterning during mouse gastrulation. *Genes & Dev.* **8**: 3032-3044.

Yamaguchi, T. P., Takada, S., Yoshikawa, Y., Wu, N., and McMahon, A. P. (1999). *T* (Brachyury) is a direct target of Wnt3a during paraxial mesoderm specification. *Genes and Development* **13**: 3185-3190.

Yamamoto, S., Hikasa, H., Ono, H., and Taira, M. (2003). Molecular link in the sequential induction of the Spemann organiser: direct activation of the *Cerberus* gene by Xlim-1, Xotx-2, Mix.1, and Siamois, immediately downstream from Nodal and Wnt signalling. *Developmental Biology* **257**: 190-204.

Yamamoto, M., Saijoh, Y., Perea-Gomez, A., Shawlot, W., Behringer, R. R., Ang, S. –L., Hamada, H., and Meno, C. (2004). *Nodal* antagonists regulate the formation of the anterior-posterior axis of the mouse embryo. *Nature* **428**: 387-392.

Yoshikawa, Y., Fujimori, T., McMahon, A. P., and Takada, S. (1997). Evidence that absence of *Wnt-3a* signalling promotes neuralization instead of paraxial mesoderm development in mouse. *Dev. Biol.* **183**: 234-242.

Zernicka-Goetz, M. (1998). Fertile offspring from mammalian eggs lacking either animal or vegetal poles. *Development* **125**: 4803-4808.

(http://www.sickkids.ca/rossant/protocols/BrdU_embryoStain.asp)

Appendix I

M2 embryo dissection media

Stock Solution	Component	Final Concentration (mM)	Vol/L (ml)
Solution A:	NaCl	94.66	**100**
	KCl	4.78	
	KH_2PO4	1.19	
	$MgSO_4 \cdot 7H_2O$	1.19	
	Sodium lactate	23.28	
	Glucose	5.56	
Solution B:	$NaHCO_3$	4.15	**16**
	Phenol Red	0.00028	
Solution C:	Sodium Pyruvate	0.33	**10**
Solution D:	$CaCl_2 \cdot 2H_2O$	1.71	**10**
Solution E:	HEPES	20.85	**84**
	Phenol Red	0.00028	
	(NaOH to adjust pH to 7.4)		

Stock solutions were made up in advance, filter sterilised and stored at -20 °C.

To make 1 litre of M2 the appropriate volumes of each solution were added to 700 ml of tissue culture water (Gibco). 100ml of tissue culture characterised Fetal Calf Serum and 10 ml of 100X Penicillin/Streptomycin solution was added and the final volume made up to 1 litre with additional tissue culture water.

Appendix II

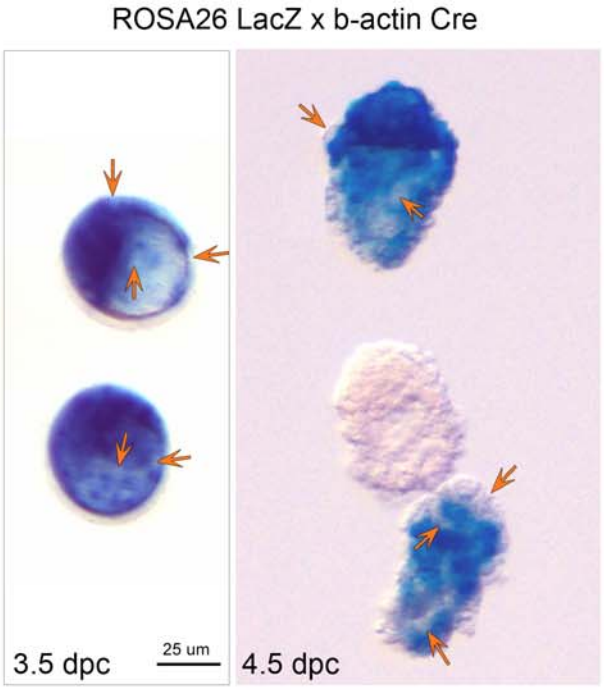

Blastocysts at 3.5 and 4.5 dpc derived from a ROSA26 LacZ X beta-actin Cre cross. Blue colour indicates positive beta-galactosidase-expressing cells. Orange arrows indicate a selection of unstained cells.